2018

DESIGN AND ANALYSIS OF CURCUMIN CONJUGATED POLY(BETA-AMINO ESTER) NETWORKS FOR CONTROLLED RELEASE IN OXIDATIVE STRESS ENVIRONMENTS

Carolyn T. Jordan
University of Kentucky, carolyntjordan@gmail.com
Author ORCID Identifier:
https://orcid.org/0000-0002-1243-0038
Digital Object Identifier: https://doi.org/10.13023/ETD.2018.224

STUDENT AGREEMENT:

I represent that my thesis or dissertation and abstract are my original work. Proper attribution has been given to all outside sources. I understand that I am solely responsible for obtaining any needed copyright permissions. I have obtained needed written permission statement(s) from the owner(s) of each third-party copyrighted matter to be included in my work, allowing electronic distribution (if such use is not permitted by the fair use doctrine) which will be submitted to UKnowledge as Additional File.

I hereby grant to The University of Kentucky and its agents the irrevocable, non-exclusive, and royalty-free license to archive and make accessible my work in whole or in part in all forms of media, now or hereafter known. I agree that the document mentioned above may be made available immediately for worldwide access unless an embargo applies.

I retain all other ownership rights to the copyright of my work. I also retain the right to use in future works (such as articles or books) all or part of my work. I understand that I am free to register the copyright to my work.

REVIEW, APPROVAL AND ACCEPTANCE

The document mentioned above has been reviewed and accepted by the student's advisor, on behalf of the advisory committee, and by the Director of Graduate Studies (DGS), on behalf of the program; we verify that this is the final, approved version of the student's thesis including all changes required by the advisory committee. The undersigned agree to abide by the statements above.

Carolyn T. Jordan, Student

Dr. Thomas D. Dziubla, Major Professor

Dr. Thomas D. Dziubla, Director of Graduate Studies

DESIGN AND ANALYSIS OF CURCUMIN CONJUGATED POLY(BETA-AMINO ESTER) NETWORKS FOR CONTROLLED RELEASE IN OXIDATIVE STRESS ENVIRONMENTS

DISSERTATION

A dissertation submitted in partial fulfillment of the
requirements for the degree of Doctor of Philosophy
in the College of Engineering at the University of Kentucky

By

Carolyn Therese Jordan

Lexington, Kentucky

Co-Directors: Dr. Thomas D. Dziubla, Professor of Chemical Engineering
and Dr. Douglass S. Kalika, Professor of Chemical Engineering

Lexington, KY

ABSTRACT OF DISSERTATION

DESIGN AND ANALYSIS OF CURCUMIN CONJUGATED POLY(BETA-AMINO ESTER) NETWORKS FOR CONTROLLED RELEASE IN OXIDATIVE STRESS ENVIRONMENTS

Oxidative stress, the imbalance of free radical generation with antioxidant defenses, leads to cellular inflammation, apoptosis and cell death. This compromised environment results in debilitating diseases, such as oral mucositis (OM), atherosclerosis, and ischemia/reperfusion injury. Antioxidant therapeutics has been a proposed strategy to ameliorate these imbalances and maintain homeostatic environments. However, the success of these approaches, specifically curcumin, has been limited due to characteristics such as hydrophobicity and high reactivity when released as bolus doses to contest to oxidative stress induced diseases. The development of a controlled release system to aid in protection of the antioxidant capacity of curcumin, as well as a tunable system to aid in proper rate of release for disease can overcome these limitations. Previously, the use of a poly(beta-amino ester) (PBAE) chemistry has been developed in Dziubla and Hilt laboratories to provide desirable properties. The dynamic mechanical analysis and efficacy in cellular protection has been studied, yet the sensitivity and responsiveness of these polymers to abnormal environments found within oxidative stress compromised environments are unknown.

In this work, a series of networks were comprised of different molar ratios of modified acrylated curcumin, poly(ethylene glycol) diacrylate, and a primary diamine crosslinker to create tunable hydrolytically degradable crosslinked hydrogels. I hypothesized a consumption rate difference of free curcumin and curcumin as a released product from the crosslinked network in the presence of a free radical generating system. After the consumption profiles of each were reported differently, the experimental data was translated into a kinetic rate model to identify quantitative consumption rate parameters of curcumin and active film degradation products. The effect on the released products arose

the question of curcumin consumption in other oxidizing environments. These networks were then investigated in low concentrations of a hydrogen peroxide insult, and interestingly showed sensitivity to hydrolysis by recovering significantly more curcumin at an accelerated rate of release. Identifying the sensitivity of these tunable networks to environmental stimuli, they were then presented to a series of low pH environments, which significantly reduced the degradation time, finding a dependence of rate of release on the weight loading of curcumin present within the film. To translate these responsive materials to an application-based system, the curcumin conjugated PBAE polymers were investigated as an oral rinse drug delivery system for the treatment of radiation-induced OM in a hamster model. Radiation-induced OM onset and severity was reduced with a 20 wt% microparticle loaded mucoadhesive system that releases curcumin over 24 hours, providing promising results of a therapeutic effect from curcumin when incorporated in to a controlled release delivery system.

Overall, curcumin conjugated PBAE polymers show selectivity of hydrolysis in abnormal environments related to oxidative stress. This information is beneficial to the proper design and loading of antioxidant therapeutics within crosslinked polymers, giving the ability to tune release to treat and deliver based on the environment's insult. This can advance the potential use for antioxidant therapeutics in pharmaceutical applications in the future.

KEYWORDS: Oxidative Stress, Antioxidant Therapeutics,
Responsive Polymers, Curcumin, Oral Mucositis

Carolyn Therese Jordan

April 19, 2018
Date

DESIGN AND ANALYSIS OF CURCUMIN CONJUGATED
POLY(BETA-AMINO ESTER) NETWORKS FOR CONTROLLED RELEASE
IN OXIDATIVE STRESS ENVIRONMENTS

By

Carolyn Therese Jordan

Dr. Thomas D. Dziubla
Co-Director of Dissertation

Dr. Douglass S. Kalika
Co-Director of Dissertation

Dr. Thomas D. Dziubla
Director of Graduate Studies

April 19, 2018

ACKNOWLEDGEMENTS

My dissertation would not have been possible without all the consistent support I have had throughout my time in graduate school. I am truly blessed with the amount of caring and supportive people that I have in my life: my wonderful family and friends, both near and far, and my encouraging mentors.

I would like to express so much gratitude to my primary advisor, Dr. Tom Dziubla, who has never given up on me. He has been one of my main motivators to work hard and stay persistent. Dr. J. Zach Hilt, my co-advisor, has also played a huge part in my research career. Thank you both for providing me with the tools and guidance necessary to become an independent and innovative thinker. Over the last five years, weekly meetings quickly turned in to something I was apprehensive about to something I truly looked forward to. I enjoyed our scientific conversations, as well as the laughs along the way. Your positive words and tough love have truly made me a proud and confident scientist, and I can't thank you all enough. I am beyond excited to continue working with you in the future.

I'd like to thank my committee members, Dr. Bradley Berron, Dr. Douglass Kalika, and Dr. Craig Miller. Your insight and resources along the way have been so helpful. I'd also like acknowledge my outside examiner, Dr. Patrick Marsac. Thank you all for the taking the time to look over my dissertation.

I would like to thank my Dziubla labmates – Vinod, Prachi, Andew, Sundar, Irfan, Dustin, and Kelley—you welcomed me with open arms and provided a perfect balance of work and play when necessary. To my undergraduates—Paige Clark, Ava, and Hannah—

you have helped me grow as a mentor and a leader, as well as turned in to friends along the way. To my department friends – Anastasia, Angela, Landon, Calvin, and Dan – these five years have given me your friendships that will last a lifetime.

I'd like to the acknowledge the Center for Clinical and Translational Sciences (CCTS) and Jennifer Moylan for providing training on tissue processing and the execution of the ELISA assays, as well as Dr. Molly Housley-Smith with guidance on the analysis of hematoxylin and eosin stained slides. I'd also like to convey my appreciation to Dr. Emily Bradford for all of her advice and help – both on science and life. There will never be a day that I won't remember our hours of conversations in DLAR and the time we spent with Angus.

I have been blessed with a family that has given me unconditional love and support. Thank you to my Mom and Dad for instilling a strong work ethic in me from the beginning. For Kristen and Jeanette always providing a shoulder to lean on, even from hundreds of miles away. Our group family message is comic relief for me every day, and I love you guys so much.

And to Spencer Jordan – my husband, best friend, and partner in crime. You have been my biggest fan since day one and I love you with all my heart. Thank you for being okay with changing plans, and not living life by the books with me. You have provided me with absolute support throughout this entire feat, and I appreciate all you do for me. More than you will ever know. I dedicate this dissertation to you.

TABLE OF CONTENTS

LIST OF TABLES

LIST OF FIGURES

Chapter 1 Introduction

1.0 Introduction

Oxidative stress (OS) is the underlying cause of many devastating diseases in human pathology, including chronic obstruction pulmonary disease (COPD) [1], cancer [2], oral mucositis [3], cardiovascular disease, chronic inflammation and even the process of aging [4]. OS is characterized by the overproduction of free radicals in a cellular environment and leads to a state of cellular dysfunction that leads to mutation and apoptosis. A list found in **Table 1-1** highlights several diseases linked to oxidative stress.

Antioxidants can be used as a therapeutic to balance excessive free radical production. Flavonoids, a specific group of natural products with polyphenolic features, are a challenging class of therapeutics, as they have potent antioxidant and anti-inflammatory properties, but as a free drug are highly reactive, prone to degradation, and hydrophobic[5, 6]. They have been shown to have high therapeutic potential for the treatment of oxidative stress-induced diseases, but their low bioavailability limits their efficacy[7]. The field of drug delivery has been using drug-conjugated polymers over the last 50 years to improve the therapeutic potential of small molecules, peptides, and proteins. The design of pro-drugs, which includes properties to enhance targeting[8], loading capacity[9, 10], and solubility[11] is important for optimal delivery.

A pioneering approach to deliver these small hydrophobic molecules, used in this dissertation, is to utilize degradable drug-conjugated crosslinked networks. The active compound can be incorporated into the backbone of the network to aid in stability and preserve activity of the drug until it is released. Acrylated polyphenols are reacted upon

Michael Addition chemistry with primary diamines and form a crosslinked polymer that not only can be categorized as a hydrogel but is also hydrolytically degradable through base-catalyzed hydrolysis. The reaction scheme for PBAE films is presented in **Figure 1-1**.

PBAE networks can control drug release by changing the crosslinking density or degree of hydrophobicity with the selection of the amine and acrylate monomers, as well as the acrylate to amine ratio in the initial reaction. The ability to tune drug release is crucial in the development of pharmaceuticals and allows for this polymer chemistry to be employed for a plethora of applications. Polymeric drug delivery systems can be responsive to environmental factors such as pH, ionic strength, free radicals, and temperature, but what has yet to be discussed is the responsiveness of these hydrolytically degradable ester linkages in the presence of external stimuli other than a PBS pH 7.4 controlled environment.

In this work, we evaluate the influence environmental factors have on the polymer degradation and release of curcumin, and how polymer synthesis impacts its environmental sensitivity. The responsiveness of the polymer and consumption of curcumin was investigated in different simulated environments of insult. Interestingly, the rate of hydrolysis of the polymer backbone was dependent on the source of oxidant, and the amount of drug within the network. The polymer response was also studied in low pH environments, and an *in vivo* oral mucositis hamster model was conducted to examine the efficacy of the biopolymer system as a preventative treatment for radiation-induced oral mucositis. Lastly, efforts to enhance curcumin release from the network were also completed in an attempt to reduce the amount of curcumin monoacrylate released.

1.1 Objectives

The overall objective of this work was to investigate the material response of curcumin conjugated poly(beta-amino ester) films and microparticles with respect to the polymer degradation and activity of the curcumin release, and determine the efficacy of the microparticle treatment for radiation-induced oral mucositis, an adverse side effect linked to oxidative stress. The degradation products were also investigated in efforts to decrease the curcumin monoacrylate product release from the network. These investigations were accomplished by setting the following objectives:

1. Develop a mathematical model to describe the oxidative consumption of curcumin from a hydrolytically degradable crosslinked microparticle network in the presence of a free radical generating environment

    A. Evaluate the consumption profile of curcumin as a free molecule in the presence of 2,2'-azobis(2-amidinopropane) dihydrochloride (AAPH).

    B. Assess the consumption profile of the degradation products of curcumin conjugated poly(beta-amino ester) crosslinked microparticle networks in the presence of AAPH.

    C. Develop a kinetic rate model to describe the consumption of curcumin over time.

    D. Utilize this model to evaluate consumption of curcumin in the presence of AAPH and different release rates of curcumin.

2. Investigate the effects of bulk film polymer degradation and curcumin consumption in the presence of two oxidizing environments (AAPH, H_2O_2).

A. Evaluate the impact of AAPH and H_2O_2 concentrations on films in solutions.

B. Investigate the release rate, polymer degradation, swelling, and antioxidant activity of the released curcumin after being exposed to AAPH and H_2O_2.

3. Evaluate the pH responsive degradation of PBAE networks of different curcumin weight loading percentages.

A. Evaluate polymer mass over time, release of curcumin, and swelling ratios of different crosslinked films in the presence of buffered solutions of pH 3, 5, and 7 at a constant ionic strength.

B. Discuss differences and discrepancies on results compared to current linear poly(beta-amino ester) literature.

4. Determine the efficacy of curcumin-conjugated PBAE microparticle formulations and doses in the treatment of radiation induced oral mucositis *in vivo.*

A. Examine observational change in onset and severity of oral mucositis when curcumin treatment with controlled release microparticle systems is given.

B. Perform histological analysis to quantify inflammatory and lipid peroxidation biomarkers, and degree of tissue damage.

5. Reduce monoacrylate forms of curcumin in the degradation products of the degraded polymer system.

A. Post-modify the current synthesized films to cap free acrylate in the network.

B. Change the ratio of total acrylates to amine protons.

C. Synthesize films with higher percentage of a diacrylate in the curcumin multiacrylate starting material.

Table 1-1: Diseases Linked to Oxidative Stress.

Disease	**Source of ROS**	**References**
Atherosclerosis (Vascular complications from Diabetes)	Mitochondrial superoxide overproduction and inactivation of anti-atherosclerosis enzymes	[12-14]
Oral Mucositis	Chemotherapy or radiation therapy for the treatment of cancer (hydroxyl radical, superoxide anion, and hydrogen peroxide production)	[15-19]
Cancer	UV-exposure, smoke inhalation, pollutant ingestion	[20-22]
Kidney Failure	Activation of phagocyte oxidant enzyme generation and impaired mitochondrial respiratory system	[23, 24]
Chronic Pulmonary Obstruction Disorder	Macrophage and leukocyte infiltration after inhalation of nitric oxide, fiber degradation	[1, 25]
Alzheimer's Disease	Endothelial cell dysfunction caused by overproduction of ROS	[4, 26]
Aging	Increase in ROS production, decrease in overall antioxidant capacity	[4]
Macular Degeneration	Activation of ROS-generating enzymes (xanthine oxidase, nitric oxide synthesis) that lead to protein damage and lipid peroxidation	[27]

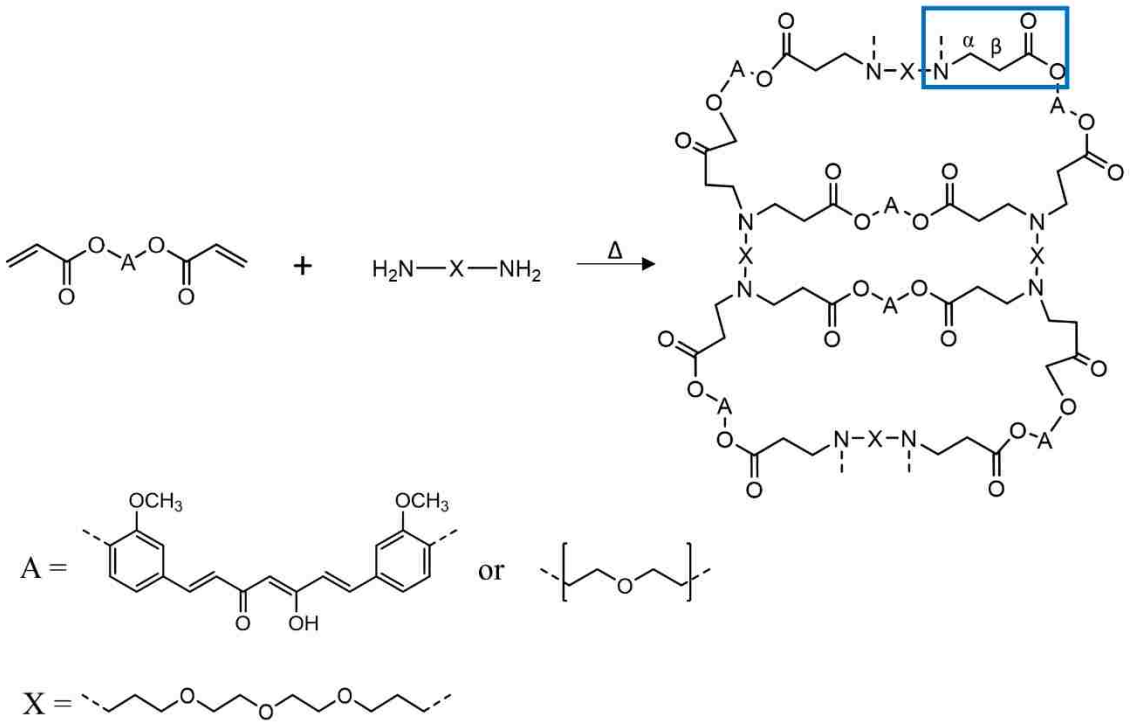

Figure 1-1: General synthesis of crosslinked poly(beta-amino ester) chemistry. (A) can either be the backbone of acrylated curcumin or poly(ethylene glycol) diacrylate, and (X) is the backbone of a primary diamine crosslinker 4,7,10-trioxa-1,13-tridecanediamine. The beta-amino ester bond is highlighted in the blue square.

Chapter 2 Background

2.1 Oxidative Stress

By 2030, worldwide cancer cases are projected to increase by 50% and affect up to 21 million people in the world [28]. Not only is there a increase in cancer cases, but cardiovascular disease, neurological disease, pulmonary dysfunction, and rheumatoid arthritis are also expected to increase with the growing adult population [4]. Although the primary damage of these diseases is targeted within specific organs of the body, a key underlying pathway is the exposure and overproduction of reactive oxygen species (ROS) or reactive nitrogen species (RNS). The imbalance of reactive oxygen species causes oxidative stress, resulting in cellular dysfunction and apoptosis, which leads to these chronic debilitating diseases [29]. ROS/RNS are characterized as chemically reactive species containing either oxygen or nitrogen; however, in constitutively low levels, they are an essential part of cellular signaling and biological regulation within a cellular environment. ROS generation can proceed from an external insult such as UV-radiation [30], cigarette smoke [31], or ingestion of pollutants [32], or can be a by-product of molecular reactions such as mitochondrial respiration [33].

2.1.1 Reactive Oxygen Species/Reactive Nitrogen Species Pathways of Oxidative Stress

Numerous pathways can generate ROS or RNS using intracellular oxidation or reduction [34] (**Figure 2-1**). Homeostatic environments demand a small concentration of these reactive species, which include oxygen containing radicals such as the superoxide anion ($O_2^{-\cdot}$), hydroxyl radical ($OH\cdot$), and the hydroperoxyl radical ($OH_2\cdot$). This class of

species also includes non-radical forming species including hydrogen peroxide (H_2O_2), hypochlorous acid (HOCl), and singlet oxygen [35].

Normal cellular metabolic function is derived off the biochemical oxidation/reduction (redox) reaction that generates reactive species as by products and is involved in cell signaling and activation pathways of a regulated cell [36]. Xanthine oxidase, a ROS generating enzyme, is a fundamental component of regulation. Xanthine oxidase oxidizes both xanthine and hypoxanthine to form uric acid [37]. Upon oxidation, superoxide anions are generated as side products, which can react with endogenous antioxidants such as manganese-superoxide dismutase (Mn-SOD) or copper/zinc superoxide dismutase (Cu,Zn-SOD) to form hydrogen peroxide (H_2O_2). The form of SOD is dependent upon the oxidation site (mitochondria vs. cytoplasm respectively). Another pathway dependent on ROS generating enzymes is when NADPH oxidase converts oxygen to superoxide anions, and with the help of sodium oxide dismutase, H_2O_2 is formed, which further converts to HOCl in the presence of myeloperoxidase, an important molecule with bactericidal properties to help neutrophils fight against microbial intrusion [38]. While hydrogen peroxide is not categorized as a free radical, its function as a radical intermediate plays a vital role in its ability to permeabilize through the lipid bilayer of a cell [39]. Fenton reactions can occur in the existence of hydrogen peroxide and iron, copper, or cobalt ions, and lead to the formation of the neutralized form of the hydroxyl radical [40], which in turn can react with fatty acids from the lipid bilayer and form a lipid radical which can further react with oxygen to cause lipid peroxidation.

2.1.2 Antioxidants

Oxidative stress can be lessened by regulating radical generation with antioxidants, which are comprised of enzymatic and nonenzymatic compounds. Nonenzymatic antioxidants work as an interruption of free radical chain reactions, where enzymatic antioxidants have the ability to break down free radicals present in the system continuously without being consumed [41]. Endogenous nonenzymatic antioxidants such as glutathione are used as cellular defense mechanisms to convert hydroxyl radicals and nitric oxide, where Coenzyme Q (CoQ), a lipid soluble antioxidant found in cellular membranes, lysosomes, and the mitochondria, functions as a protecting agent against lipid, protein, and DNA damage, and induces redox mechanisms and permeability of the cell [42]. Protein antioxidants, such as catalase and peroxidase proteins have the ability to convert hydrogen peroxide and hydroxyl radicals to stable products like water and oxygen [36, 43].

Exogenous antioxidant enzymes for antioxidant therapeutics are beneficial in that they scavenge millions of radical species before inactivity occurs; however, their scavenging capability is unique to specific radical species, are high in cost, and have stability issues [44]. Phytochemicals for antioxidant defense have become molecules of interest in pharmaceutical and cosmeceutical applications [45, 46]. Exogenous nonenzymatic antioxidants, also known as small molecule scavenger antioxidants, can be found in fruits, tea, coffee, and red wine [47]. Polyphenols are small molecule antioxidants and include curcumin[48], resveratrol[49], and quercetin[50] which are derived from turmeric, wine, and apple skins. Natural products can be introduced by ingestion or absorption through the skin or through mucosal barriers, and are consumed during radical-antioxidant interaction [51]. These antioxidants are consumed in stoichiometric

proportions by oxidizing species, and to counterbalance free radicals, a large dose is necessary to obtain balance in a diseased environment. There is risk of introducing high concentrations of antioxidants in to an environment, as antioxidants can have pro-oxidant effects at elevated levels and cause cytotoxicity [52-56] (**Figure 2-2**). This reiterates the necessity for sustained release of antioxidants over time to treat oxidative stress induced disease and will be demonstrated further in Chapter 3.

Not only do these polyphenols exhibit antioxidant properties, they also have been shown to have anti-inflammatory, anti-cancer, and anti-microbial properties, as well as chelating properties to reduce metal toxicity in humans[57, 58]. For instance, curcumin's anti-inflammatory properties were demonstrated by treating chondrocytes after IL-1β inflammatory pathways were stimulated. NF-κB activation was suppressed, which ultimately inhibited COX-2 and MMP-9 [59]. Another lab at Indian Institute of Technology showed suppression in toxicity of hypoxia induced ROS-mediated apoptosis. Lipid peroxidation, ROS production, and glutathione content were all suppressed after the treatment of free resveratrol was administered after oxygen-glucose deprivation [60].

2.2 Oral Mucositis

A specific disease that is promoted by the overproduction of reactive oxygen species is oral mucositis. Oral mucositis (OM) is a common, adverse side effect of anti-cancer therapies such as chemotherapy and radiotherapy [19, 61, 62]. 100% of head and neck cancer patients who receive fractionated radiotherapy develop severe ulcerations to the proximity of the mouth including lips, tongue, cheek, and throat [63, 64]. Ionizing radiation delivers high energy electrons using a linear accelerator, directed at the source of cancer for the inhibition of proliferative cancerous cells and ultimately apoptosis. Direct

radiation is caused by the intentional breakage of DNA strands within a cell, while indirect radiation is caused by the excitement of water molecules present in a cellular environment producing hydroxyl radicals. The reactive oxygen species present within the cell can cause a cascade of responses in the environment that lead to an imbalance of the free radicals and antioxidants present. The healthy tissue can be affected by these treatments as well, which employ a burst of reactive oxygen species, inhibiting normal cell regulation, which can cause cell mutation and death [18]. These treatments are utilized for enhanced patient quality of life and the termination of cancerous cells; however, the treatments result in detrimental and adverse side effects that can lead to death.

2.2.1 Clinical Pathology

For head and neck cancer patients, direct radiation damage to healthy epithelial tissue is challenging to inhibit. By the end of the first week of radiation, the mucosal lining of the oral cavity becomes inflamed. As the progression of OM continues, mucosal erosion begins to occur, and the development of ulcers proceed by the third week [16, 65]. These lesions are traumatically painful and can often lead to difficulty in eating and drinking. Pain is the leading impact on patients with mucositis, but some cases of severe oral mucositis can also lead to weight loss, the need of a feeding tube and hospitalization, and discontinuation of treatment. This leads to deterioration of the patient's quality of life and can result in enhanced risk of infection or pause patient treatment [62].

2.2.2 Oral Mucositis Development

Oral mucositis development can be broken down in to five stages [15] (**Figure 2-3)**. The healthy epithelium consists of proliferating basal cells with normal cell populations. In the first stage, the epithelium is exposed to radiation and a burst of reactive

oxygen species is released from the cellular environment (epithelial, endothelial, fibroblasts, and macrophages) occurring from indirect radiation, and DNA-damage occurs from direct radiation. This is known as the initiation step. Free radicals present after radiation include hydroxyl radicals, as well as superoxide anions. One study showed an increase in survival rates of mice that were given SOD before radiation over 30 days [66], converting superoxide anions present into hydrogen peroxide, which can be further broken down in to water by catalase. Increased pentose cycle activity, which produces NADPH oxidase, has also been reported minutes after radiation[36], showing additional superoxide anion generation. The hydrogen peroxide present can react with the directly linked myeloperoxidase generated in tissue during radiotherapy to form hypochlorous acid secreted by neutrophils [67], along with a buildup of nitric oxide formation catalyzed by NADPH oxidase and an amino acid, such as L-arginine, glutamine, or citrulline[68].

The second step in OM is the primary damage. Free radicals present activate secondary messengers and transmit signals to surface receptors of the cellular environment that can stimulate pro-inflammatory markers such as nuclear factor-kappa B (NF-κB), and other activator proteins such as activator protein-1 (AP-1) [69]. ROS generation can also initiate fibronectin damage and activate matrix metalloproteinases (MMPs), which can lead to apoptosis and tissue damage as well. This leads to a cascade of pro-inflammatory cytokine production, such as tumor necrosis factor (TNF), and promotes the production of ceramide synthase which results in cell apoptosis. The cascade continues and amplifies injury (Stage III), which ultimately leads to the formation of ulcers (Stage IV). During ulceration, the cellular membrane is disrupted and forms lesions that lead to enhanced cytokine production and inflammation. This is where the infiltration of bacteria can occur,

and if not treated properly, severe cases can lead to sepsis and fatality. As the environment regains integrity, the extracellular matrix initiates signal (Stage V) to induce proliferation of epithelial and endothelial cells and the network is resolved [3, 64].

2.2.3 Current Treatments

Management of radiation-induced OM can be categorized into pain control, nutritional support, oral decontamination, palliation of dry mouth, management of bleeding, and therapeutic interventions [70]. Currently, there is no single US-FDA approved treatment for the general treatment of oral mucositis, but many treatments are used in preclinical and clinical studies on patients in attempt to alleviate pain and severity of symptoms. One FDA approved drug on the market is a recombinant human keratinocyte growth factor, Palifermin, which decreases the incidence and duration of severe oral mucositis by protecting and promoting epithelial growth. Unfortunately, it is selectively used in patients with hematological cancers, as keratinocyte growth factors could promote cancer cell growth in patients other than bone cancer[71]. Treatments specifically for radiation-induced oral mucositis include localized topical agents that have mucoadhesive, analgesic, and antimicrobial properties[72]. Viscous lidocaine is widely recommended for alleviation of localized pain. Oral narcotics are used to treat pain symptoms, and oral rinses, such as Mugard®, a 510(k) cleared medical device, have shown to reduce severity of symptoms [73]. Turmeric rinses also have been studied as a preventative and ameliorative treatment in radiation-induced oral mucositis. In one study, patients were asked to rinse with 10 mL of 5 mg/mL turmeric water for 2 minutes at a time, which included 4 rinses per time point, 6 times per day [74]. The highly involved regimen is due to low percentages

by weight of curcumin in turmeric (0.3-5.4%) as well as its low absorption and bioavailability[75].

The current treatments on the market today require several applications or rinses at one time and results in low patient compliance. This also requires the purchase of significant amounts of materials and ultimately leads to expensive medical bills, estimating that patients spend up to $17,000-$22,500 or more on remedies after OM is diagnosed in patients undergoing treatment [3, 76].

2.3 Polymeric Drug Delivery Systems

Natural and synthetic polymers have been used in delivery of therapeutics to deliver drugs to vascular[77], gastrointestinal[78], ocular[79], vaginal[80], and dermal[81] sites. Depending on the desired site of delivery, these can be designed in the form of oral tablets, microparticles, nanoparticles, or implantable devices, all which can be synthesized into various geometries and sizes for optimal delivery[8, 82]. These can include polymeric nanocarriers such as spherical micelles, ellipsoidal disks, and rods. Polymers are not only used as the foundation of drug delivery carriers, but are also commonly used as excipients to form amorphous solid dispersions (ASD) to enhance drug solubility in formulations [83]. Polymeric drug delivery design is used to achieve (1) controlled drug release, (2) site specific delivery without rapid clearance from the body, and (3) enhanced bioavailability. While designing polymeric systems, it is also important to select biomaterials that are non-cytotoxic as biomaterials, as well as remain non-cytotoxic if degradable. Synthetic polymers include poly(ethylene glycol) (PEG), poly(acrylamide) and poly(N-vinyl pyrrolidone), while polysaccharide-based natural polymers such as chitosan and alginate are also commonly used[84].

2.3.1 Hydrogels

Hydrogels are three-dimensional crosslinked polymer networks that can incorporate hydrophobic and hydrophilic monomers which allow for swelling in many solvent and aqueous systems. They are widely used in tissue engineering and regenerative medicine due to their appealing physical properties. The hydrophilic nature of hydrogels make them great biocompatible candidates, as well as their mechanical integrity. Dependent on the selection of starting material, hydrogels can have high mechanical integrities and glass transition temperatures[85]. These durable hydrogels can be used as bone or cartilage scaffolds, whereas hydrogels with lower glass transition temperatures remain in a rubbery state and can easily conform and adapt to abnormal spaces or wounds for topical healing-based platforms. These properties are all based on the selection of biomaterials used in synthesis. The porous matrix of hydrogels also provides excellent loading spaces for drugs. These encapsulated drugs undergo diffusion-based release and are dependent solely on the diffusion coefficient of the drug through the gel network. This also causes limitations when used as a controlled release drug delivery system where homogeneity of drug incorporation in to a network could be complicated and the pharmacokinetics are limited by the drug-network interaction driving force rather than a dependence on the environment.

Hydrogels can be formed by physical crosslinks or chemical crosslinks [86]. In physical crosslinks, hydrogen bonding or ionic interaction can allow for polymers to form complexes. Many physically crosslinked hydrogels, such as poly(acrylic acid) and poly(methacrylic acid) complexed with poly(ethylene glycol) absorb liquid and swell at low pH based on the protonation of groups present [87]. Monomers such as

poly(urethanes), and poly(esters) can be chemically conjugated in to nondegradable or degradable networks by capping the ends with functional groups[88, 89]. Nondegradable crosslinked networks can be formed by UV-polymerization, gamma and electron beam polymerization, or thermal initiated free radical polymerization with acrylate capped monomers[86, 90]. Nondegradable crosslinked networks can encapsulate free drug in to the network, and upon stimulated response, swell and release drugs via diffusion (**Figure 2-4A**). Degradable crosslinked networks can be formed using Michael Addition chemistry by conjugating acrylate-amine, or amine-thiol functional groups and result in hydrolytically degradable bonds [91-93] or through Stagelich esterification and result in enzymatically degradable bonds[94]. Drugs can be modified and conjugated in to the network [11]. Upon stimulated response, hydrolysis in this case, the hydrogel will degrade labile bonds and the free drug will be released over time (**Figure 2-4B**).

2.3.2 Stimuli-Triggered Response of Drug Delivery Systems

Recently, the design of drug delivery systems that respond to chemical or physical stimuli are used to regulate or trigger drug release. Stimuli can include temperature, pH, ROS, light, or mechanical stress. Materials can have a reversible response to stimuli, or an irreversible response where chemical bonds are broken, or oxidation occurs [95]. The stimuli present in a diseased environment can include an increase in ROS concentration, pH-changes, and irregular biochemical upregulation. Materials that incorporate or encapsulate drugs can be tailored with groups sensitive to these environments to design optimal delivery that can trigger degradation, and enhanced swelling ultimately using the environment to obtain sustained release of a drug.

2.3.2.1 Thermoresponsive Polymers

Thermoresponsive polymers have swelling/collapsing capabilities based on the material's lower critical solution temperature (LCST) or upper critical solution temperature (UCST), which are the temperature points below and above the state in which the polymer and solvent are miscible[96]. Poly(N-isopropylacrylamide) is a common polymer used in biomedical applications as its LCST is close to body temperature (32°C) [97]. This polymer content can be varied with hydrophobic comonomers to tune and shift to lower LCSTs [98]. One specific biomedical application for thermoresponsive polymers are injectables that are delivered as a liquid to the body, and once exposed to physiological temperatures form semi-solid drug depots [99]. These thermo-gelling materials can be designed as using chitosan-based mucoadhesive drug carriers for ocular diseases and intranasal delivery[100].

2.3.2.2 pH-Responsive Polymers

Many chemotherapeutic nanocarriers use the acidic environment found intracellularly and within the leaky vasculature of tumors [101], where polymers can be triggered to degrade or release in acidic environments[102]. Other pH-responsive materials are utilized for non-viral nucleic acid delivery where the degradation of designed poly(beta-amino ester) and other poly(esters) remain stable at neutral pH and then rapidly degrade after being internalized in to low pH environments[103].

2.3.2.3 ROS-Responsive Polymers

ROS-induced degradation and solubility is another important stimulated response for drug release and degradation of biomaterials. In an excellent review on the progression of ROS-responsive materials, Sung et al. classified poly(propylene) sulfides, and co-block

polymers containing selenium undergo oxidative cleavage and enhance release of drug in the presence of super oxide anions, peroxynitrate anions, and H_2O_2. This mechanism is based on redox changes in the backbone of the polymer that increase solubility of the materials during phase change [104]. Materials that undergo ROS-induced degradation by H_2O_2 and superoxide anions include boronic esters, silicon, proline oligomers, and poly(thioketals). Poly(beta-amino ester) crosslinked network's inherent property is the hydrolytically degradable ester bond formed through Michael Addition chemistry; however, it was discovered that this network is also susceptible to accelerated degradation in the presence of hydrogen peroxide, with dependence on the antioxidant loading in the polymer. This phenomenon is discussed in detail in Chapter 5.

2.4 Polyphenolic Antioxidant Drug Delivery Systems

The promising effect of polyphenolic antioxidants for drug therapy has been documented for decades, but their hydrophobicity and reactivity continue to limit the impact on human pharmaceuticals [105]. Antioxidants such as curcumin and resveratrol have become molecules of interested in the treatment for stroke related injuries and renal failure due to their high antioxidant and anti-inflammatory potential [106], but the translation of free active polyphenol therapies is unsuccessful and tends to fail when translated into clinical trials[107]. A promising solution to delivering small hydrophobic antioxidant molecules is to encapsulate them in a delivery vehicle to provide protection and allow for the drug to remain active until the target site is reached. For the use of antioxidant therapies for delivery to vital organs, the delivery vehicle can be found in the form of nanoparticles for target specificity, which can easily be internalized by cells. This has been previously shown in literature using grape seed extract loaded chitosan and

hyaluronic acid nanoparticles to reduce oxidative stress in endothelial progenitor cells that were exposed to a hydrogen peroxide insult [108]. Other studies have shown photothermal-responsive rotaxane-functionalized mesoporous silica nanoparticles that upon light and heat, tethered rotaxane gates are switched and curcumin is able to diffuse out in to the site of delivery [109].

While these applications are promising, they still risk premature release or degradation of the active drug, as well as additional materials necessary for clearance and noncytotoxic effects. Antioxidant polymers can be incorporated into the backbone of polymer networks to overcome these potential limitations and are advantageous as they have tunable properties based on the selection of the starting material. Since the drug itself makes up the backbone of the drug delivery system, it has high weight loading of drug compared to other polymeric-encapsulated systems where the payload is low compared to the material that is carrying it. Controlled release of antioxidants using PBAE chemistry can not only be in the form of bulk films (**Chapters 4 and 5**), but can be in a multitude of geometries including microparticles (**Chapter 3 and 6**), and nanogels [110]. As the development and control of the reaction conditions and purification of the acrylated actives are better understood, this drug delivery mechanism can progress to linear PBAE polymers, and the applications can expand further in to areas such as aerosols, and surface coatings.

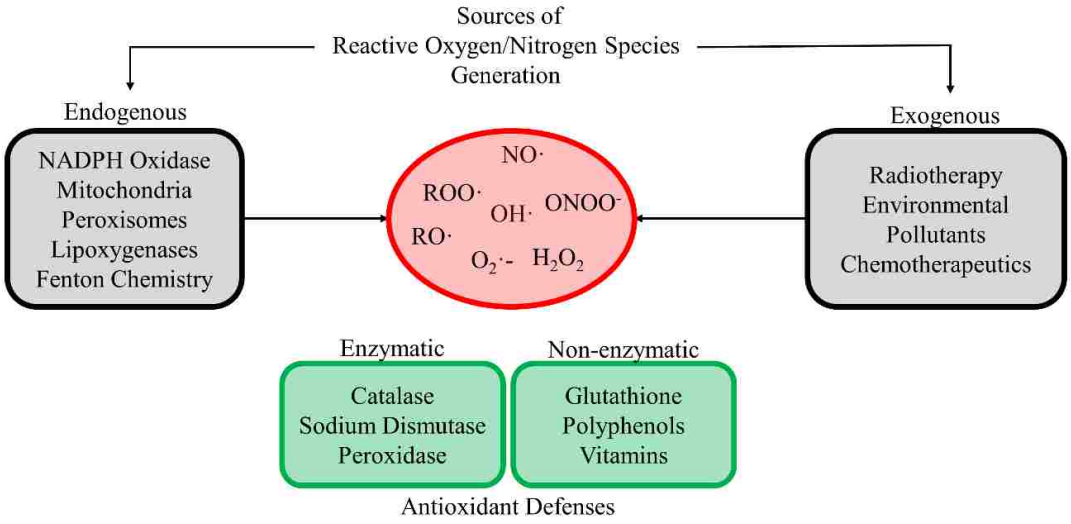

Figure 2-1: Endogenous and exogenous sources of reactive oxygen and nitrogen species (ROS/RNS) and the enzymatic and non-enzymatic antioxidant defenses to maintain homeostasis.

NO·: Nitric Oxide, ROO·: Peroxyl Radical, RO·: Alkoxyl radical, O_2^{-}·: Superoxide Anion, H_2O_2: hydrogen peroxide, $ONOO^-$: peroxynitrate, OH·: Hydroxyl radical

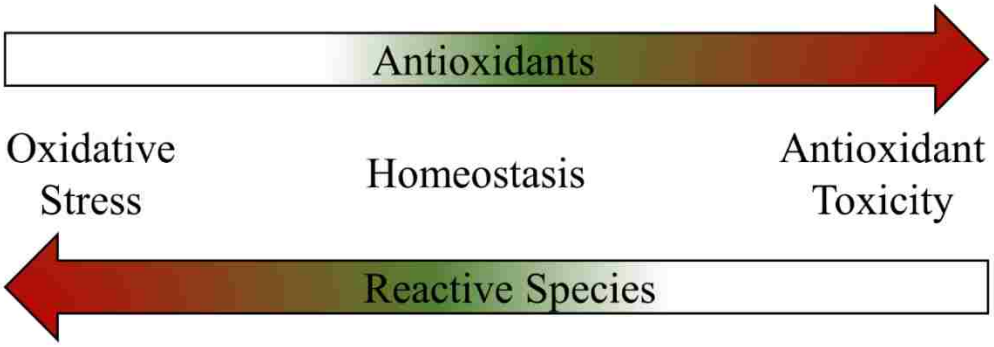

Figure 2-2: Schematic demonstrating effects of overproduction of reactive species or antioxidant in a cellular environment.

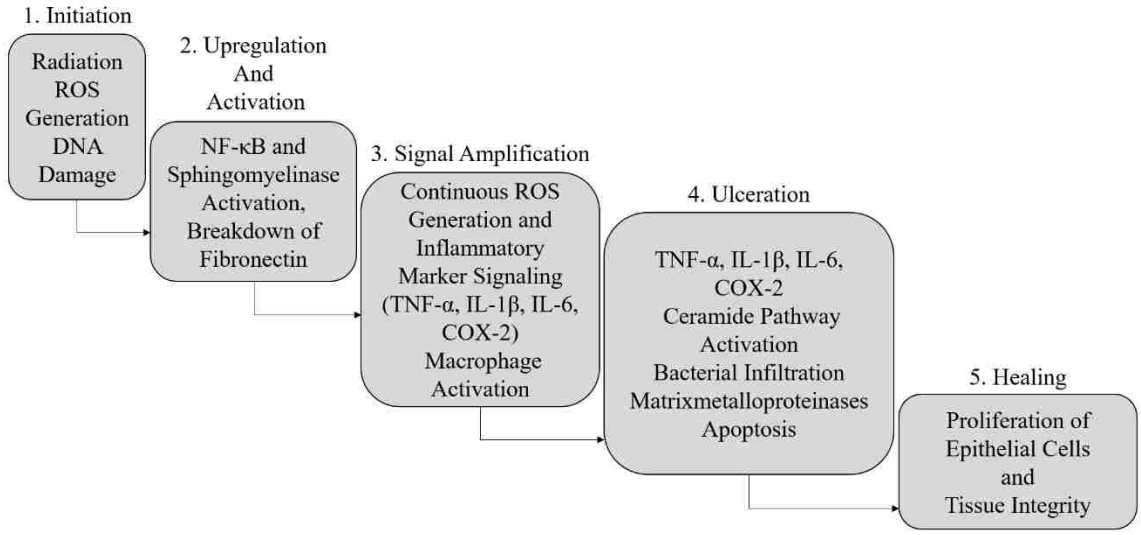

Figure 2-3: The five stages of oral mucositis development.

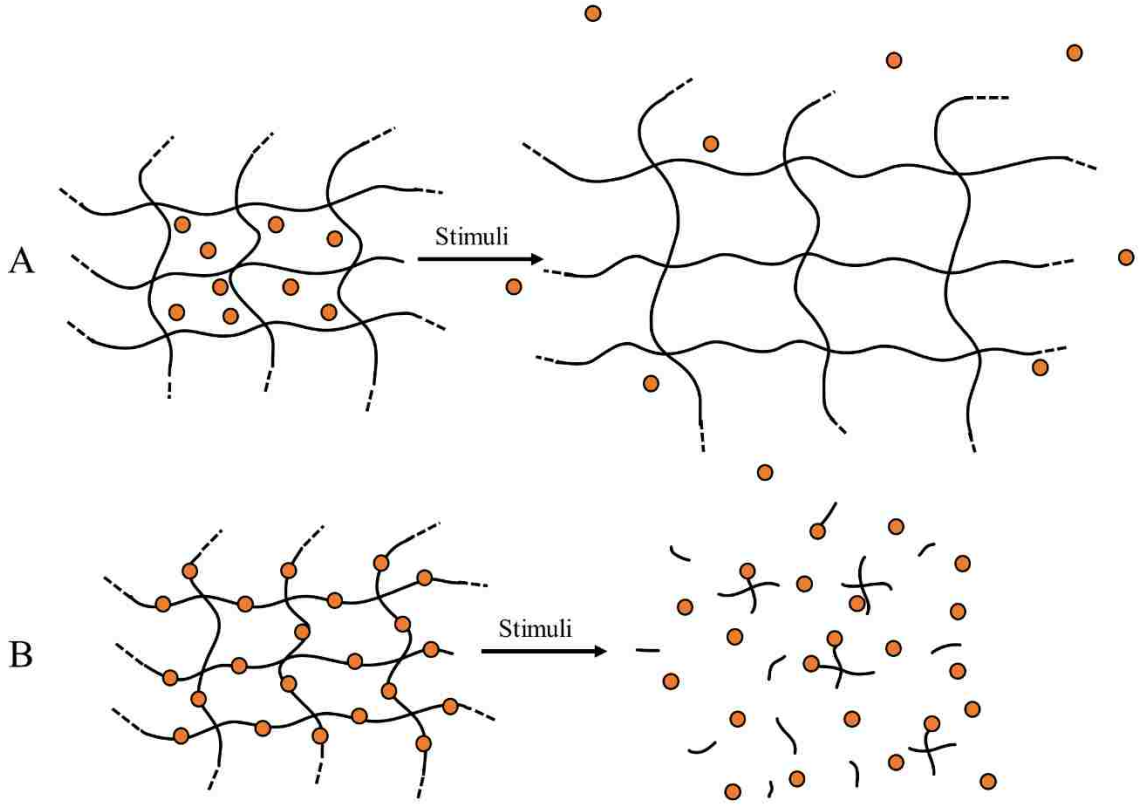

Figure 2-4: Schematic for drug release out of a nondegradable polymeric network due to stimuli-responsive swelling (A), and drug release out of a degradable polymeric network where the drug is conjugated into the network and is released upon stimuli-responsive hydrolysis.

Chapter 3 Modeling the Oxidative Consumption of Curcumin from Controlled Released Poly(beta-amino ester) Microparticles in the Presence of a Free Radical Generating System

3.1 Introduction

The cytosolic balance between reactive oxygen species and antioxidants is essential to the physiological health of a cell [38]. However, under a variety of pathophysiological conditions (e.g., radiation injury [15], inflammation [111], acute lung injury [112]), cells are no longer able to maintain this balance, resulting in an accumulation of free radicals, defined as oxidative stress [113].

Oral mucositis, an adverse side effect of head and neck cancer radiotherapy, is one of many specific examples of the potentially debilitating effect that oxidative stress can induce [70]. The exposure of healthy epithelial tissue to ionizing radiation initiates breaks in the DNA and inhibits rapid replication of cells in the submucosa. Water molecules found within the cell can also interact with electrons and upon interaction, form hydroxyl radicals [15, 64, 65]. This interferes with the intracellular regulation, leading to the formation of superoxide anions. These free radicals are linked to a specific inflammasome, NRLP1, that activates pro-inflammatory cytokines, such as IL-1β [114]. These secondary messengers transmit signals to stimulate pro-inflammatory markers such a nuclear factor-kappa B (NF-κB), and activator proteins, such as activator protein-1 [69]. The activation and upregulation of these receptors cause fibronectin damage and activate matrix metalloproteinases (MMPs), which leads to apoptosis and cell death [18]. These detrimental cell signaling cascades continue to inhibit proliferation of healthy epithelial

cells, which ultimately lead to the formation of severe ulcers within the oral cavity [65]. Despite the prevalence of this disorder, there exists few treatments other than palifermin, a keratinocyte growth factor. Although palifermin has been shown to reduce onset and severity of OM, it is a therapeutic limited to only patients with hematologic malignancies [71]. Temporary treatments such as topical anesthetics and analgesics are implemented during prognosis [70]. However, a universal drug to scavenge free radicals and reduce the onset of oral mucositis for all patients does not exist and is in high demand.

Curcumin, a potent antioxidant, has been a promising candidate for the control of inflammation and serves as a free radical scavenger [115]. However, up to now, no double-blinded, placebo controlled clinical trial of curcumin has shown a positive benefit [107]. Due to curcumin's hydrophobicity and severe sensitivity to oxygen and light, a controlled delivery system to release curcumin successfully as a therapeutic agent in oxidative stress-induced diseases is of critical need. Recent literature, such as Pauli et al., expresses concern on the use of curcumin as a successful nutraceutical with the countless failures in translational attempts from lab bench to person [107]. Treatments using excessive amounts of free curcumin have been reported to obtain minimal absorption in serum levels, which not only highlights the failure as a free molecule but risks toxicity, due to high localized concentrations of antioxidant at the site of delivery [54]. The high promise for curcumin, yet consistent failure, has made even high impact journals endorse the skepticism of curcumin [107]. The ability to understand and even predict the interaction between a delivered antioxidant and a free radical promotes the design of a mathematical kinetic rate model that describes the rate of consumption and radical scavenging ability. With this

method of design, it is highly promising in the development of a delivery system that will be consistently successful in treatment.

An innovative delivery system, curcumin conjugated poly(beta-amino ester) (PBAE) polymer networks, has been developed previously in the Dziubla and Hilt laboratories at the University of Kentucky to enhance curcumin's stability, solubility, and resistance to aggregation—all problematic attributes presented with curcumin as a free drug [116]. The incorporation of curcumin into the backbone of a hydrolytically degradable crosslinked hydrogel can eliminate the concern of curcumin's pitfalls and allow for a tunable network with high drug loading capacity that also provides protection to the agent until released. These degradable hydrogels, which can be prepared in a multitude of forms (e.g. films, microparticles, and nanoparticles), have been studied on the synthesis, swelling and degradation properties in controlled temperature PBS environments [11], as well as the dynamic mechanical analysis of different network compositions [116]. They have successfully prolonged suppression of oxidative stress in cells [11] as well as inhibited H_2O_2 induced mitochondrial oxidative stress [110].

Controlled release systems are beneficial in that they are able to provide a constant therapeutic concentration of drug in a system for a controlled period of time [117]. Specific for antioxidant delivery, knowledge of consumption rates of active curcumin released from microparticle systems can provide insight in dosing and treatment regimens to unique oxidative environments to maintain a regulated environment [52]. Kinetic modeling can be used to model curcumin conjugated PBAE microparticles to verify the consumption rates of active curcumin and degradation products in the presence of free radicals. We

hypothesize that curcumin released from microparticles of different compositions will be consumed based on the concentration of free radicals present and rate of drug release.

In this chapter, we report on the consumption of curcumin as a free molecule and the degradation product release and consumption profile from three controlled release curcumin conjugated PBAE microparticle systems. Two concentrations of 2,2-azobis(2-amidinopropane) dihydrochloride (AAPH) solution were used *in vitro* as a test oxidative environment due to its ability to degrade into alkyl radicals when introduced to temperatures of 37°C.

Studies quantifying curcumin degradation in an oxidative environment were utilized to develop a set of mathematical expressions to describe the oxidative consumption rates of both curcumin as a free molecule and curcumin and its residual degradation product, curcumin monoacrylate, after it has been released from the PBAE crosslinked network. The rate constants of consumption can be used to model theoretical curcumin levels over time and change in concentration of reactive oxygen species in an environment. The model also demonstrates the benefit of controlled release versus single dose delivery methods and the effect both delivery methods have on the theoretical baseline levels of reactive oxygen species that are necessary in a regulated cellular environment.

3.2 Materials and Methods

3.2.1 Materials

Curcumin was purchased from Chem-Impex International, Inc. (Wood Dale, IL). 4,7,10-Trioxatridecane-1,13-diamine, Tween 80, and 2,2'-azobis(2-amidinopropane) dihydrochloride, triethylamine, and acryloyl chloride were purchased from Sigma Aldrich (St. Louis). Poly(ethylene glycol) diacrylate, MW 400, was obtained from Polysciences

Inc. (Philadelphia, PA). Dichloromethane, tetrahydrofuran and acetonitrile were purchased from Pharmco-Aaper (Brookfield, CT). No additional purification steps were conducted after materials were received.

3.2.2 Curcumin Conjugated Poly(beta-amino ester) (PBAE) Microparticle Synthesis

Curcumin multiacrylate was prepared using an acid chloride-alcohol esterification reaction, as described in Patil et al[118]. Briefly, curcumin and acryloyl chloride were reacted in a 1:3 molar ratio in anhydrous THF in the presence of triethylamine for 24 hours in the dark to comprise a curcumin multiacrylate system of 45% curcumin diacrylate, 55% curcumin triacrylate, and 0.9% curcumin monoacrylate.

PBAE films were synthesized as previously stated in Patil et al [116] and the reaction schematic can be found in **Figure 1-1**. Curcumin multiacrylate and poly(ethylene glycol) diacrylate (MW 400) (PEG(400)DA) were reacted with a diamine crosslinker, 4,7,10-trioxatridecane-1,13-diamine, at a ratio of total acrylates to amine protons of 1.0 (RTAAP = 1.0) with two different compositions (26 wt% curcumin and 32 wt% curcumin loading). Upon Michael addition, crosslinked poly(beta-amino ester) bonds were formed. 1.5 times the total monomer mass of the film of anhydrous dichloromethane was used as the reaction medium. Curcumin was dissolved in half of the anhydrous dichloromethane (aDCM). PEG(400)DA was dissolved in a separate centrifuge tube with the remaining amount of aDCM. TTD was added to the PEG(400)DA/DCM solution and vortexed immediately. After 5 minutes of reaction time on the bench top at room temperature, the PEG(400)DA/TTD solution was vortexed while CMA was added dropwise quickly and the pre-polymer solution was immediately poured into casting ring on aluminum covered glass

plates and left at room temperature for 1 hour. The film was then transferred to 50°C convection oven for 24 hours to complete the reaction and evaporate excess solvent.

Crosslinked films of 0.4 mm thickness were washed with anhydrous acetonitrile (5 times) to remove any unreacted monomers. Films were placed under vacuum at 50°C overnight to complete drying. Microparticles were obtained by cutting the film into small pieces and placed into a milling tube with 1 wt% magnesium stearate as a lubricant. Using a 6775 Freezer/Mill Cryogenic Grinder, the film was milled for 10 minutes at 15 cycles per second CPS (max), with a pre-cool and post cool setting of 3 minutes. Microparticles were left on the bench top until the tube reached room temperature to prevent any moisture from condensing in to tube. Microparticles were then collected and dried overnight on a lyophilizer to remove any excess moisture and stored in -20°C conditions in a sealed bag with desiccator pack until future use.

3.2.3 Free Curcumin Stability and Consumption in the Presence of AAPH

Curcumin was dissolved at 80 mg/mL in anhydrous DMSO (aDMSO) and 6.25 µL was added under constant vortexing to a 10 mL 0.1% (w/v) Tween 80 phosphate buffered saline (PBS) (pH 7.4) solution to reach a final concentration of 50 µg/mL curcumin. Periodic samples were collected and read at 420 nm using a Cary 50 UV-Vis Microplate Reader spectroscopy instrument to monitor absorbance of solution over 24 hours. Curcumin of the same concentration was also introduced to a 10 mM AAPH and 100 mM AAPH 0.1 w/v% Tween 80 PBS solution and periodic samples were collected and read directly at 420 nm.

3.2.4 Microparticle Degradation Profiles in the Presence of AAPH

Microparticle systems were degraded in a 0.1% (w/v) Tween 80 PBS (pH 7.4) solution, 10 mM AAPH/0.1 w/v% Tween 80 PBS (pH 7.4) or a 100 mM AAPH/0.1 w/v% Tween 80 PBS (pH 7.4) solution for over 24 hours at the same theoretical final release concentration of curcumin. 1 mL samples of the supernatant of the control were collected every two hours and analyzed under UV-Visible Spectroscopy. The volume was replenished after each time point. Independent samples for each time point were prepared for the microparticle release in AAPH solution so the concentration of free radicals to curcumin ratio was consistent throughout the 24-hour study.

3.2.5 Microparticle Degradation Product Consumption in the Presence of AAPH

Microparticles were fully degraded in a 0.1% (w/v) Tween 80 PBS solution at pH 7.4. AAPH was added to the degradation products to a concentration of either 10 or 100 mM and analyzed directly over time using reverse-phase HPLC (Water Phenomenex C18 column, 5 μm, 250 mm (length) x 4.6 mm (ID) on a Shimadzu Prominence LC-20 AB HPLC system attached to a Waters Refractive Index Detector) at 420 nm to analyze curcumin and residual acrylated curcumin peaks over time in the presence of AAPH.

3.2.6 Kinetic Rate Model Development

3.2.6.1 Oxidative Consumption Rate of Curcumin

Based on the experimental data collected regarding the consumption profiles of curcumin as a free molecule, a kinetic rate model was developed to describe the oxidative consumption of curcumin. Observing the interactions between three main components in solution (AAPH, free radicals produced, and curcumin) using a first principles approach, a

set of rate equations were established. It was assumed that curcumin consumption was solely dependent on the interaction with the radical formed by thermal decomposition.

In an AAPH solution, the compound can thermally decompose into either alkyl radicals or peroxyl radicals in the presence of molecular oxygen:

$$AAPH \xrightarrow{\Delta} 2R\cdot \xrightarrow{O_2} 2ROO\cdot \quad (1)$$

It is assumed that radicals are generated upon thermal decomposition of AAPH. As such, a first order rate was assumed ($k_A = 1.26x10^{-6}\ min^{-1}$) based on Werber et al [119], and can be expressed in the following equation:

$$\frac{dC_A}{dt} = -k_A C_A \quad (2)$$

Where C_A is the concentration of AAPH. The thermal decomposition of AAPH produces 2 molecules of radicals for every 1 molecule of AAPH. Based on the instability of general alkyl/peroxyl radicals, the fast half-life and elimination of the free radicals produced are on the order of 1 millisecond [120], which is assumed to be first order ($k_{el} = 4.16x10^{4}\ min^{-1}$). In an AAPH solution, the concentration of free radicals present can be simplified as:

$$\frac{dC_R}{dt} = 2k_A C_R - k_{el} C_R \quad (3)$$

Where C_R is the concentration of free radicals. The change in curcumin concentration is dependent on both the concentration of curcumin and free radicals present over time:

$$\frac{dC_C}{dt} = -k_C C_C C_R \qquad (4)$$

Where C_C is the concentration of curcumin in solution. In the presence of curcumin, equation (3) can be modified to incorporate the dependence of free radical concentration on the interaction with curcumin present.

$$\frac{dC_R}{dt} = 2k_A C_R - k_{el} C_R - k_C C_C C_R \qquad (3a)$$

3.2.6.2 Oxidative Consumption Rates of Curcumin and Curcumin Monoacrylate Released from the Microparticle Network

To better model the consumption rate parameters of the released curcumin (k_c) and curcumin monoacrylate (k_{CM}) from microparticles, an additional equation, dependent on the free radical concentration, was added to describe the change in concentration of curcumin monoacrylate in the system over time:

$$\frac{dC_{CM}}{dt} = -k_{CM} C_R C_{CM} \qquad (5)$$

The free radical concentration is then also dependent on the concentration of curcumin monoacrylate modifying Equation (3a) to the following:

$$\frac{dC_R}{dt} = 2k_A C_R - k_{el} C_R - k_C C_C C_R - k_{CM} C_{CM} C_R \qquad (3b)$$

The set of mathematical expressions for the free molecule and degradation products were solved simultaneously using ODE15s in MATLAB while the unknown consumption rate parameters were minimized over the experimental data by sum of squared errors (fminsearch). These parameters were then used to find consumption rate parameters of

curcumin monoacrylate within the solution from the fully degraded microparticle system and the correlation factor was calculated to evaluate the degree of fit.

3.2.7 Demonstration of Controlled Release Antioxidant Delivery

Six zero order rates of curcumin release were investigated and compared to a one-time bolus of the equivalent amount of curcumin over 1440 minutes. The specified rate was added to the curcumin concentration equation (4) as follows:

$$\frac{dC_C}{dt} = specified\ rate - k_C C_C C_R \quad (4a)$$

For one-time delivery treatments, AAPH initial concentration was kept at 10 mM and the only information modified in the model was the initial concentration of curcumin present.

3.3 Results and Discussion

3.3.1 Poly(curcumin) Microparticle Synthesis

After poly(curcumin) films (**Figure 3-1A**) were successfully synthesized and cryomilled (**Figure 3-1B**), a Size Analyzer (Shimadzu SALD-7101) utilizing ultraviolet laser diffraction was used to measure size. Size distribution of particles were 25-100 μm (**Figure 3-1C**). Degradation studies of the two systems individually and blended at a 50:50 ratio of 26 and 32 wt% curcumin were conducted in a 0.1% (w/v) Tween 80 PBS (pH 7.4) solution to quantify the cumulative release of curcumin over time (**Figure 3-1D)**. Curcumin release was monitored using an ultra-violet visible spectroscopy at curcumin's maximum absorbance wavelength of 420 nm. Upon introduction of PBAE microparticles to a 0.1% (w/v) Tween 80 PBS solution, base-catalyzed hydrolysis occurred and the ester bond was cleaved by a nucleophilic attack from a water group present; however, the rate of hydrolysis

was dependent on the degree of hydrophobicity of the polymer backbone. As hydrophobicity increased, the rate of release decreased, slowing the curcumin release rate. The 26 wt% loaded curcumin microparticles, with a higher incorporation of the hydrophilic co-monomer, PEG400DA, released curcumin over 8 hours until the absorbance values plateaued. When incorporating a higher molar ratio of curcumin multiacrylate:PEG400DA in to the backbone of the network, the rate of release was extended over a 12 hour period. For each bulk film system, there was a point at which the integrity of the film is lost and a burst release can be observed. Due to the increase in surface area of the microparticle system, the burst release phenomenon was minimized and the release profile appears more linear compared to bulk film degradation (as seen in **Chapter 4**). To form a constant release, the 26 wt% and 32 wt% loaded curcumin microparticles were blended at a 50:50 ratio. By incorporating the 26 wt% microparticle system and the 32 wt% microparticle system, the faster release from more hydrophilic particles took place initially and the slower rate of release dominated after 6 hours, taking on a constant rate of release with an $R^2 = 0.98$ when comparing to a constant slope trendline (**Figure 3-1D**).

3.3.2 Consumption Profiles of Curcumin

The absorbance of a 50 μg/mL curcumin solution in 0.1% (w/v) Tween 80 PBS (pH 7.4) was monitored to evaluate curcumin stability at 37°C (**Figure 3-2A**). As shown, there was no significant change in absorbance, as well as no precipitation in solution, suggesting that curcumin was stable for over 24 hours in aqueous solution. However, when in the presence of AAPH, curcumin's absorbance profile dramatically changed over time. As free radicals are generated, curcumin protons are abstracted leading to destabilization of the molecule and degradation of curcumin. As curcumin degrades, it loses its

characteristic absorbance at 420 nm. The rate of curcumin consumption was correlated to the initial concentration of AAPH in solution. 10 mM AAPH solution results in 90% of curcumin consumed within the first 8 hours, whereas 100 mM AAPH solution results in 90% of curcumin consumed within the first hour.

The three forms of curcumin (curcumin, curcumin demethoxycurcumin, and bisdemethoxycurcumin) were consumed in order of antioxidant activity [48], being that the curcumin peak diminished at a faster rate than demethoxycurcumin, and bisdemethoxycurcumin (**Figure 3-3**). Overall, curcumin appeared to be highly susceptible to depletion in AAPH solutions at all times as its hydroxyl sites on each curcuminoid were always exposed free in solution.

3.3.3 Microparticle Degradation Profiles in the Presence of AAPH

26 wt% curcumin loaded PBAE MPs were introduced to both 10 and 100 mM AAPH 0.1% (w/v) Tween 80 PBS solutions at pH 7.4 in a 37°C agitating shaker bath (**Figure 3-2B**). The profile of the microparticle release in the presence of AAPH changed significantly compared to the release profile with 0 mM AAPH. Incorporating curcumin in to the backbone of PBAE crosslinked network provided protection from oxidation until released from the network. As the network hydrolytically degraded and released intact curcumin, its exposed protons were able to be abstracted from the free radicals present. As curcumin was released, it was also consumed at a rate in which it is interacting with the free radical. Once the curcumin was released in its entirety and the microparticles are fully degraded after 8 hours, the residual curcumin released into solution began to be consumed; however, the rate of consumption appeared to be slower compared to free curcumin and after 24 hours there was still curcumin present based on absorbance. The controlled release

of curcumin allowed for sustained concentrations of curcumin over an extended period of time compared to the exponential consumption seen of curcumin as a free drug.

32 wt% curcumin loaded PBAE MP was also introduced to AAPH (**Figure 3-2C**). Initially less curcumin was recovered in the system, due to its slower release rate. The time at which the maximum amount of curcumin in solution was observed with AAPH changed, where 40% of the absorbance was retained from the first 8 hours in the 26 wt% MP to 12 hours in the 32 wt% MP system. Again, after all the curcumin was released, the absorbance started to decrease as the free curcumin in solution was consumed, but likewise to the other system, 10% of the absorbance remained even after 24 hours. Similar trends were seen at high concentrations of AAPH for both 26 and 32 wt% MP networks; however, the peak absorbance recovery was shifted by 2 hours, the overall recovery is lower, and all the colorimetric products were consumed by 24 hours. For 100 mM AAPH, no color absorbance was seen after 12 hours and 20 hours respectively.

In efforts to extend curcumin in solution, the 50:50 MP blend was evaluated as well (**Figure 3-2D**). Within the first 8 hours, 42% of recovery was obtained from the microparticle system; however, due to the extended release contribution from the 32 wt% microparticles in solution, the recovery at 40% was held constant between 8 and 10 hours, before absorbance decreased. Similarly, the blend in the presence of the 100 mM AAPH was consumed at a faster rate, but also had a constant recovery of 15% for 2 hours before it began to be consumed over the remaining 18 hours. When free curcumin was observed in the presence of 10 mM AAPH and 100 mM AAPH, the amount of curcumin decreased to 20% after 4 hours and 20 minutes respectively. For the controlled release mechanisms, curcumin sustained recovery above 20% for up to 16 hours out of the 24 hour duration.

For the 100 mM AAPH solution, the recovery of curcumin was highest in 26 wt% as the rate of release of curcumin dominates the generation of radicals that would consume the active component over time. The slower release rate of the 32 wt% microparticles provided a slow enough rate to allow for consistent consumption of curcumin over time, where curcumin recovery levels were low throughout the entire duration of release.

Due to the residual absorbance retained at 24 hours in all release curves interacting with 10 mM AAPH (**Figure 3-2B-2D**) and the change in extent of consumption after the microparticles were fully degraded, HPLC analysis was used to verify the degradation products present after the microparticle system had been completely degraded. After running the supernatant of a fully degraded microparticle system via HPLC, all three forms of curcumin (curcumin, demethoxycurcumin, and bisdemethoxycurcumin) peaks were observed in **Figure 3-4A** at an elution time of 5-6.5 minutes; however, residual curcumin monoacrylate peaks at elution times between 8-9 minutes were observed as well, verified by a curcumin multiacrylate standard. The residual acrylates found in the supernatant could be a result of the curcumin triacrylate group being unable to fully crosslink at all three sites due to steric hindrance of the curcumin molecule during film synthesis. This would allow for hydrolysis to retain 2 hydroxyl groups, but leave a residual unreacted acrylate group on the molecule.

26 wt% microparticles were fully degraded in a 0.1% (w/v) Tween 80 PBS solution at pH 7.4. 10 mM AAPH was introduced to the solution with degradation products, and the consumption profiles of curcumin and curcumin monoacrylate were monitored using HPLC (**Figure 3-4B**). Curcumin was consumed over time at a consistent rate similar to the free molecule (**Figure 3-2A**); however, curcumin monoacrylate concentration did not

decrease until 4 hours after the addition of 10 mM AAPH. This lag could be due to decrease in antioxidant activity with the presence of the acrylate group on close to 40% of the curcumin molecules that were released; however, it was able to still be consumed over time. There was also residual concentration of curcumin monoacrylate at 24 hours. The additional acrylate moiety found on the molecule appeared to influence susceptibility of consumption, explaining the residual color left in solution over 24 hours and the change in overall rate of consumption.

3.3.4 Development of the Oxidative Consumption Rate Model of Free Curcumin

Using the experimental data obtained from curcumin in the presence of 10 mM AAPH (**Figure 3-2A**), equations (2), (3a), and (4) were solved simultaneously using MATLAB ODE15s solver and the fminsearch function to find the unknown consumption parameter, k_C, to be 200 $\mu M^{-1}min^{-1}$ with $R^2 = 0.895$ in comparison to the experimental data (**Figure 3-5**). Equation (4) is plotted in the first subplot, where Equation (2) and (3a) are plotted in the second and third subplot. The model was verified by plotting the expected profile of curcumin consumption in a 100 mM AAPH solution and was compared to actual data of curcumin consumption over time. The consumption profile of curcumin exponentially decreased, and the entirety of curcumin was theoretically consumed within the first hour. Although the finality of curcumin consumptiom was not until 8 hours experimentally, the majority of curcumin was consumed within the first hour, just as the model described. The consistency in predicted curcumin consumption profile verified second order degradation kinetics to describe the consumption of curcumin in the presence of AAPH. Correlation factor values are provided in **Table 3-1**. AAPH concentration decreased over time as the thermal decomposition of the molecule of takes places. The

concentration of free radicals started to increase as the free radicals were generated and then began to decrease as the elimination constant within the equation dominated after all the curcumin was consumed. This model was able to predict the consumption profile of curcumin over time in a solution of higher radical concentration at a correlation factor of 0.92.

3.3.5 Modeling the Consumption of Released Products in the Presence of AAPH

Equation (5) was added to the set of equations to describe the consumption rate of the curcumin monoacrylate degradation product released. Equations (2), (3b), (4), and (5) were solved simultaneously as previously described and k_C and k_{CM} were minimized fitting the HPLC experimental results to 75 and 25 $\mu M^{-1}min^{-1}$, respectively (**Figure 3-6**). It is here we note that the oxidative consumption rate of curcumin has decreased in comparison to the oxidative consumption rate of curcumin as a free molecule. This suggests the activity of curcumin was slightly inhibited in the presence of residual degradation products from the polymer network in solution or from being integrated within the network. The model was then used with the minimized parameters to predict consumption profiles of curcumin and curcumin monoacrylate in the presence of 100 mM AAPH and overlaid with experimental data. Indeed, the rate parameter of curcumin monoacrylate was lower; however, when predicting consumption profiles in a higher concentration of free radicals, the model fit well at a correlation factor of 0.924, again providing validity to the second order kinetic rate model for the products released from the network (**Table 3-2**).

The free radical levels present over time in this model (**Figure 3-6, subplot 3**) appeared to be more constant than in the curcumin model with a low but instantaneous

production of free radicals, thus decreasing slightly over time due to the elimination rate term.

For the treatment of an oxidative stress induced disease such as oral mucositis, the application of curcumin conjugated PBAE microparticles to the surface of the buccal cheek pouch could allow for controlled release of curcumin to suppress free radical production that activates pro-inflammatory markers [121]. When translating this model into a human or *in vivo* trial, other pathways of elimination of curcumin may be added. A potential missing term or "piece to the puzzle" would be a rate to describe the wash out of particles, which would account for any loss of curcumin that was removed before release. This would take in to account the retention time of particles on the surface of the buccal tissue. Retention time can be enhanced by using a vehicle such as a mucoadhesive solution, but this term would and should be incorporated in future development of models to predict lasting effects *in vivo.*

Another factor that could play a role in the discrepancy of the consumption profiles is the rate of hydrolysis versus rate of swelling. While PBAE crosslinked networks are degradable, they are also classified as hydrogels as well due to their swelling properties [116, 122]. The domination of swelling effects in initial release profiles can be demonstrated, where in each independent microparticle network, there is a point at which microparticle integrity is lost, allowing for the remainder of the curcumin to be released. The consumption equations developed could then be added to describe the products of interest in the presence of AAPH.

The model developed demonstrates the ability to describe curcumin and curcumin monoacrylate in the presence of a free radical, like AAPH, and has promising results to

better understand free radical interaction of curcumin *in vivo.* The consumption rate of curcumin and curcumin monoacrylate in the presence of AAPH was successfully described by this nonlinear model; however, consumption rates of these compounds could change based on the origin and property of the free radical present. It has been shown that the activity of scavenging potential changes based on the interaction of radicals. Curcumin has been presented as having a high reducing power to transition metals, a value correlated to antioxidant capacity, but when investigated with specific free radical interactions, lower scavenging potentials are found for superoxide anions and H_2O_2 compared to AAPH[123]. In the future, this model could be investigated and compared against consumption profiles of other free radical molecules to better understand the degree of translation in other environments and the authenticity this model has to AAPH specifically.

3.3.6 Demonstration of Controlled Release Antioxidant Delivery

The deviation of free radical concentrations by adding curcumin at a constant rate or at one initial amount were compared. The theoretical baseline generated at a concentration of 10 mM AAPH was the point of deviation. The plot shown in **Figure 3-7A** represents the concentration deviation from the baseline concentration of free radicals over time in the presence of bolus curcumin doses or constant release rates of equivalent curcumin over 24 hours ($C(t=0) = 0$ μM). For 10 and 25 μM curcumin initial concentrations, the change in free radical concentration was $0.25x10^{-5}$ and $0.6x10^{-5}$ μM initially and reverted to baseline within less than 2 hours after all of the curcumin had been consumed. Bolus delivery of low concentrations allowed for a fast, initial consumption of radicals present, and deviated significantly from the baseline level of radical concentration. The curcumin was then quickly consumed, and the initial free radical levels were

maintained. Higher initial concentrations such as 225 µM curcumin deviated significantly at t = 0 min by $3.25x10^{-5}$ µM and did not reach baseline until after 24 hours. The greater the initial dose of curcumin the longer it took for the free radical concentration to reach baseline, which initially could appear as a benefit; however, the greater the deviation in antioxidant/oxidant levels, the higher the risk in implementing imbalance to the cellular environment. This could ultimately create an antioxidant toxicity effect by shifting the redox equilibrium in the environment. This model represents the potential risk of toxicity by showing the drastic change in concentration initially.

When looking at the model with curcumin being released constantly over 24 hours, the deviation of free radical concentration did not appear as significant compared to the initial dose delivery method. Unlike initial doses of curcumin, the controlled release of even the highest theoretical delivery of 225 µM over 24 hours only deviated from baseline levels by $0.6x10^{-5}$ µM at any time in the 24 hour period evaluated. To understand the degree of curcumin's scavenging potential and the degree in change of the free radical environment, the area under the curve (AUC) for each delivery method was evaluated (**Figure 3-7B**). For the curcumin rates of release, the AUC ranged from $3.34x10^{-4}$ – $7.3x10^{-3}$ µM*min, and for initial doses of curcumin, the AUC ranged from $3.84x10^{-4}$ – $8.3x10^{-3}$ µM*min (Figure 3-7C). For all bolus deliveries, the AUC was higher than all the controlled release models, showing higher change of antioxidant/oxidant levels in bolus deliveries for each theoretical dose equivalence.

3.4 Conclusions

In these novel controlled delivery systems, the consumption of curcumin was protected as it was incorporated into the backbone of the microparticle network until

hydrolyzed and released into the environment. The experimental findings in this work showcased the ability to deliver a constituent amount of curcumin over time through a controlled release system compared to rapid consumption as a free drug. Experimental data provided a foundation to develop a second order kinetic rate model to describe the oxidative consumption of curcumin as a free molecule and the oxidative consumption of the materials released from the microparticle network utilizing a first principles process. This gives insight on the incorporation of an antioxidant into the backbone of a polymer and how the addition of curcumin into a network allows for more consistent delivery and protection of curcumin over time. It also showed that controlled release can suppress levels of free radicals theoretically over time consistently rather than dramatically, which is not possible with bolus delivery of curcumin. This model will continue to be developed to advance the pharmacokinetics of curcumin conjugated poly(beta-amino ester) networks and implement them into clinical practice in the future.

Table 3-1: Oxidative consumption rates of curcumin in the presence of AAPH.

Model	k_c ($\mu M^{-1}min^{-1}$)	R^2
Curcumin + 10 mM AAPH	200	0.895
Curcumin + 100 mM AAPH	200	0.915

Table 3-2: Oxidative consumption rates of curcumin and curcumin monoacrylate release from microparticle networks.

Model	k_C ($\mu M^{-1}min^{-1}$)	k_{CM} ($\mu M^{-1}min^{-1}$)	R^2
Degradation Products + 10 mM AAPH	75	25	0.876
Degradation Products + 100 mM AAPH	75	25	0.924

Table 3-3: Summary of the total area under the curve of each theoretical dose.

Initial Dose (μM)	AUC (μM*min)	Rate of Release (μM/min)	AUC (μM*min)
10	3.84×10^{-4}	**0.0070**	3.34×10^{-4}
25	8.72×10^{-4}	**0.0175**	7.56×10^{-4}
75	2.7×10^{-3}	**0.0515**	2.6×10^{-3}
100	3.7×10^{-3}	**0.0678**	3.3×10^{-3}
150	5.5×10^{-3}	**0.1031**	4.9×10^{-3}
225	8.3×10^{-3}	**0.1548**	7.2×10^{-3}

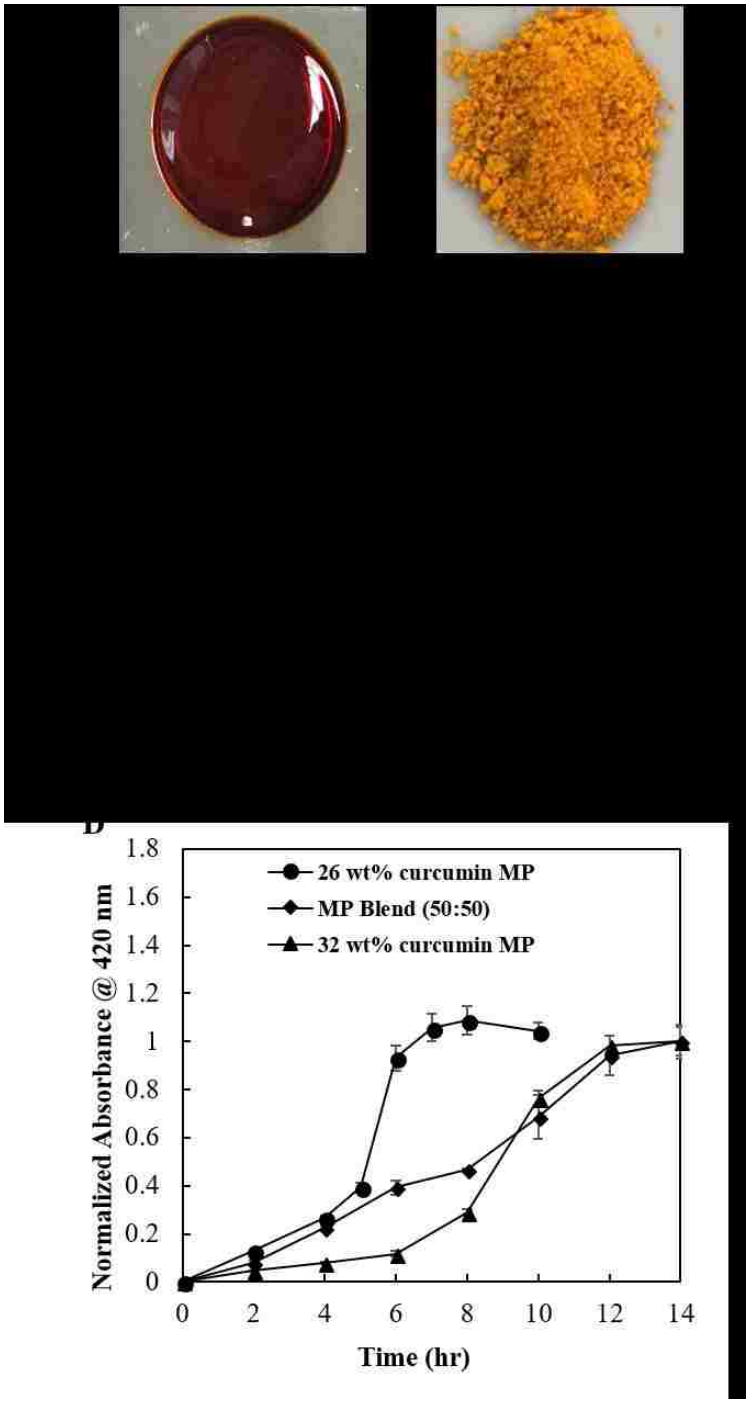

Figure 3-1: Characterization of curcumin conjugated PBAE microparticles (MPs). (A) Curcumin conjugated poly(beta-amino ester) (PBAE) film. (B) Cryomilled curcumin conjugated PBAE MPs. (C) Distribution of MP size. (D) Degradation profiles of 26 wt%, 32 wt%, and 50:50 blend of 26 and 32 wt% curcumin MP. (Mean ± SEM, n = 3)

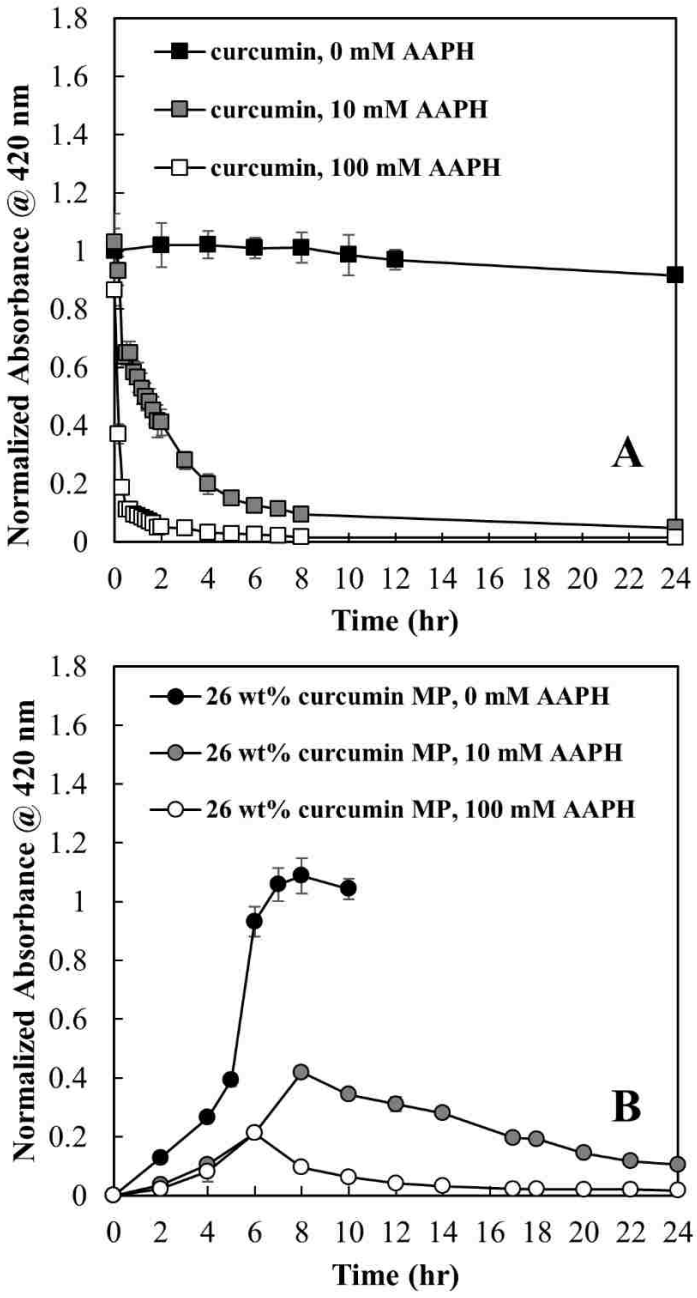

Figure 3-2: Release and consumption profiles of curcumin and curcumin MPs. (A) Curcumin, (B) 26 wt% curcumin loaded PBAE MP, (C) 32 wt% curcumin loaded PBAE MP, and (D) 50:50 blend of 26 and 32 wt% loaded MPs in the presence of 0, 10 and 100 mM AAPH over 24 hours. (Mean ± SEM, n = 3)

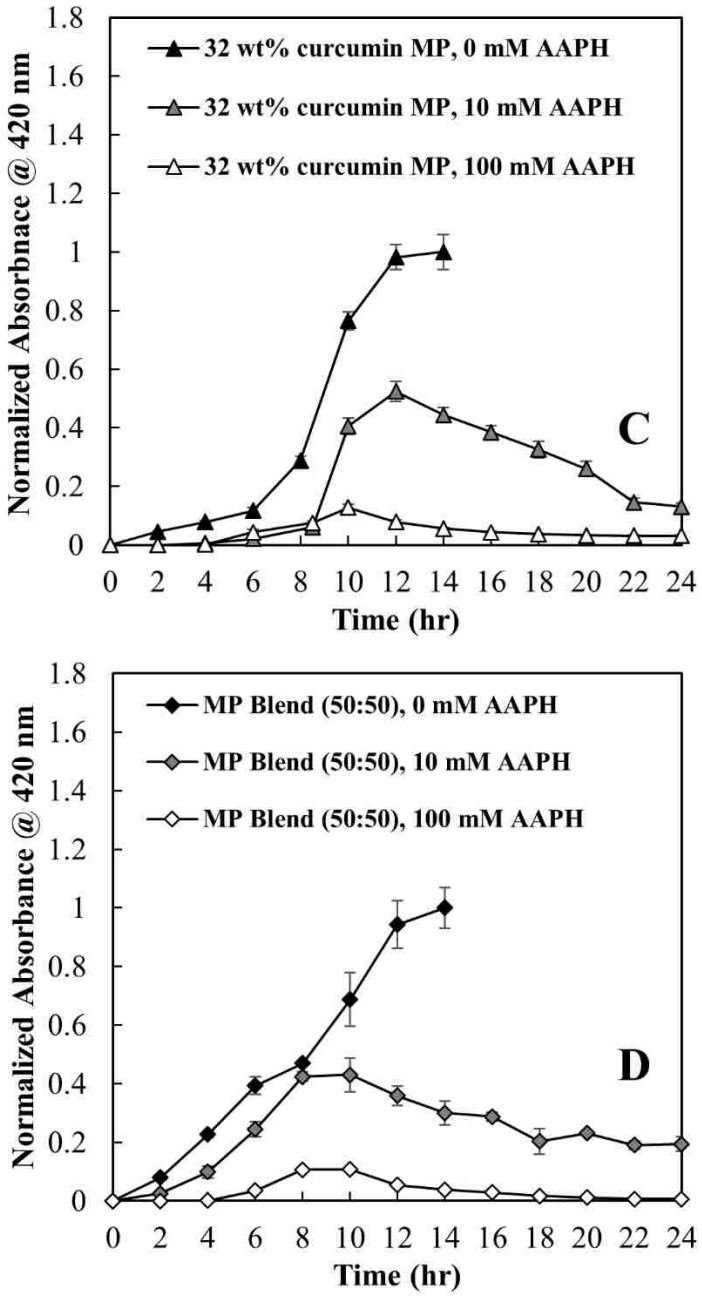

Figure 3-2 (continued): Release and consumption profiles of curcumin and curcumin MPs. (A) Curcumin, (B) 26 wt% curcumin loaded PBAE MP, (C) 32 wt% curcumin loaded PBAE MP, and (D) 50:50 blend of 26 and 32 wt% loaded MPs in the presence of 0, 10 and 100 mM AAPH over 24 hours. (Mean ± SEM, n = 3)

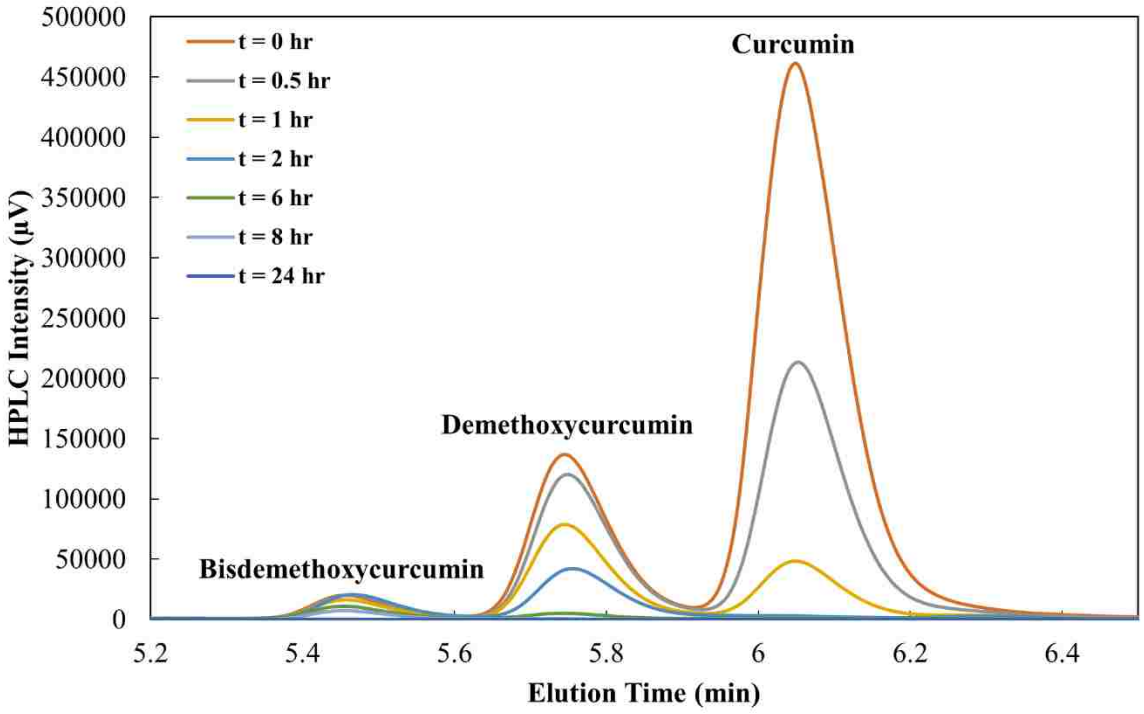

Figure 3-3: Curcuminoid consumption susceptibility by 10 mM AAPH over time.

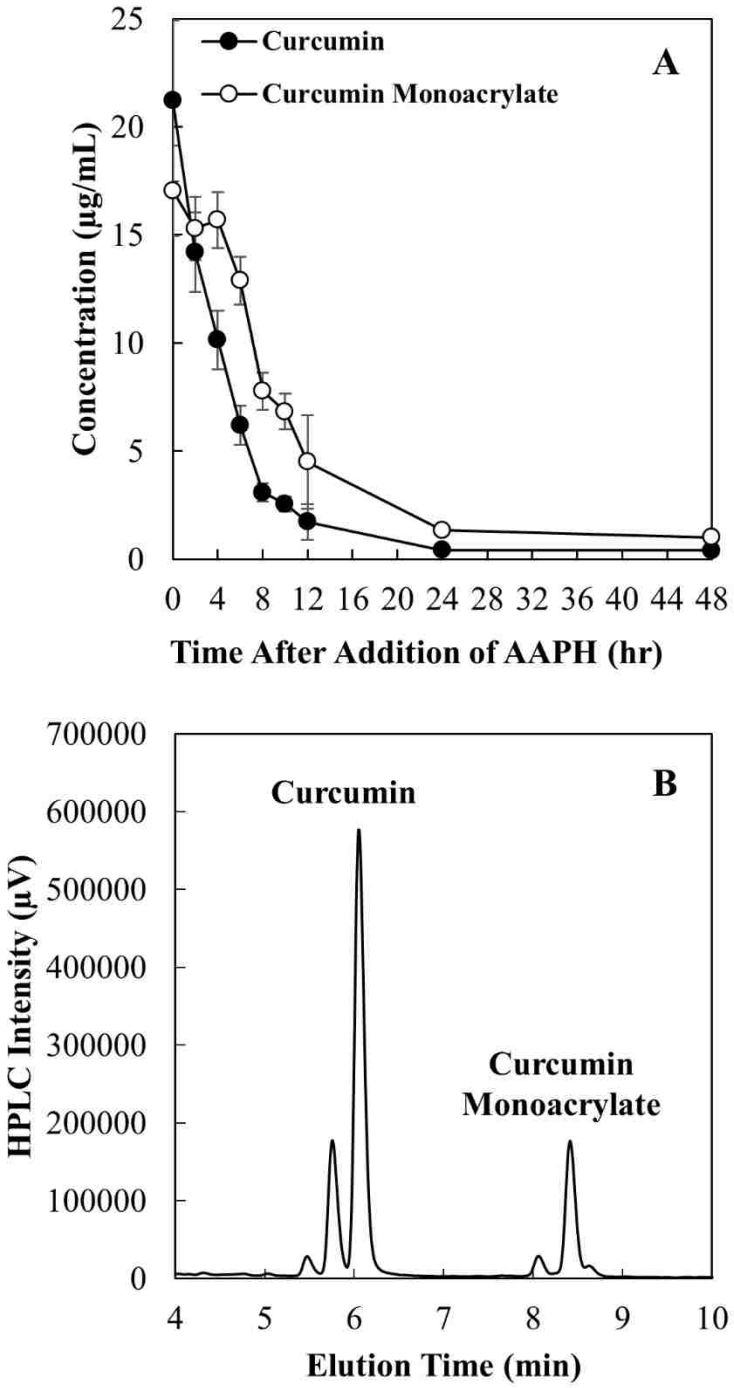

Figure 3-4: (A) Consumption profiles of curcumin and curcumin monoacrylate in the presence of 10 mM AAPH and (B) the HPLC chromatogram of curcumin and curcumin monoacrylate peaks in the release products (Mean ± SEM, n = 3).

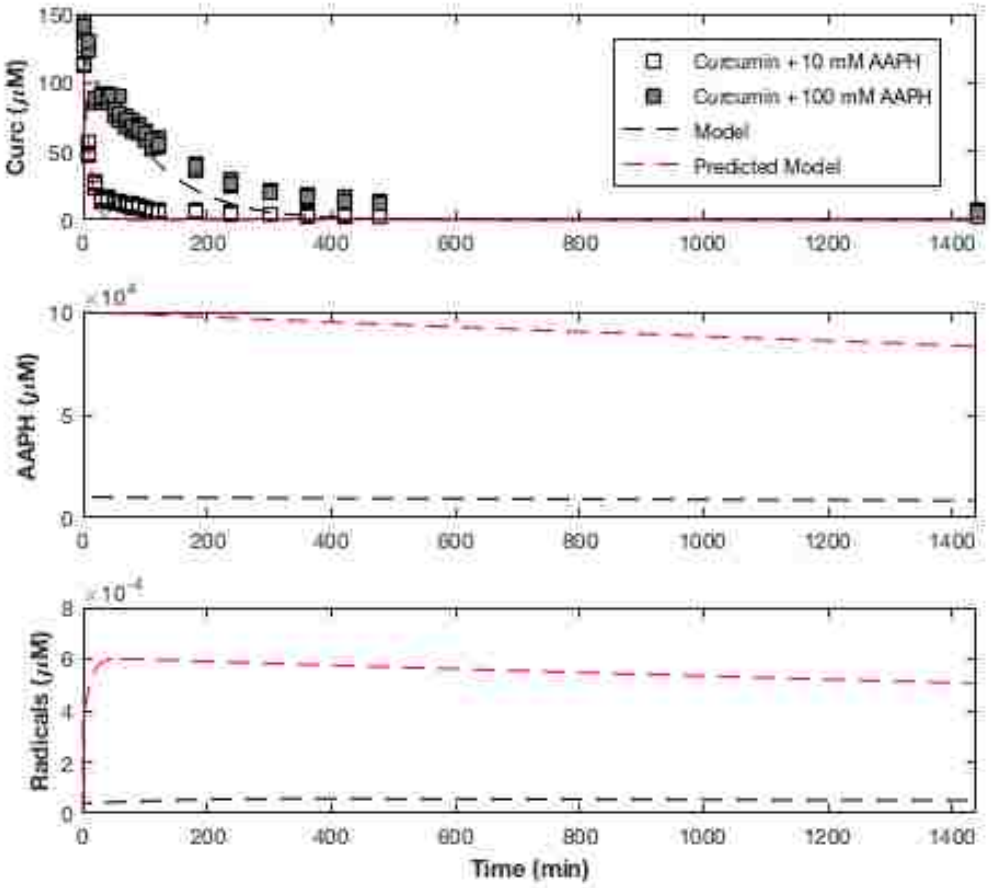

Figure 3-5: Curcumin consumption rate model. Model for curcumin consumption (--) minimized based on raw experimental data of degradation products in the presence of 10 mM AAPH and verified by overlaying predicted model (--) with raw experimental data with higher initial AAPH concentration.

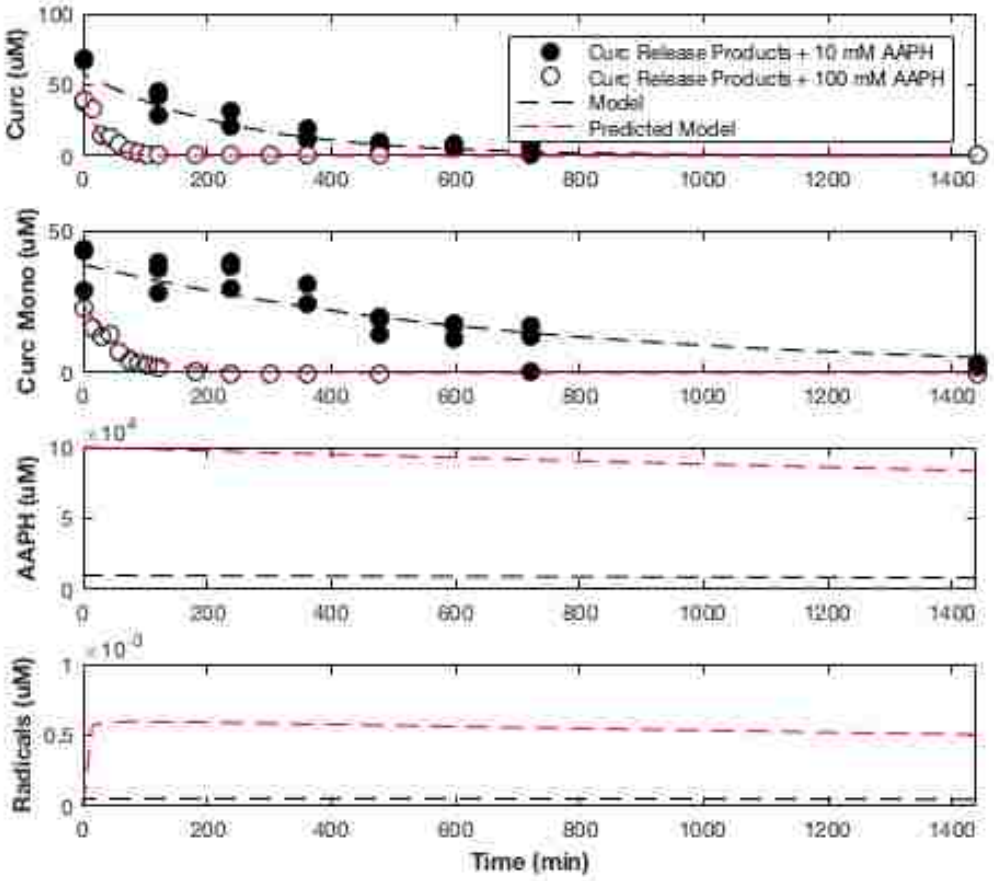

Figure 3-6: Curcumin and curcumin monoacrylate consumption rate model. Model (--) minimized based on experimental data of degradation products in the presence of 10 mM AAPH and verified by overlaying predicted model (--) with experimental data with higher initial AAPH concentration.

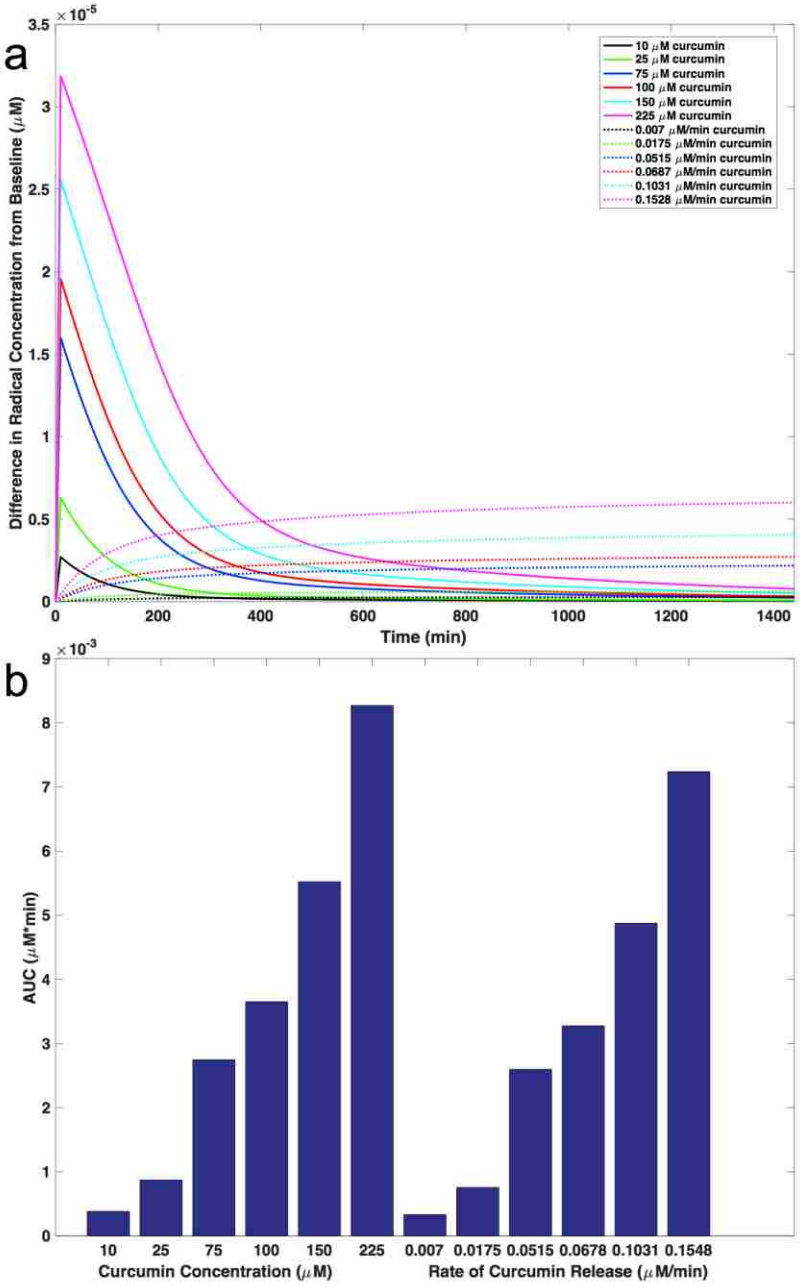

Figure 3-7: Demonstration of bolus and controlled release of curcumin in a free radical generating environment. The deviation of free radical concentration (μM) when the addition of a one-time theoretical injection of free curcumin is added to a 10 mM AAPH solution or the rate equivalent to the total amount added over 24 hours (a) and the AUC values (μM*min) reported as a bar graph (b).

Chapter 4 Responsive Poly(beta-amino ester) Bulk Films in Oxidizing Environments

4.1 Introduction

Oxidative stress diseases are often initiated by an external insult that causes a detrimental oxidant-antioxidant imbalance [40]. A specific example is the onset of chronic obstruction pulmonary disease (COPD) from smoking [25]. Patients not only have elevated levels of hydrogen peroxide from acute exacerbations from the disease [124], but also depleted levels of endogenous antioxidants in the alveolar macrophages, which allows for the oxidants present to amplify the imbalance of many molecular mechanisms [1]. Normal concentrations of hydrogen peroxide are found between 10-100 μM within a regulating cellular environment [125]. When oxidative stress occurs from an indirect insult or amplified concentrations accumulate due to a shift in regulation, the concentration of reactive oxygen species and hydrogen peroxide will increase beyond basal value. This can cause the upregulation of gene transcription factors and an increase in cytokine production, which allows for the imbalance to cascade [126]. Antioxidant therapeutics for the treatment of COPD have been studied, but are still not readily used due to their lack of bioavailability as a free molecule [127].

As the imbalance of free radicals has been found to lead to deleterious effects, the thought of ROS-responsive materials to deliver and overcome these concentrated environments has been a popular topic of investigation [104]. Triggered cleavage and release of drug from polymer in the presence of hydrogen peroxide has been reported, such as poly(ester-amides) and co-poly(oxalate) nanoparticles [128, 129], with the release from these polymer systems being specifically regulated by hydrogen peroxide. Other materials

reported to have ROS-induced degradation include, boronic esters, silicon, proline oligomers, and poly(thioketals) [104].

Up until now, the hydrolysis of the poly(beta-amino ester) networks has been thought to be predominantly controlled by base catalyzed hydrolysis, where water acts as the nucleophile to attack at the ester site to induce hydrolysis [11, 92, 110, 116, 130, 131]. Responsiveness of linear PBAE polymer degradation to external stimuli has been studied by many laboratories including Langer et. al to deliver plasmid DNA for gene therapy using DNA/polymer complexes [132], as well as tuning the degradation of linear PBAE polymers in acidic environments by adding acid sensitive monomers [133]. Poly(beta-amino esters)s have also been designed to be bioreducible for intracellular delivery of siRNA by the Green group at Johns Hopkins University [134], utilizing unique disulfide PBAE linkages, which degrade specifically from redox potential through thiol-disulfide exchange in the cytosol where high concentrations of glutathione are present [135]. However, the response to oxidative environments, specifically hydrogen peroxide, in crosslinked PBAE networks has yet to be studied.

In this chapter, we present the discovery that low levels of hydrogen peroxide in solution can trigger accelerated hydrolysis of the crosslinked PBAE network, releasing curcumin at a self-regulating rate dependent upon the concentration of hydrogen peroxide. This triggered release mechanism can release antioxidant therapeutics in a self-regulated fashion, where the levels of hydrogen peroxide present control the “as needed” delivery mechanism to counterbalance oxidative environments. This triggered release is compared to another oxidizing environment, 2’2-azobisdiamidinopropane dihydrochloride (AAPH), a thermally decomposing free radical generator, which appears to have negligible effect on

the hydrolysis of the network but promotes consumption of curcumin once released in to the environment. This triggered release allows the design to take advantage of the oxidizing environment, which regulates the delivery of the drug necessary for treatment and balance, and will help to deliver extended amounts of curcumin over a time desired to counteract oxidative stress induced diseases.

4.2 Materials and Methods

4.2.1 Materials

4,7,10-Trioxatridecane-1,13-diamine (TTD), Tween 80, 2,2'-azobis(2-amidinopropane) dihydrochloride (AAPH), 2,2'-azino-bis(3-ethylbenzothizoline-6-sulphonic acid) (ABTS), ammonium persulfate (APS), triethylamine, hydrogen peroxide, and acryloyl chloride was obtained from Sigma Aldrich (St. Louis). Curcumin was purchased from Chem-Impex International, Inc. (Wood Dale, IL). Poly(ethylene glycol) (MW 400) diacrylate (PEG(400)DA), was obtained from Polysciences, Inc (Philadelphia, PA). Dichloromethane, tetrahydrofuran and acetonitrile were purchased from Pharmco-Aaper (Brookfield, CT). No additional purification steps were conducted after materials were received.

4.2.2 Synthesis of Bulk PBAE Films

Poly(beta-amino ester) thin films of four different weight loading percentages of curcumin were synthesized similar to Patil et al [116]. The compositions are found in **Table 4-1**. Briefly, to modify curcumin into a multiacrylate system, curcumin was dissolved in anhydrous tetrahydrofuran. In the presence of triethylamine, acryloyl chloride was added at a 1:3 molar ratio under purged nitrogen and ice. The acid-chloride esterification reaction was left for 16 hours to modify the hydroxyl sites of curcumin to acrylate groups, forming

a curcumin multiacrylate mixture. The curcumin multiacrylate product was purified by removing the excess acrylic acid and TEA-HCl salts formed as by products during the reaction, and the product was verified by high performance liquid chromatography (HPLC).

Poly(beta-amino ester) films were synthesized using Michael Addition chemistry, reacting curcumin multiacrylate and PEG(400)DA at different ratios with a primary diamine crosslinker, TTD, at a ratio of total acrylate to amine protons (RTAAP) of 1.0 in anhydrous dichloromethane at 1.5 times the total monomer mass of the film. Films were left at room temperature for 1 hour and then transferred to a 50°C convection oven for 24 hours. Films were then washed five times in anhydrous acetonitrile at 40 mL/1 g of film to remove unreacted monomers from the network. After five washes, films were then dried at 50°C under vacuum and stored with a desiccant until use.

4.2.3 Swelling Profiles in the Presence of AAPH or Hydrogen Peroxide

Circular discs from a bulk film of 0.4 mm thickness were punched and placed in 20 mL of 0, 0.5, and 5 mM hydrogen peroxide (H_2O_2) solutions, or 0.5 and 5 mM 2,2'-azobio(2-methylpropionamidine dihydrochloride (AAPH) solutions below the solubility limit of curcumin in a 0.1% (w/v) Tween 80 PBS solution (pH 7.4). These samples were submerged in an agitating shaker bath at 37°C. At desired time points, films were removed from the bath, blotted dry on a tissue, and the mass was measured. The swelling ratio is defined as:

$$Swelling\ Ratio = M_S/M_I \quad (1)$$

where M_S is the mass of the swollen film and M_I is the mass initial dry film. The swelling ratio was observed until the film lost integrity and was unable to be handled.

4.2.4 Total Polymer Content in the Presence of AAPH or Hydrogen Peroxide

Individual films (n = 3) for each time point were measured to obtain the percent of polymer mass remaining over time in a 0.1% (w/v) Tween 80 PBS (pH 7.4), and compared to solution with AAPH or hydrogen peroxide. Empty microcentrifuge tubes were weighed. At each desired time point, films were removed from the bath, blotted dry on a tissue, and the swollen mass was measured. The swollen polymer mass was then collected in the microcentrifuge tube and placed in the freezer until frozen. The films were then freeze dried overnight, and the mass of the microcentrifuge tube plus the dried mass was measured. Knowing the mass of the swollen polymer (M_s) and the initial mass of the polymer (M_I), the amount of water retained by the film is known (M_w) and calculated using the following equation:

$$M_W = M_S - M_I \quad (2)$$

After the swollen film was freeze-dried, the salts from the buffer remained. The theoretical amount of residual salts was calculated from the mass of the known water and the salts were subtracted from the dried polymer mass to obtain the mass of the dried film. The mass remaining percentage is defined as the following:

$$\%\ Mass\ Remaining = M_{FR}/M_I \quad (3)$$

where M_{FR} is the mass of the film dried that remained. Films were compared by looking at the time at which 50% of the total polymer mass remains and will be referred to as MT50.

4.2.5 Release Profiles in the Presence of AAPH or Hydrogen Peroxide

The release of curcumin and acrylated curcumin degradation products from the film were measured via reverse-phase high performance liquid chromatography (HPLC) (Water Phenomenex C18 column, 5 µm, 250 mm (length) x 4.6 mm (ID) on a Shimadzu Prominence LC-20 AB HPLC system attached to a Waters Refractive Index Detector) at 420 nm in the presence of 0, 0.5 and 5 mM hydrogen peroxide solutions and 0, 0.5 and 5 mM AAPH solutions. The supernatant of the individual samples measured for the mass remaining studies were collected at each time point. Curcumin and curcumin multiacrylate standards were used to quantify the concentration of active released.

4.2.6 Antioxidant Capacity of Released Degradation Products over Time

A Trolox Equivalent Antioxidant Capacity (TEAC) assay was used to measure the total antioxidant activity of the degradation products after being released from the network in the presence of AAPH or hydrogen peroxide. ABTS at 8 mg/mL and APS at 1.32 mg/mL were reacted overnight in the dark to produce ABTS free radical cations. Samples or a trolox standard were added to the ABTS free radical cation working solution for 5 minutes and then directly read at 734 nm using a UV-visible spectrophotometer microplate reader. Trolox was used as the reference antioxidant to directly compare the sample's antioxidant capacity. These values were reported as the Trolox Equivalence Antioxidant Concentration (TEAC) (mM). TEAC assays were completed at room temperature to inhibit any increase in free radical generation present in solution from thermal decomposition of AAPH throughout the duration of the assay.

4.3 Results and Discussion

4.3.1 Bulk Film Synthesis and Characterization

Curcumin, a small hydrophobic polyphenol with high antioxidant capacity has promise as a therapeutic, but because of curcumin's high reactivity and instability as a free molecule [136, 137], there is motivation to find a way to keep its active sites preserved until antioxidant treatment is desired in an environment. To do this, curcumin was converted to a curcumin multiacrylate monomer by an acid-chloride alcohol esterification reaction as seen by Wattamwar et al [11]. By converting the hydroxyl groups to acrylates, the polyphenolic compound was incorporated in to the backbone of a crosslinked network. Four different compositions of PBAE crosslinked networks (**Table 4-1**) were synthesized using a ratio of CMA (hydrophobic monomer) and PEG(400)DA (hydrophilic monomer), and a primary diamine crosslinker, TTD. TTD, acting as a Michael donor, reacted with the alkene group of either acrylate and formed a PBAE bond. The four amine proton reaction sites on the primary diamine allowed for a crosslinked network to form. The introduction of water allowed the ester bond to hydrolyze, which released curcumin in its active state.

The swelling ratios (**Figure 4-1** and **Figure 4-5)** and total polymer content (**Figure 4-2** and **Figure 4-6**) over time of four different film compositions were obtained in a control 0.1% (w/v) Tween 80 PBS (pH 7.4) environment. In the absence of oxidizing environments, the 0, 10, 26, and 32 wt% curcumin conjugated films degraded in 3, 2.5, 8, and 13 hours respectively. The rate of degradation time increased as the hydrophobicity of the network increased, although the integrity of the network appeared lower in the 10 wt% loaded curcumin film compared to the 0 wt% loaded curcumin film. This could be due to poor conjugation of CMA into the network. Analysis of the release profiles (controls in

Figure 4-3 and **Figure 4-7)** and trolox equivalent concentrations (controls in **Figure 4-4** and **Figure 4-8**) of the released antioxidant was also completed for the three compositions that incorporated curcumin into the network. Swelling profiles, the total polymer content of the films over time, the release products, and the activity of curcumin were all compared in the presence of two oxidizing environments to observe selectivity and sensitivity to different abnormal environments for antioxidant release.

4.3.2 2,2'-Azobio(2-methylpropionamidine) dihydrochloride (AAPH) Investigation

4.3.2.1 Swelling Profiles in the Presence of AAPH

In 0.1% (w/v) Tween 80 PBS (pH 7.4), films that had no curcumin conjugated into the network (**Figure 4-1A**) had increased water uptake compared to curcumin-conjugated films due to extent of hydrophilicity and swelled 7.09 ± 1.3 times its original mass over 3 hours before losing integrity. In the presence of 0.5 and 5 mM AAPH, the swelling ratios over time increased to 6.17 ± 0.53 and 7.77 ± 0.46 times its original mass, losing integrity at 3 hours as well. The equilibrium swelling ratios were not statistically different. For 10 wt% curcumin loaded films (B), the observed maximum swelling ratios of the films in 0, 0.5 and 5 mM AAPH were 6.98 ± 0.15, 6.98 ± 0.27, and 6.48 ± 0.50 over 1.5 hours. The equilibrium swelling decreased and time before integrity was lost increased as the hydrophobicity of the network increased. This was due to the decrease in hydrophilicity of the network and the incorporation of more curcumin multiacrylate, a more hydrophobic molecule than PEG(400)DA. 26 wt% curcumin films swelled over 5 hours before losing integrity with a maximum swelling ratio of 4.09 ± 0.29 in PBS with no free radical generator. Films in the presence of 0.5 and 5 mM AAPH swelled at similar rates over 5

hours until the last point of integrity, where the maximum swelling ratios are slightly lower but within error at 3.5 ± 0.04 and 3.6 ± 0.16 respectively.

Similarly, there was no significant effect on the swelling profiles of the 32 wt% curcumin film in 0, 0.5 and 5 mM AAPH solution. The maximum swelling ratios were 2.8 ± 0.16, 2.6 ± 0.036, 2.3 ± 0.13 respectively and the integrity of all three films was lost over 9 hours.

4.3.2.2 Total Polymer Content in the Presence of AAPH

The mass of the total polymer content of the curcumin conjugated poly(beta-amino ester) films was investigated to observe the degradation of the films present in the presence of AAPH. The time at which 50% of the polymer mass remained was calculated (MT50) for each composition in each solution. For AAPH, a slight shift in the MT50 values was observed in the presence of AAPH (**Table 4-2**). There was an increase in MT50 for 0 wt% curcumin films and 32 wt% curcumin films in 0.5 and 5 mM AAPH, where the rest of curcumin conjugated films shift to the left. This could be due to the slight variability between networks depending on localized hydrophobicity or hydrophilicity depending on the neighboring bonds of the crosslinked network. Significant change in the mass remaining MT50 value was compared to the control using a paired t-test. The 0 wt% curcumin film's MT50 in the 0.5 mM AAPH solution was 5.4 minutes slower than the control ($p<0.05$) and the MT50 value in 5 mM AAPH was 14.4 minutes slower compared to the control ($p<0.05$). The 10 wt% film MT50 value shifted less than 30 minutes in the presence of each solution when compared to the control film ($p>0.05$), and a 20 minute change was seen for the 26 wt% films when compared in 5 mM AAPH ($p>0.05$). For all the curcumin conjugated films, the total degradation time was insignificant. AAPH solution

did not appear to have a significant effect on the total polymer content remaining throughout the degradation study as the rate of degradation of the polymer containing no curcumin was rapid in the control solution.

4.3.2.3 Release Profiles in the Presence of AAPH

As the films hydrolyze and release curcumin over time in different oxidizing environments, samples were collected, and the release products were analyzed via HPLC coupled with UV-visible detector and the absorbance at 420 nm was reported as a chromatogram. In **Figure 4-3**, the release profiles of three different compositions are plotted in a control solution (0.1% (w/v) Tween 80 PBS, pH 7.4), 0.5 and 5 mM AAPH. The two active release products are curcumin and curcumin monoacrylate, verified by standards in the HPLC chromatogram. These acrylate forms are from curcumin multiacrylate monomer not being fully crosslinked within the network, leaving free acrylate groups present in the degradation products. Within the 10 wt% curcumin film, curcumin was fully released from the network after 2.5 hours at 6 μg/mL curcumin concentration, and 3 μg/mL curcumin monoacrylate. The same samples were collected over time in the presence of the free radical generator AAPH. The films released over the same 2.5 hour period; however, after the curcumin was fully released, a decrease in concentration was seen for all products due to consumption of the active products. This decrease in concentration was due to the abstraction of the hydrogen of the active hydroxyl groups on curcumin, thus destabilizing the molecule in the presence of the peroxyl radicals formed as AAPH thermally decomposes over time. This consumption phenomenon was even more pronounced in the presence of 5 mM AAPH, where the recovery of the curcumin concentration was only 3 μg/mL and 1.23 μg/mL for curcumin monoacrylate.

For the 26 wt% curcumin films over 8 hours, 55 µg/mL curcumin and 34 µg/mL curcumin monoacrylate was released. These degradation studies were repeated in the presence of AAPH, and similar to the 10 wt% films, the recovery of the degradation products was lower over time from the instantaneous consumption of curcumin as its hydrolyzed and released in to solution. The recovery appeared to be lower, but the rate of release was proportional, showing no notable change in release time other than consumption of the active component. The change in recovery was observable due to the controlled rate of release, allowing for more free radicals to generate within the system before curcumin is hydrolyzed in to solution.

32 wt% curcumin films in release profiles showed a noteworthy change in release in the presence of AAPH, recovering 60.5 g/mL curcumin and 36.8 g/mL in the control environment, where in the 0.5 and 5 mM AAPH, the peak concentration of curcumin and curcumin monoarylate was hour 12 rather than 13 (**Figure 4-3)**. Comparing this to the slight increase in degradation time from **Figure 4-2D**, there is a slight effect on the rate of hydrolysis in the presence of high concentrations of AAPH, where curcumin incorporation is highest. Again, after the films are fully degraded and the total loading of curcumin was released, the consumption of curcumin and curcumin monoacrylate in solution started to occur. This decrease in recovery was seen throughout the 26 wt% curcumin films. This could be due to the faster rate of release over 8 hours which allowed for the rate of free radical production and rate of curcumin and curcumin monoacrylate release/consumption to be proportional. Due to the hydrophobic nature of the 32 wt% curcumin film, the swelling occurred over 9 hours, so the concentration of free radicals in solution was highest

as the network loses integrity and a significant amount of curcumin was released, allowing for a notable amount of curcumin to be consumed within the last two hours of degradation.

4.3.2.4 TEAC Assay on the Degradation Products in the Presence of AAPH

The antioxidant capacity of the supernatant of the degradation products was measured using a trolox equivalence antioxidant capacity assay. The concentration of the active antioxidant in a solution was reported as the theoretical equivalent concentration to that of a known antioxidant, Trolox. The 10 wt% curcumin film degradation products appeared less stable from both the release profiles (**Figure 4-3**) and the TEAC assay profiles (**Figure 4-4**) and began to lose activity after the films were fully degraded compared to the control solution (0.1% (w/v) PBS, pH 7.4). Interestingly, there was no observable effect on the antioxidant capacity of the curcumin released from the 26 wt% film in to the solution with a free radical generator. This could be due to the low concentration of free radicals present over time. If the release was at a lower concentration, or the free radical concentration were increased, an effect on the antioxidant capacity could potentially be seen.

The 32 wt% curcumin film cumulative TEAC profile was similar to the cumulative release profile seen in **Figure 4-3.** There was an increase in antioxidant activity at 9 hours, when the integrity of the film was lost and the curcumin began to hydrolyze and release from the network; however, there was no significant change in the TEAC values at the final degradation times points of 12-13 hours, where release profiles show decay in absorbance. This could be due to the consumption or degradation of curcumin from the free radical present, resulting in curcumin degradation products that could obtain antioxidant capacity.

4.3.3 Hydrogen Peroxide Induced Degradation

4.3.3.1 Swelling Profiles in the Presence of Hydrogen Peroxide

The same compositions of films were investigated in the presence of 0, 0.5 and 5 mM H_2O_2 added to 0.1% (w/v) Tween 80 PBS (pH 7.4) (**Figure 4-5)**. Between each composition of film, hydrogen peroxide solutions decreased the time in which the films swelled and the time in which the film's integrity was lost. 0 wt% curcumin in a control 0.1% (w/v) Tween 80 PBS (pH 7.4) solution swelled over 2.5 hours, until integrity was lost. In the presence of 0.5 and 5 mM H_2O_2, the maximum swelling ratio was not affected, but the point of integrity decreased to 2 and 1.5 hours respectively (**Figure 4-5A**).

10 wt% curcumin films had a different swelling response, where the rate of swelling in the presence of 5 mM H_2O_2 was significant, although the maximum swelling rate was still only 30 minutes faster than the control film in a normal solution (**Figure 4-5B**). Interestingly, as the loading of curcumin increased within the film, the sensitivity of the film response appeared to change significantly. The swelling of 26 wt% films in the presence of hydrogen peroxide increased over 5 hours but appeared to maintain integrity throughout all 5 hours, similar to the control film; however, the swelling ratio tapers off between 4 and 5 hours, rather than continuing to swell. This "tapering" effect could point to bulk erosion degradation, where degradation could occur directly at the surface rather than within the network. This same effect was seen in 5 mM H_2O_2, where the films swelled for the first 1.5 hours, but the maximum swelling rate plateaued rather than continuing to swell (**Figure 4-5C**). Similarly, a significant difference was seen in swelling profiles in 32 wt% curcumin films, where the point of integrity was lost after 6 hours compared to 9 hours in a 0.5 mM H2O2 solution, and after 2 hours in a 5 mM H2O2 (**Figure 4-5D)**. Note the

maximum swelling ratio decreased in the presence of hydrogen peroxide solutions as well. This could express accelerated rate of hydrolysis that is competitive with the rate of uptake. In the presence of hydrogen peroxide, the rate of hydrolysis appeared to be more selective than the rate of swelling, and this sensitivity increased with higher incorporation of curcumin in to the network.

4.3.3.2 Total Polymer Content in the Presence of Hydrogen Peroxide

The films conjugated with curcumin dramatically decreased in polymer mass remaining over time due to accelerated degradation (**Table 4-2**). Observing each curcumin-conjugated film composition, increasing the hydrogen peroxide in solution decreased the MT50 value significantly, and accelerated degradation was enhanced upon the increase of the weight percent of curcumin. (**Figure 4-6**). The 32 wt% film had the largest change in MT50, where the MT50 in the control PBS solution was 10.7 hours and in 5 mM H_2O_2, the MT50 was 3.10 hours. The presence of hydrogen peroxide enhanced base catalyzed hydrolysis of the network, and accelerated polymer degradation. The most significant H_2O_2 response on polymer degradation was 20x greater than polymer response to AAPH. The MT50 values of the films in the presence of 0, 0.5 and 5 mM AAPH, and H_2O_2 are provided for direct comparison in **Table 4-2**.

4.3.3.3 Release Profiles in the Presence of Hydrogen Peroxide

The release profiles of the three curcumin-conjugated films in the presence of 0, 0.5, and 5 mM H_2O_2 are shown in **Figure 4-7**. 26 wt% curcumin films were punched from a film (n = 3 for each treatment solution) and the release products, curcumin and curcumin monoacrylate, were observed by collecting supernatant over the 8-hour degradation period. 26 wt% curcumin films in 0.1% (w/v) PBS (pH 7.4) did not release a significant amount

of curcumin until hour 6. Comparing this value to the swelling profile, this was 1 hour after films lose integrity. The final recovery concentration of curcumin and curcumin monoacrylate is 115.5 ± 21.7 and 36.3 ± 6.8 μg/mL, respectively. In the presence of 0.5 mM H_2O_2, the concentration of curcumin monoacrylate decreased to 12.9 ± 4.9 μg/mL and curcumin increased to 163.5 ± 6.7 μg/mL as full degradation was accelerated to 6 hours. With 10-fold increase in H_2O_2 concentration, the curcumin monoacrylate was hydrolyzed and 191.7 ± 13.7 μg/mL curcumin was recovered after 4 hours. Not only was the hydrolysis within the network sensitive to the hydrogen peroxide, but the acrylate group on the curcumin monoacrylate degradation product hydrolyzes, recovering only free curcumin at 5 mM H_2O_2. The sensitivity of hydrolysis appeared dependent upon the amount of curcumin conjugated to the network.

At 0.5 mM H_2O_2, 26 wt% curcumin films degraded 33% faster than in a control PBS solution, where 32 wt% curcumin films degraded 62.5% faster than in a control PBS solution and 10 wt% curcumin films had no change in total degradation time. In 5 mM H_2O_2, 26 wt% curcumin films degradation time increased by 100% than the control solution, where the shift in degradation significantly increased to 160% faster when curcumin is responsible for 32% of the total weight of the polymer. Even at high concentrations of hydrogen peroxide, there was no ultimate change in the rate of release at low weight percent loadings of curcumin.

The films that were comprised of only PEG(400)DA appeared to be the least affected hydrogen peroxide. The rate of hydrolysis between the beta-amino ester bond neighboring the ethylene oxide chains versus the beta-amino ester bond neighboring the benzene ring could be more sensitive, promoting the rate of hydrolysis to increase when

more curcumin was incorporated in to the network. Another potential reason for enhanced sensitivity could be due to a shift in antioxidant-oxidant balance in solution, promoting the release of curcumin to neutralize the system.

4.3.3.4 Trolox Equivalent Antioxidant Capacity on Degradation Products

The antioxidant capacity of the release products into solution were investigated after being exposed to the hydrogen peroxide. At these lower concentrations of hydrogen peroxide, the activity profile mimics the release curve profile. As active curcumin is released into solution, the equivalent antioxidant capacity, using Trolox as an antioxidant reference compound, increased as well, showing active products accumulating in the environment as the network degrades. There was a slight increase in the antioxidant potential for all three film compositions when degraded in H_2O_2. The could be due to the hydrolysis of the acrylate group on the curcumin monoacrylate degradation product, which would increase the antioxidant capacity of the molecule, thus increasing the equivalent antioxidant capacity in solution.

4.4 Conclusions

The accelerated release of curcumin in the presence of low concentrations of hydrogen peroxide introduces a self-regulating drug delivery system where rate of release of drug is controlled by the environment in which the system is introduced. Interestingly, not all oxidizing environments have the same effect on the hydrolysis of the crosslinked network. Although the peroxyl radicals had a higher affinity to consume the curcumin release products from the polymer, the hydrogen peroxide aided in accelerated polymer degradation. Not only was curcumin released at a faster rate, the acrylate found on

curcumin monoacrylate was further hydrolyzed, enhancing the release of free active curcumin.

This discovery illustrates the necessity for tunable drug delivery systems to provide the proper therapeutic doses in abnormal environments. Further investigation will continue on pulsatile release to look at the effects of the polymer degradation when exposed to abnormal concentrations of hydrogen peroxide and then back in to a neutral environment. This interesting concept will help to modify the monomer selection pending the environment balance required for homeostatic environments.

Table 4-1: Compositions of curcumin conjugated poly(beta-amino ester) films.*

CMA (mol%)	PEG(400)DA (mol%)	Curcumin (wt%)
0	100	0
20	80	10
50	50	26
60	40	32
*all synthesized at a ratio of total acrylate to amine proton moles (RTAAP) of 1.0		

Table 4-2: Comparison of time at which 50% mass of the polymer remains in the control, 0.5, and 5 mM AAPH and H_2O_2 solutions.

		Film Composition (wt% curcumin)			
Solution	**MT50 Values (hr)**	**0**	**10**	**26**	**32**
0.1 (w/v)% PBS (pH 7.4)	**-**	2.45	2.04	5.89	10.7
AAPH (pH 7.4) (mM)	**0.5**	3.10	1.60	5.80	11.2
	5	3.00	1.58	5.56	11.1
H_2O_2 (pH 7.4) (mM)	**0.5**	1.89	1.56	4.71	6.41
	5	1.76	1.35	2.02	3.06

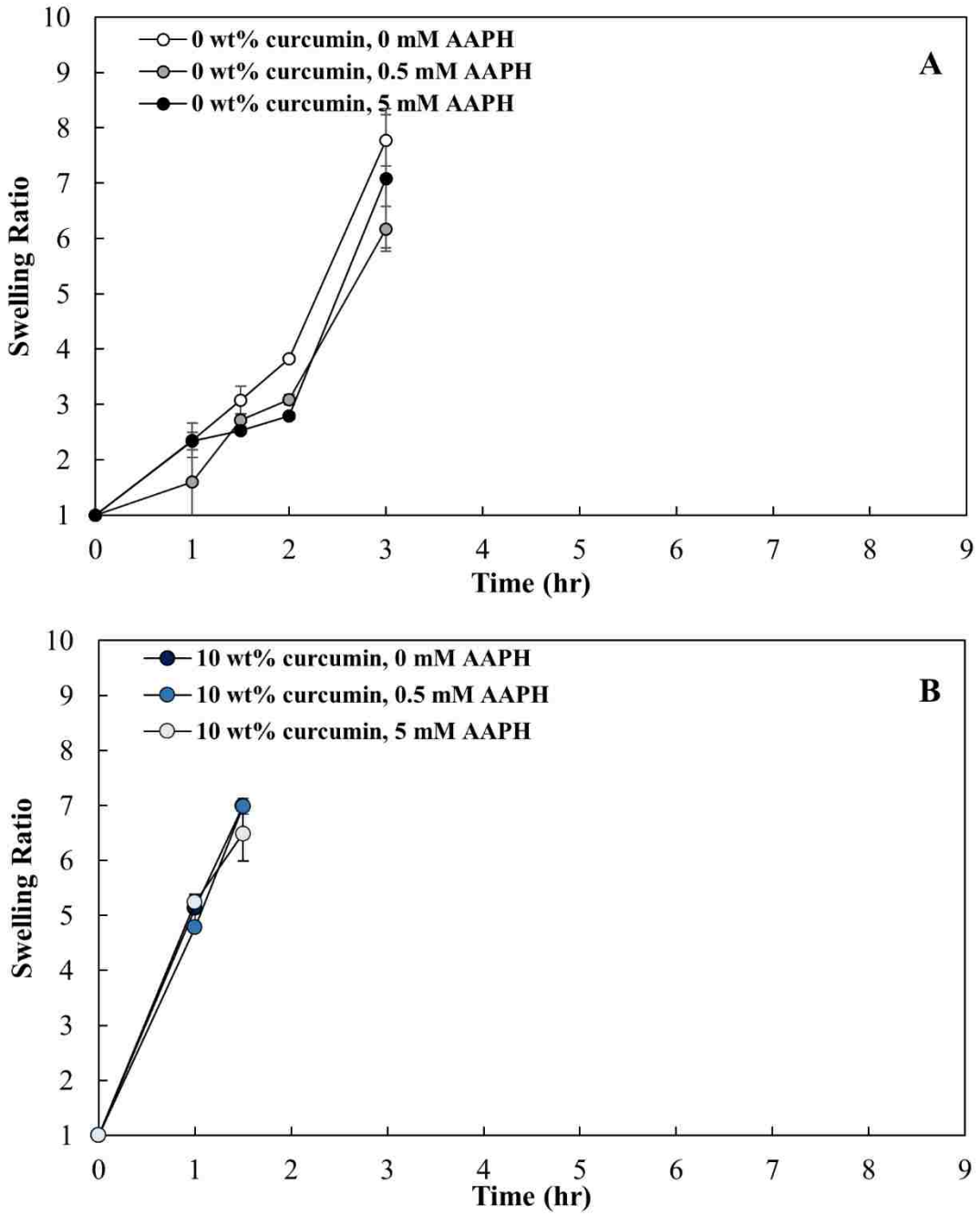

Figure 4-1: Swelling ratio profiles of (A) 0 wt%, (B) 10 wt%, (C) 26 wt%, (D) 32 wt% curcumin-conjugated PBAE films in the presence of 0, 0.5 and 5 mM AAPH solution. (Mean ± SEM, n = 3)

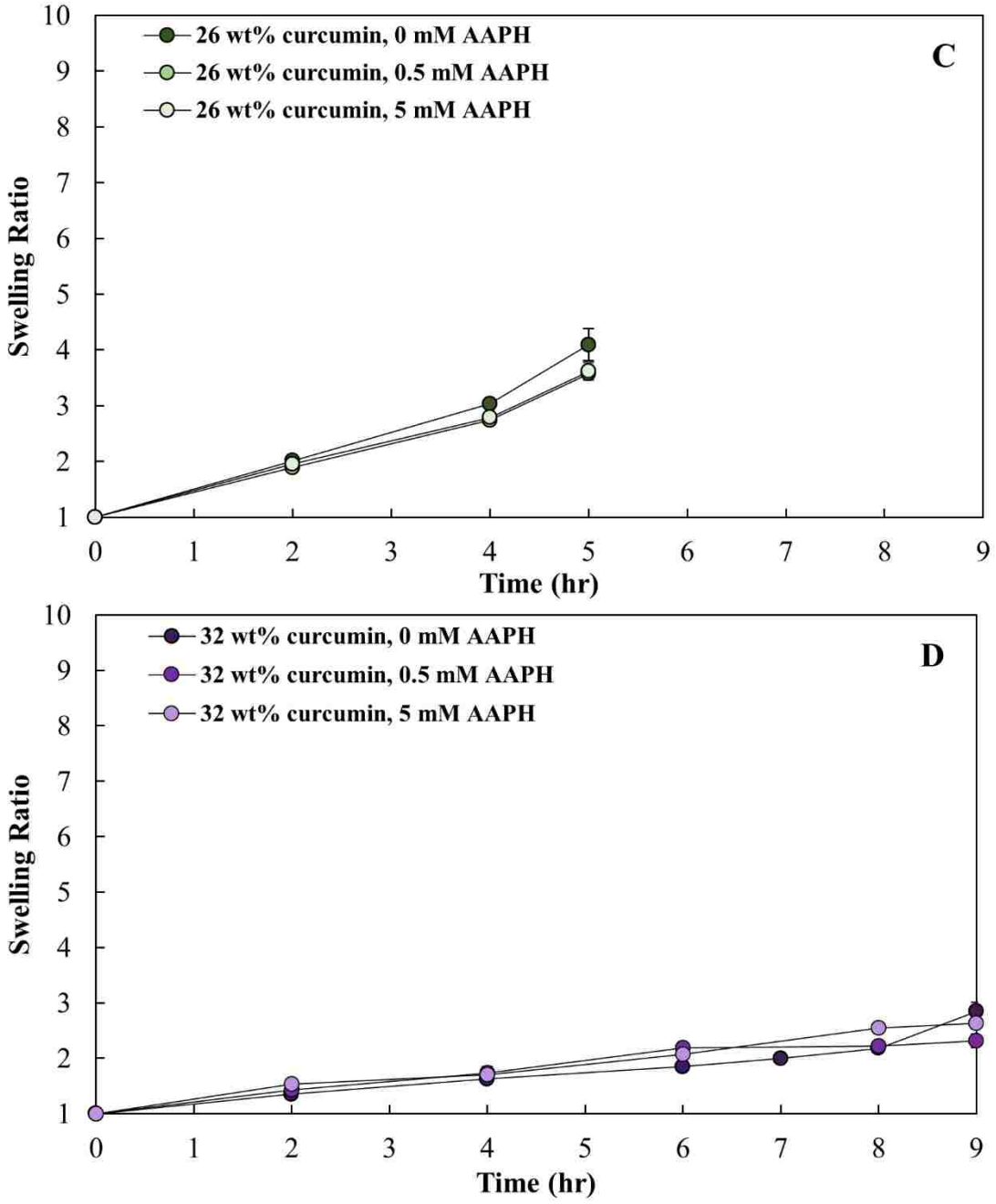

Figure 4-1 (continued): Swelling ratio profiles of (A) 0 wt%, (B) 10 wt%, (C) 26 wt%, (D) 32 wt% curcumin-conjugated PBAE films in the presence of 0, 0.5 and 5 mM AAPH solution. (Mean ± SEM, n = 3)

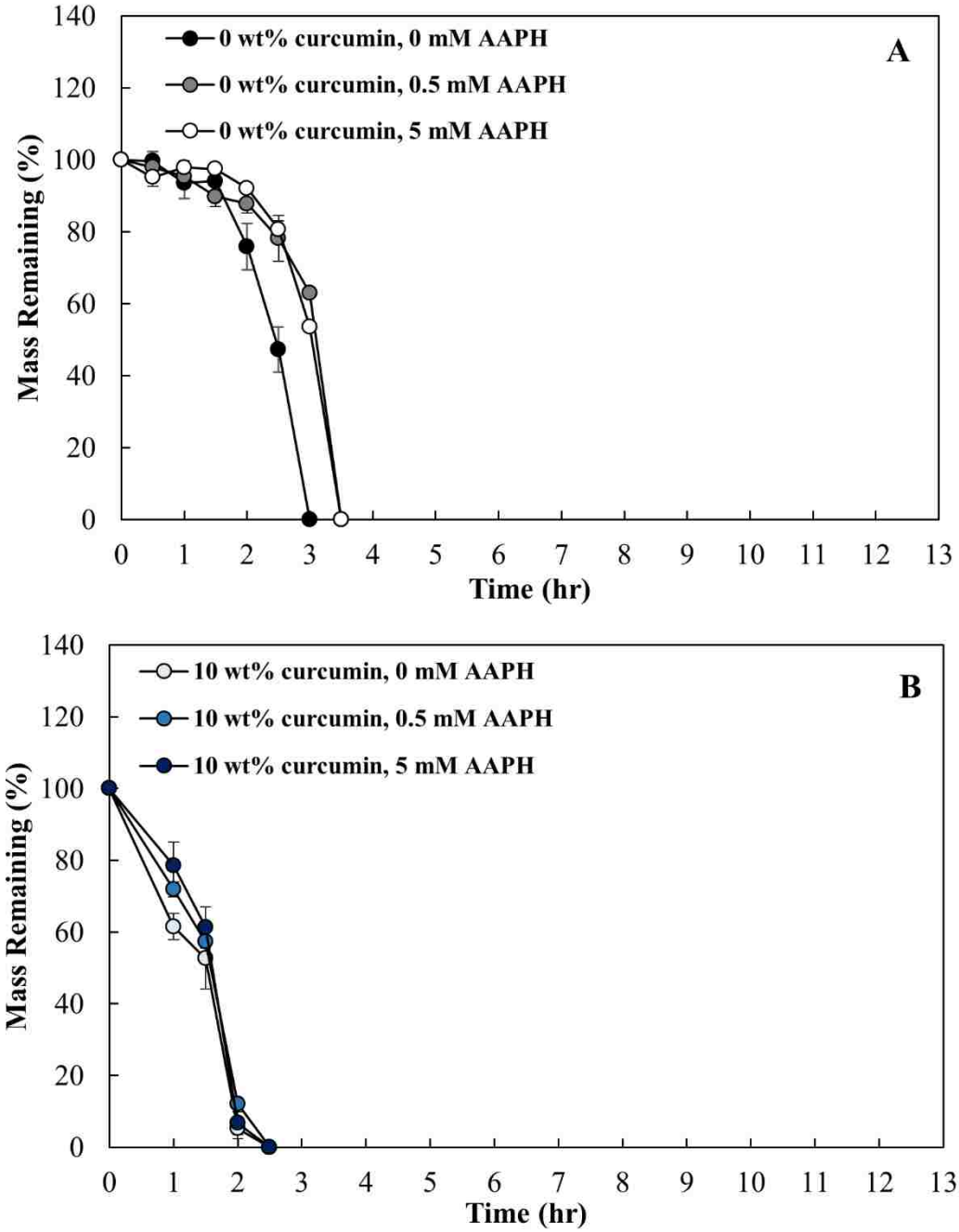

Figure 4-2: Mass remaining profiles of (A) 0 wt%, (B) 10 wt%, (C) 26 wt%, and (D) 32 wt% curcumin films in the presence of 0, 0.5 and 5 mM AAPH. (Mean ± SEM, n =3)

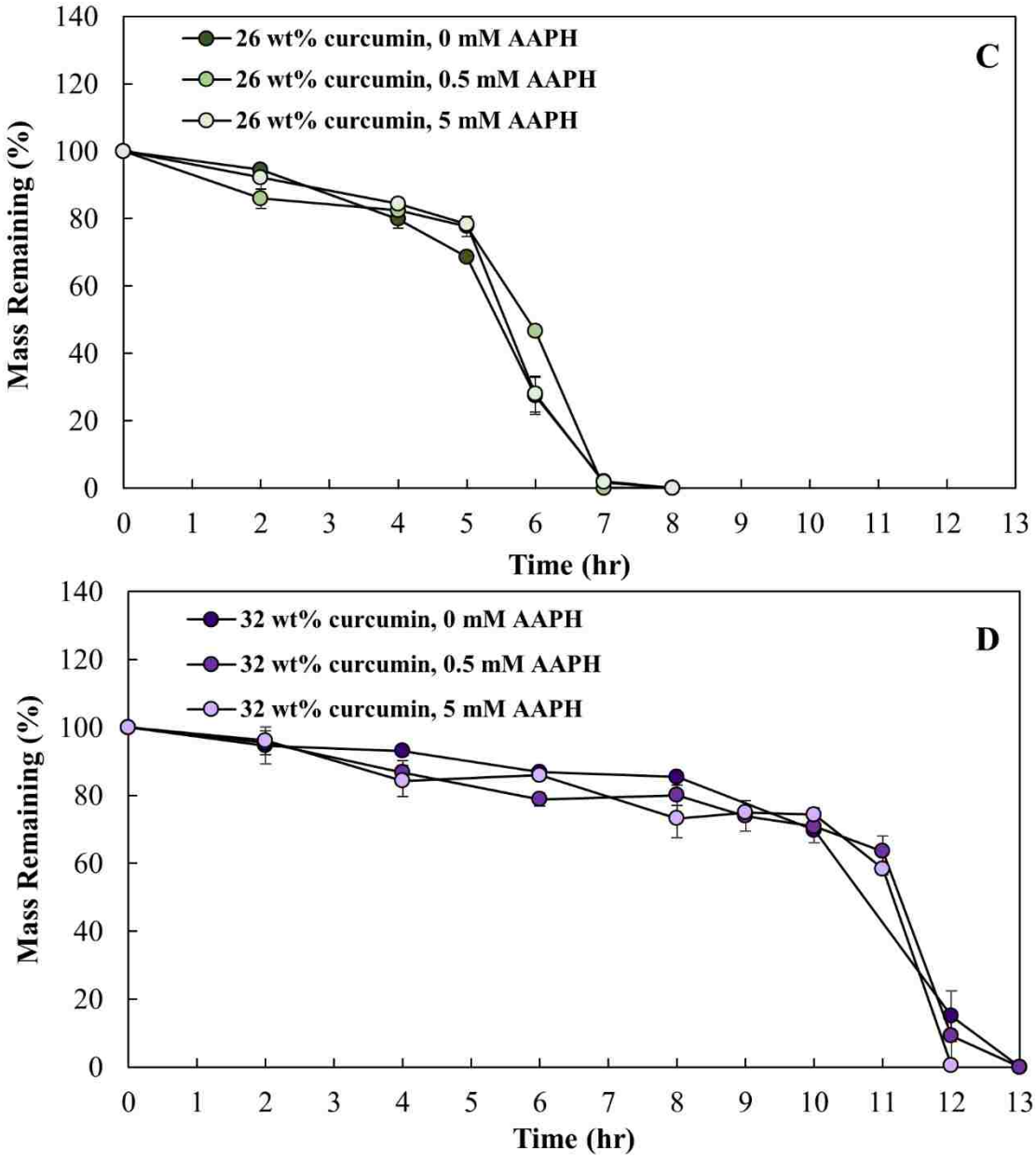

Figure 4-2 (continued): Mass remaining profiles of (A) 0 wt%, (B) 10 wt%, (C) 26 wt%, and (D) 32 wt% curcumin films in the presence of 0, 0.5 and 5 mM AAPH. (Mean ± SEM, n =3)

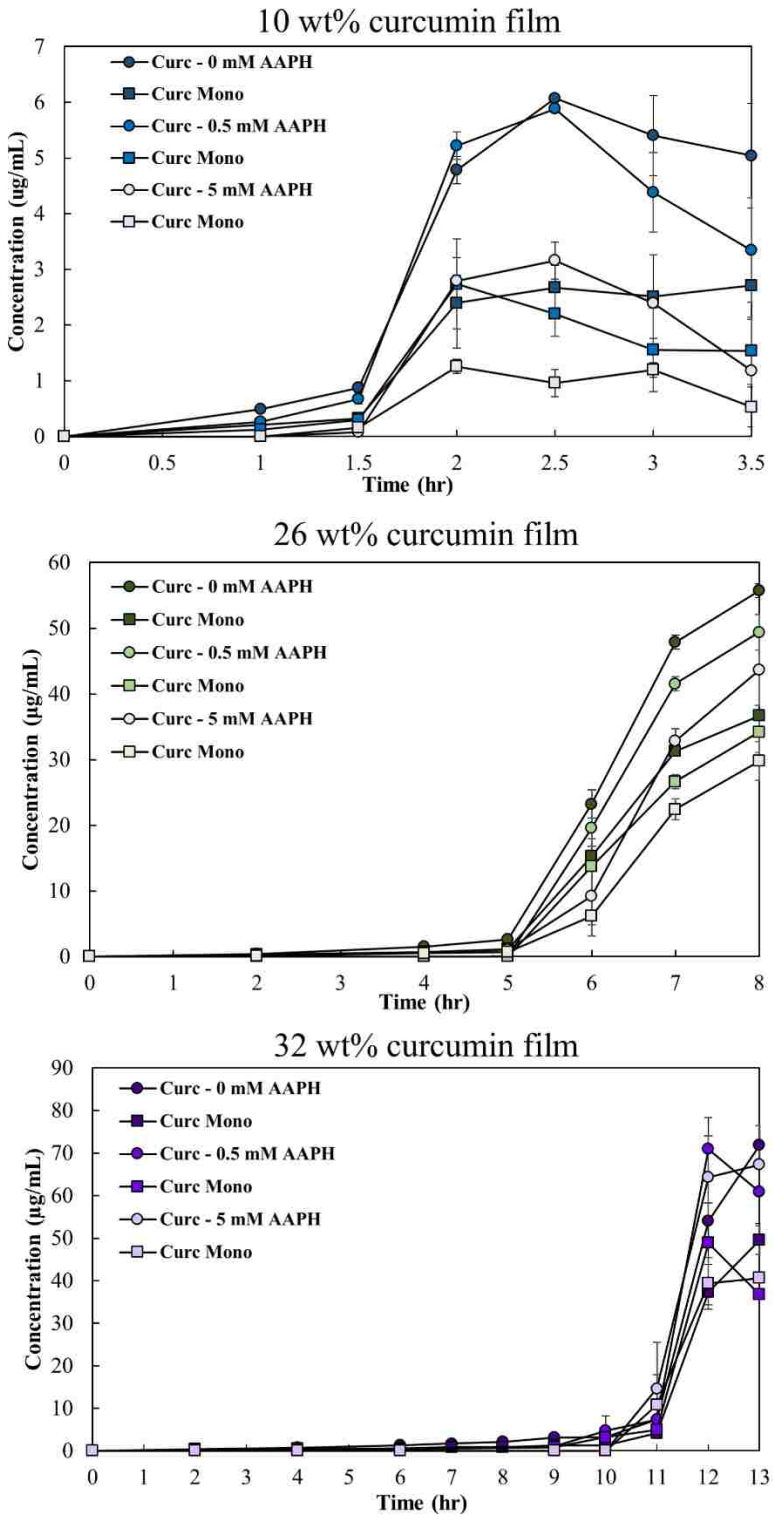

Figure 4-3: HPLC analysis of the curcumin release products in the presence of 0, 0.5 and 5 mM AAPH solutions. (Mean ± SEM, n =3)

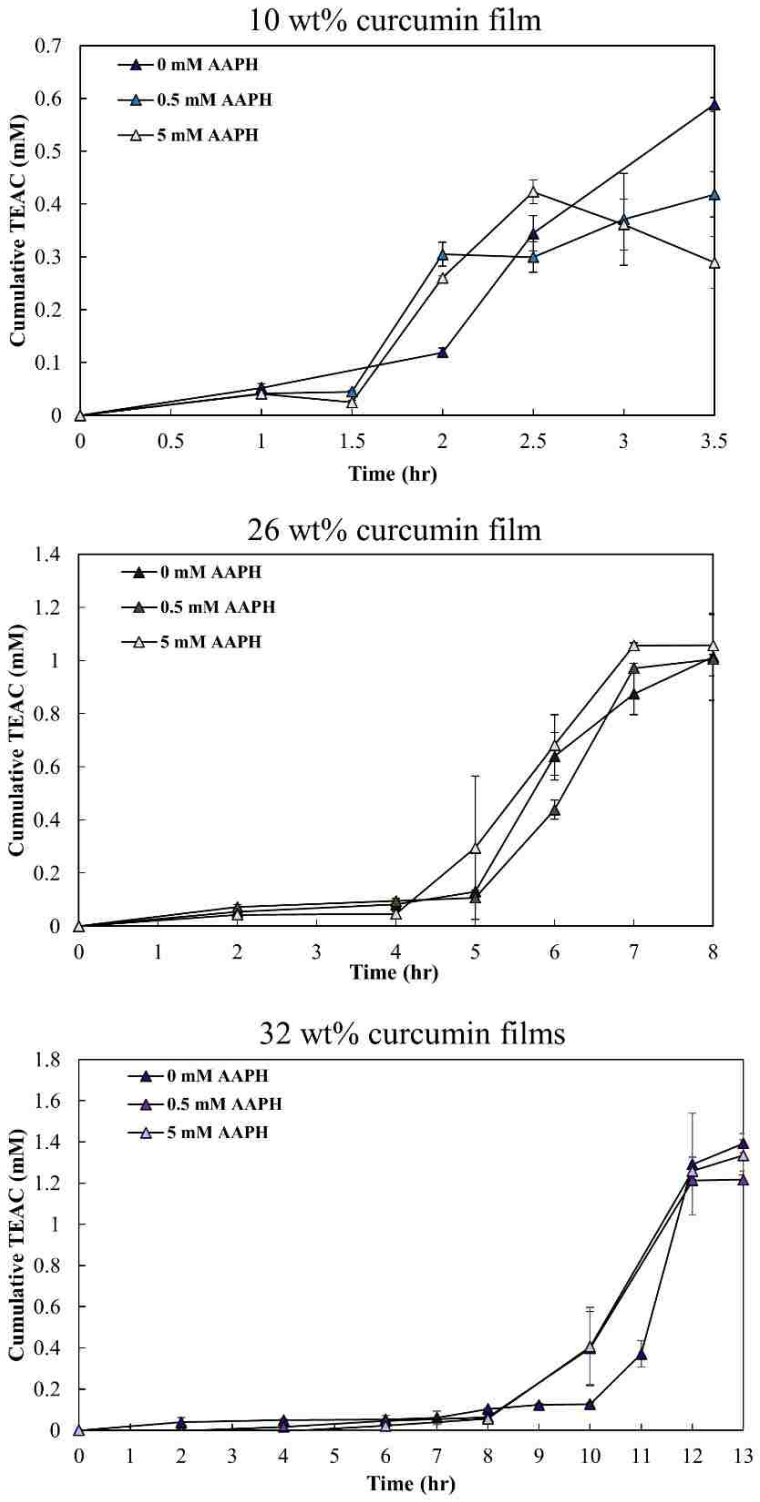

Figure 4-4: Cumulative trolox equivalence antioxidant concentration (TEAC, mM) of 10, 26, and 32 wt% films in the presence of 0, 0.5, 5 mM AAPH. (Mean ± SEM, n =3)

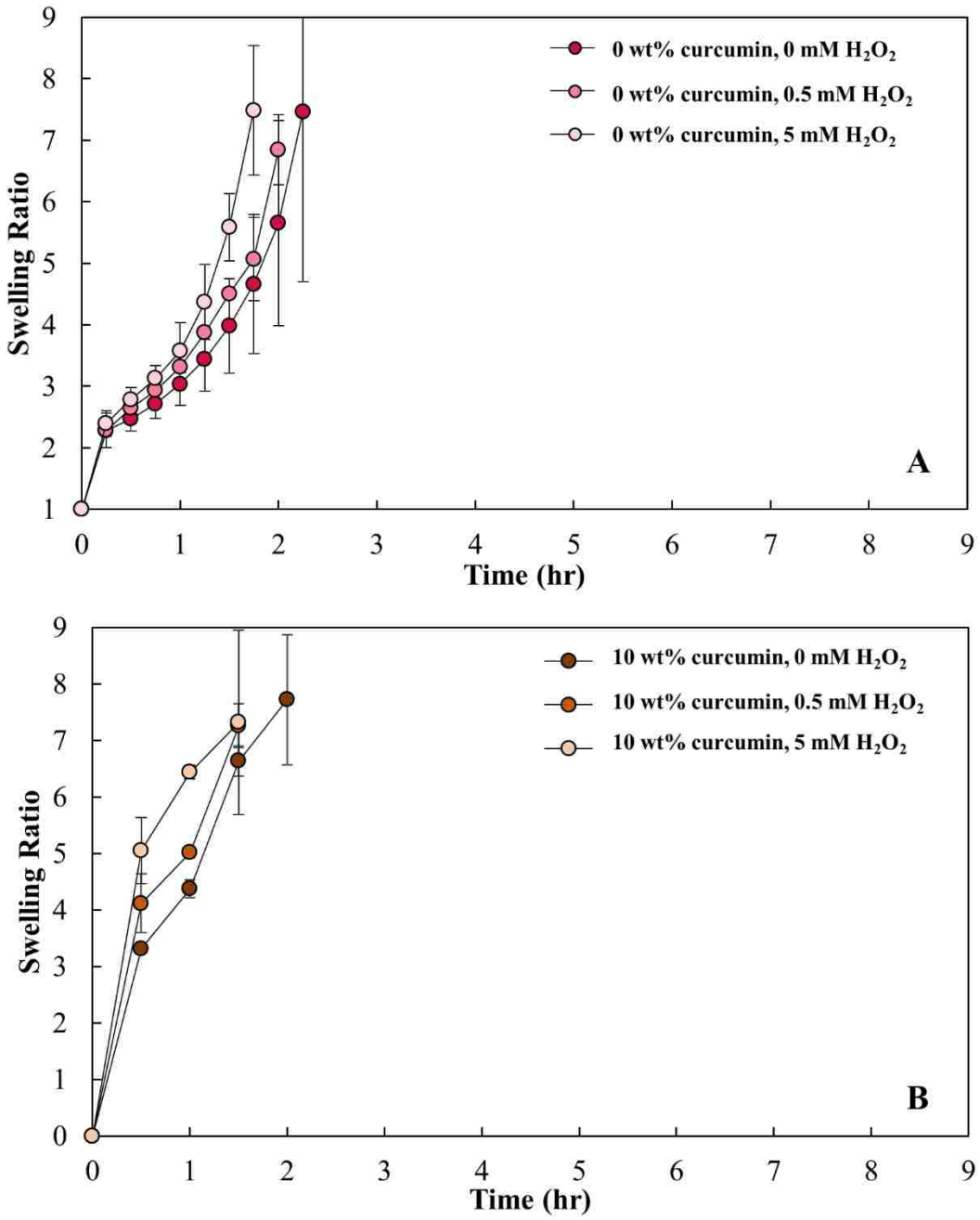

Figure 4-5: Swelling ratio profiles of 0 wt% (A), 10 wt% (B), 26 wt% (C), and 32 wt% (D) curcumin-conjugated PBAE films in the presence of 0, 0.5 and 5 mM H_2O_2. (Mean ± SEM, n = 3)

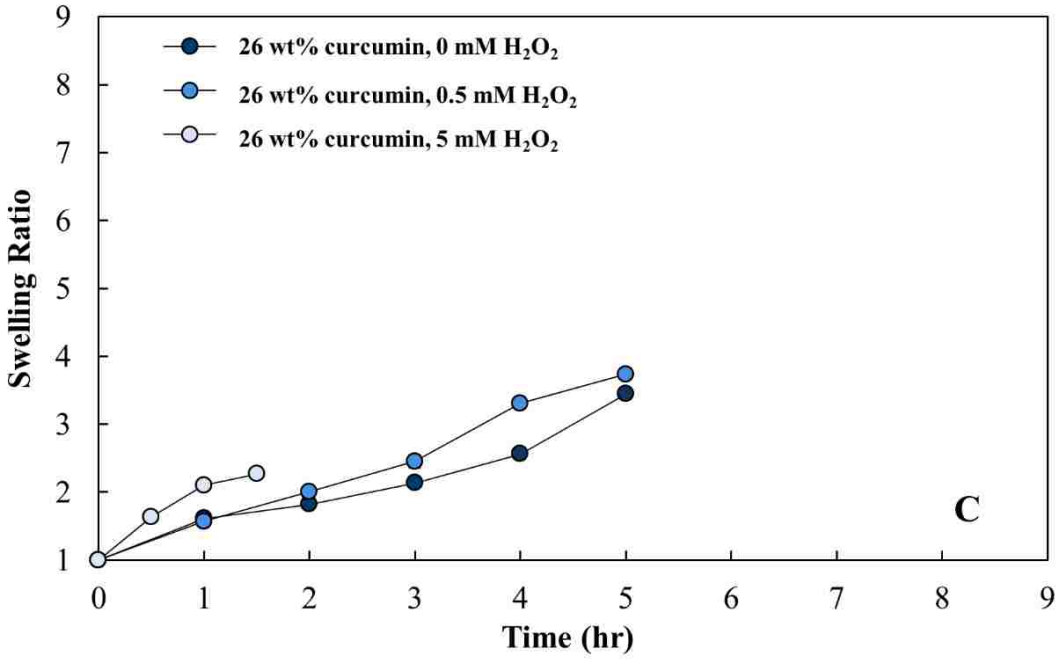

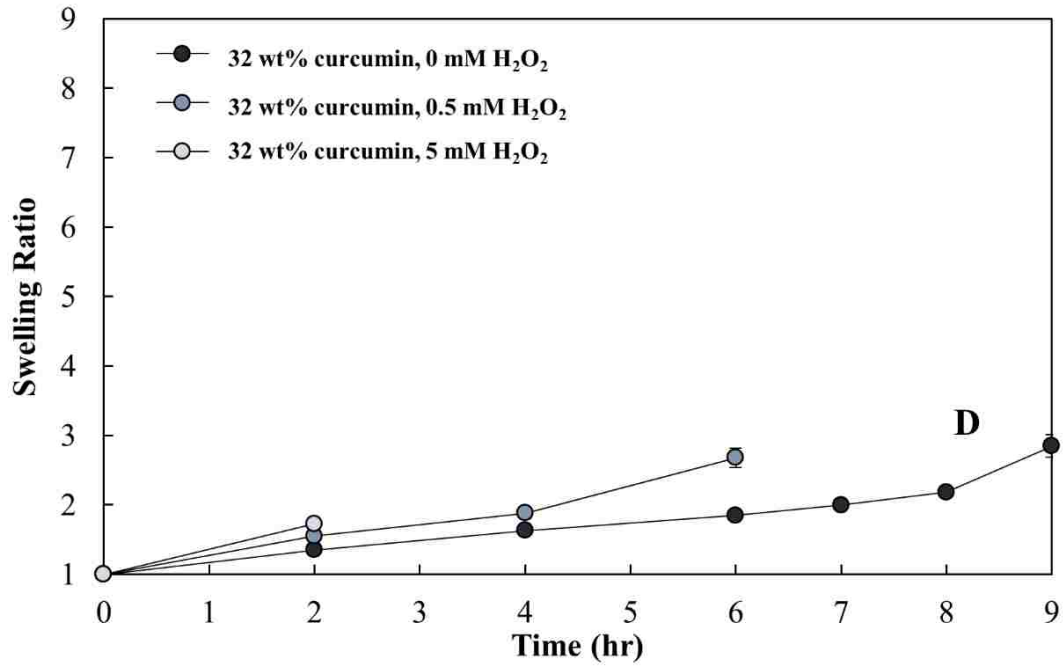

Figure 4-5 (continued): Swelling ratio profiles of 0 wt% (A), 10 wt% (B), 26 wt% (C), and 32 wt% (D) curcumin-conjugated PBAE films in the presence of 0, 0.5 and 5 mM H_2O_2. (Mean ± SEM, n = 3)

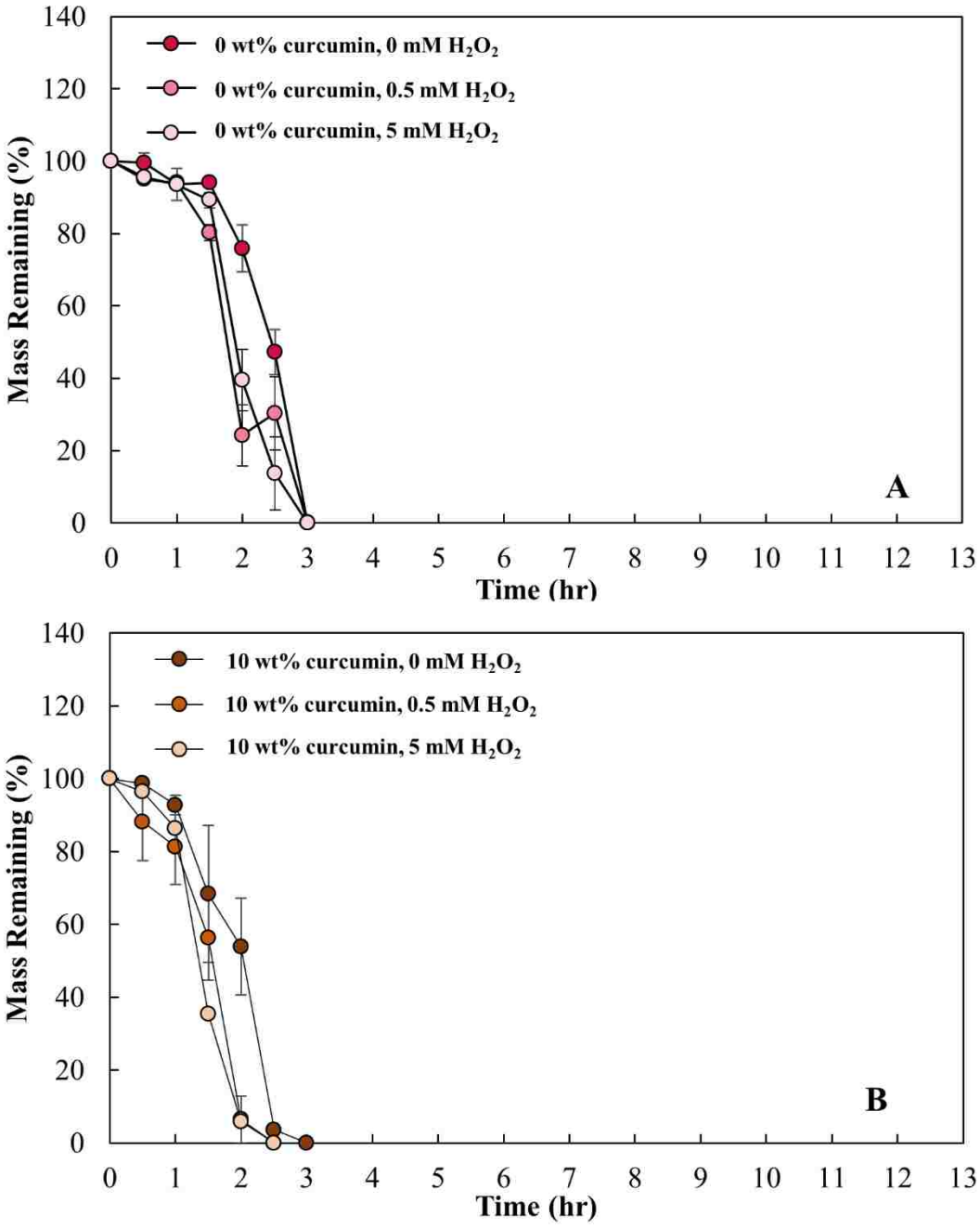

Figure 4-6: Mass remaining profiles of (A) 0 wt%, (B) 10 wt%, (C) 26 wt%, and (D) 32 wt% curcumin films in the presence of 0, 0.5 and 5 mM H_2O_2. (Mean ± SEM, n = 3)

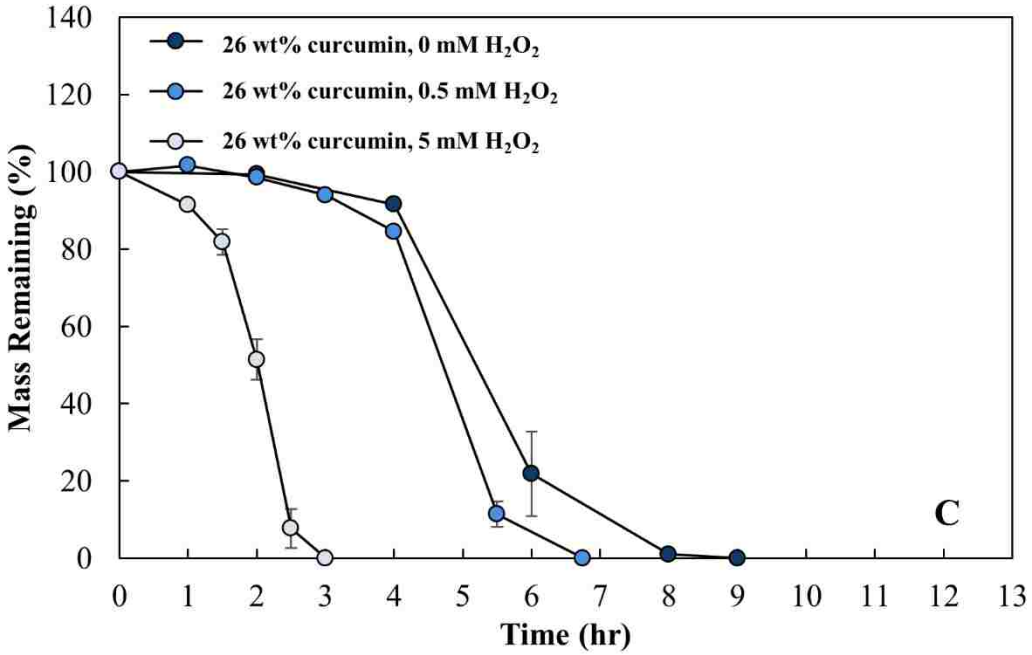

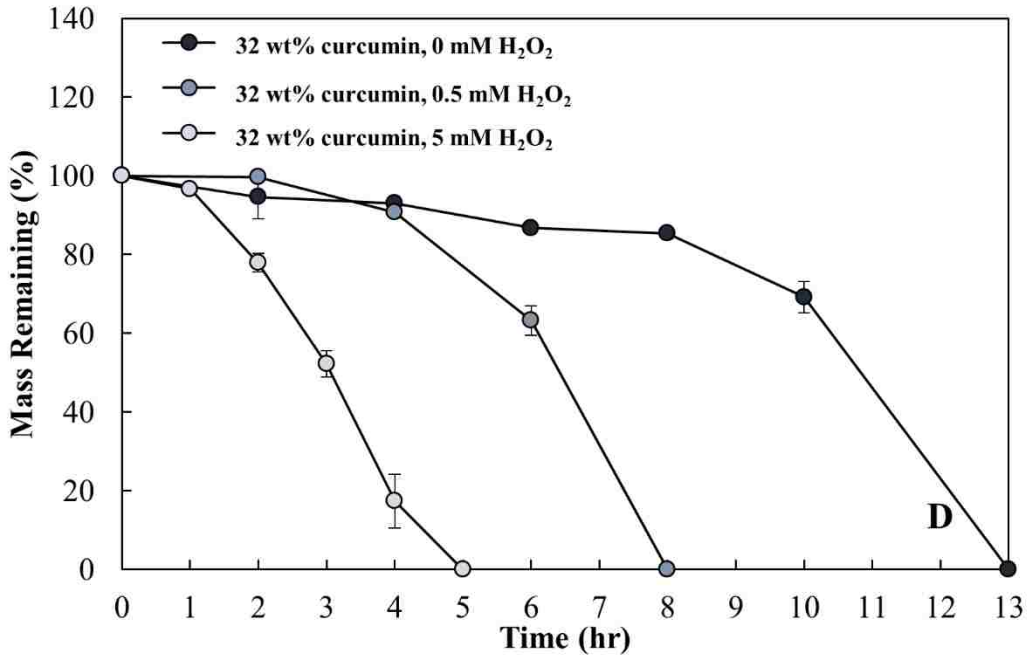

Figure 4-6 (continued): Mass remaining profiles of (A) 0 wt%, (B) 10 wt%, (C) 26 wt%, and (D) 32 wt% curcumin films in the presence of 0, 0.5 and 5 mM H_2O_2. (Mean ± SEM, n = 3)

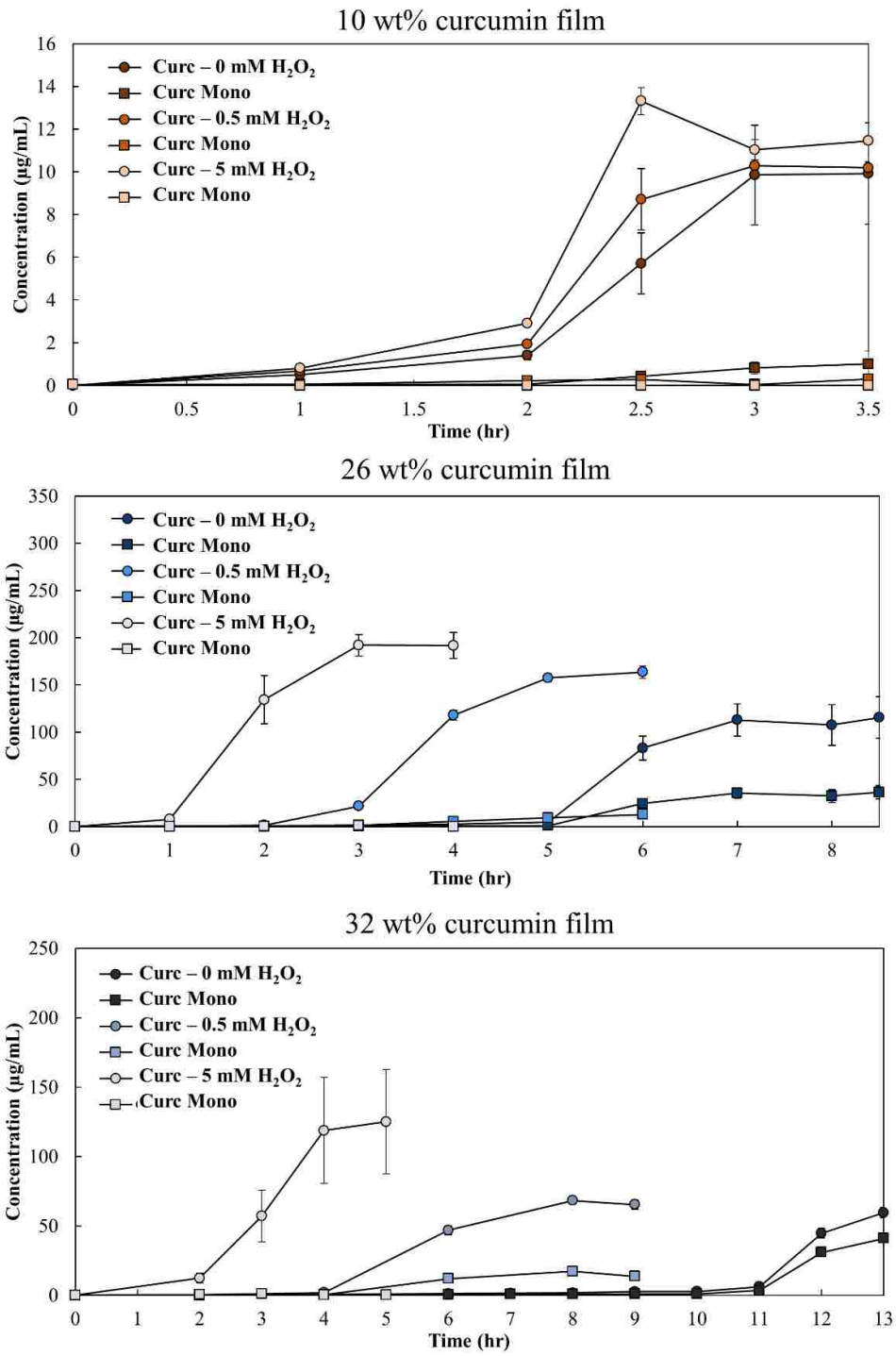

Figure 4-7: Release profiles of curcumin and curcumin monoacrylate from 10, 26, and 32 wt% curcumin PBAE films. (Mean ± SEM, n =3)

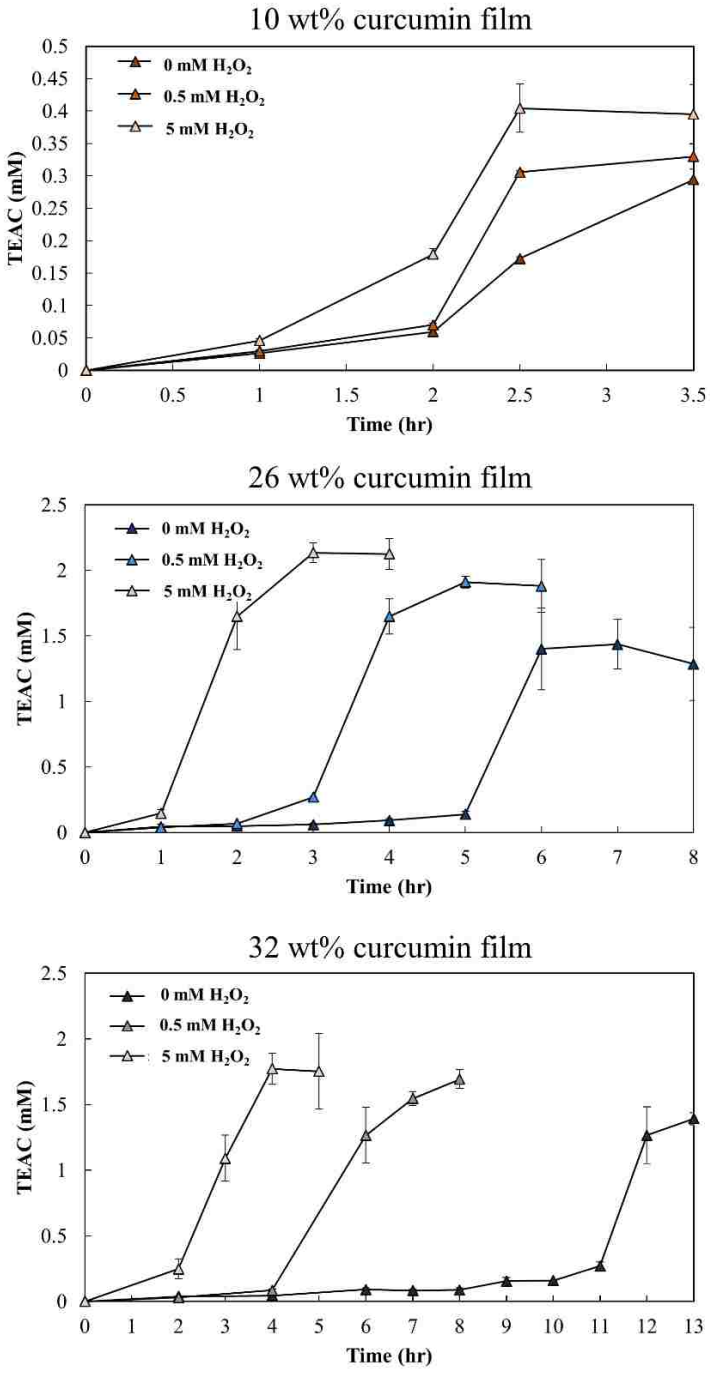

Figure 4-8: Cumulative antioxidant capacity reported as an equivalent trolox concentration (mM) for 10, 26, and 32 wt% curcumin films in the presence of hydrogen peroxide. (Mean ± SEM, n =3)

Chapter 5 pH-Responsive Behavior of Hydrolytically Degradable Curcumin Conjugated Poly(beta-amino ester) Hydrogels

5.1 Introduction

Biologically compatible polymers have been extensively studied for their use in drug delivery with pH-responsive systems of particular interest as polymeric carriers [9, 138, 139]. Buffered pH solutions have been used to mimic endosomal and lysosomal storage conditions, as well as pH changes at different mucosal surfaces (e.g. GI tract, vaginal, and oral) to understand vehicle stability and drug delivery at varying sites [140-142].

Poly(beta-amino esters) are a specific class of pH-responsive polymers that show great promise in drug delivery due to their biocompatibility and low toxicity. These polymers have been used for gene delivery [132, 143] and the synthesis of hydrogels [11, 116, 133]. By incorporating primary diamines into the synthesis, the PBAE linkages can form crosslinked hydrolytically degradable networks rather than linear polymers and can conjugate acrylated drugs in to the system. Through the modification of their phenol groups to form acrylates, antioxidants can be incorporated into a polymer via Michael Addition chemistry [110]. Antioxidant release occurs during hydrolytic cleavage of the ester bond between the acrylate monomers and amine crosslinker in the presence of water. It has been consistently documented that linear PBAE polymers are pH-sensitive and experience rapid degradation and accelerated swelling in acidic environments because their mechanism of hydrolysis is acid-catalyzed [144-147]. Despite the consistent story that PBAE polymers are acid-sensitive, the effect of pH on the degradation of crosslinked PBAE networks has

not been studied. In this chapter, the hydrolysis of crosslinked PBAE polymers was shown to be base-catalyzed. Although not directly related, environments of oxidative stress can be coupled with acidic environments, such as in the process of tissue ischemia, where acidic environments are produced by ischemic/hypoxic insult [148]. Since these materials will ultimately be utilized to counterbalance free radicals present in oxidative stress induced diseases, environmental stimuli other than free radicals is a key factor to consider when characterizing the responsiveness and stability of the material.

In this study, we compare three different polymer systems by investigating the total polymer content, swelling ratio, and release of a polyphenolic antioxidant, curcumin, over time. By incorporating poly(ethylene glycol) (400) diacrylate (PEG(400)DA), the hydrophilicity and the release rate of the polymer can be controlled at neutral pH. As the incorporation of curcumin increases in the network, so does the hydrophobicity. This results in longer release times for curcumin from the hydrogels. Additionally, the ester bonds in all three polymers are stabilized in acidic pH, decreasing the release rate of curcumin significantly based on its initial degradation time. These results aid in our understanding of the impact that physicochemical properties have on pH behavior in polymers. It may also allow for the fine tuning of polymers to create precise pH release points, increasing the sensitivity to physiological cues. Additionally, it holds potential for the design of water-sensitive pharmaceuticals that could be stored in acidic environments for short or extended periods of time.

5.2 Materials and Methods

5.2.1 Materials

Curcumin was purchased from Chem-Impex International, Inc (Wood Dale, IL). Poly(ethylene glycol) (400) diacrylate (PEG(400)DA) was obtained from Polysciences, Inc. (Philadelphia, PA). 4,7,10-Trioxatridecane-1,13-diamine (TTD), sodium hydroxide, hydrochloric acid, and Tween 80 was purchased from Sigma Aldrich (St. Louis, MO). Citric acid and sodium phosphate dibasic dodecahydrate was purchased from VWR (Radnor, PA). Dichloromethane, tetrahydrofuran (THF), and acetonitrile was obtained from Pharmco-Aaper (Brookfield, CT). No additional purification steps were conducted after materials were received.

5.2.2 Synthesis of Curcumin Multiacrylate

Curcumin was functionalized into curcumin multiacrylate (CMA) by reacting its three hydroxyl sites with acryloyl chloride using an acid-esterification reaction similar to Patil et al. Briefly, 30 g of curcumin was dissolved in 600 mL of anhydrous THF. TEA was added in a 1:3 (curcumin:TEA) molar ratio. After the addition of TEA, acryloyl chloride was added at a 1:3 (curcumin:acryloyl chloride) ratio. The reaction was purged under nitrogen and then left to react in the dark for 18 hours. The product was then filtered to remove any TEA-HCl salts, and the THF was evaporated using a rotary evaporator. The product was reconstituted in anhydrous dichloromethane and two liquid-liquid extraction washes were executed with 0.1M HCl and 0.1M K_2CO_3 to remove any residual TEA, acryloyl chloride, and acrylic acid. The organic phase was collected and introduced to anhydrous magnesium sulfate to remove any residual water. The solution was then filtered once more and dried completely using a rotary evaporator to result in crystallized CMA.

The product was run at 50 µg/mL in acetonitrile using a reverse-phase high performance liquid chromatography unit (HPLC) with an attached UV detector at 420 nm (Phenomenex C18 column, 5 µm, 250 mm (length) x 4.6 mm (ID) on a Shimadzu Prominence LC-20 AB HPLC system attached to a Waters Refractive Index Detector) to verify complete conversion of curcumin to curcumin multiacrylate product and stored at -20°C away from light until use.

5.2.3 Synthesis of Poly(beta-amino ester) Films

Poly(beta-amino ester) films were synthesized similar to Patil et al[116]. Briefly, CMA and PEG(400)DA were reacted with TTD to form a crosslinked amphiphilic network utilizing Michael Addition chemistry in anhydrous dichloromethane (aDCM). The molar ratio of CMA to PEG(400)DA was varied (**Table 5-1**). The ratio of total acrylates to amine protons was set to a value of 1.0, and 1.5 times the total monomer mass of aDCM was used for the reaction. CMA was solubilized in half of the desired aDCM. PEG(400)DA and TTD were added to the remaining aDCM in a separate tube for 5 minutes to allow for initial crosslinking. CMA was added directly to the PEGDA/TTD mixture while mixing on a Vortex-mixer and the entire reaction solution was added to a casting ring on a leveled platform and covered with a watch glass and left for 1 hour at room temperature. After 1 hour, the film was placed in a convection oven at 50°C for 24 hours. Synthesized films were washed at 40 mL of anhydrous acetonitrile per 1 gram of total polymer 5 times at 1 hour each to remove any unreacted monomers. Washed films were dried under vacuum at 50°C for 24 hours.

5.2.4 Conversion of CMA to Curcumin in the Presence of HCl and NaOH

100 μg/mL CMA was exposed to three different concentrations of NaOH or HCl in a 0.1% (w/v) Tween 80 phosphate-buffered saline (PBS) solution. After 30 minutes, solutions were adjusted back to pH 7.4 to maintain consistent colorimetric properties of CMA and samples were analyzed using HPLC with an attached UV detector at 420 nm. Conversion of curcumin was quantified using a standard curve of curcumin and compared to the initial concentration of CMA in solution.

5.2.5 Total Polymer Content of PBAE Films in Acidic Environments

Individual films (n = 3) for each time point were measured to obtain the percent of polymer mass remaining over time of the three compositions of hydrogels in citrate-phosphate buffer solutions at pH of 3, 5, 7 with the ionic strength kept constant at 0.5M (I = 0.5M) in an agitating shaker bath at 37°C. The buffer recipes were taken from Elving et al [149] with the addition of Tween 80 at 0.1% (w/v). Empty microcentrifuge tubes were weighed. At each desired time point, films were removed from the bath, blotted dry on a Kimwipe®, and the swollen mass was measured. The swollen polymer mass was then collected in the microcentrifuge tube and placed in the freezer until frozen. The films were then freeze dried overnight, and the mass of the microcentrifuge tube plus the dried mass was measured. Knowing the mass of the swollen polymer (M_s) and the initial mass of the polymer (M_I), the amount of water retained by the film is known (M_w) and calculated using the following equation:

$$M_W = M_S - M_I \quad (1)$$

After the swollen film was freeze-dried, the salts from the buffer remained. The theoretical amount of residual salts was calculated from the mass of the known water and

the salts were subtracted from the dried polymer mass to obtain the mass of the dried film. The mass remaining percentage is defined as the following:

$$\%\, Mass\ Remaining = M_{FR}/M_I \quad (2)$$

where M_{FR} is the mass of the film dried that remained.

5.2.6 Swelling Response of PBAE Films in Acidic Environments

Circular disks were punched out of a bulk film of each composition of material and submerged in citrate-phosphate buffered solutions of pH of 3, 5, and 7 with a constant ionic strength of 0.5M and placed in a 37°C shaking water bath. At each desired time point films were removed from buffer, and excess buffer solution was removed with a Kimwipe®, and weighed for swollen polymer mass. Mass was recorded until films lost integrity and were unable to be handled. The swelling ratio of the film is defined as:

$$Swelling\ Ratio = M_S/M_I \quad (3)$$

where M_S is the mass of the swollen film and M_I is the mass initial dry film.

5.2.7 Release Profiles of Curcumin Conjugated PBAE Films in Acidic Environments

The cumulative release profiles of the PBAE films with curcumin incorporated into the network were investigated in pH 3, 5, and 7 solutions with a constant ionic strength of 0.5M. The same discs used to measure swelling profiles were used. At desired time points, one milliliter of supernatant was collected and analyzed using UV-Visible Spectroscopy at 420 nm to quantify curcumin release products and the sample was replenished with fresh buffer. The replenishing step was compensated for in the cumulative release calculations to keep the volume constant throughout the degradation.

5.3 Results and Discussion

5.3.1 pH-Dependent Conversion of CMA to Curcumin

The integrity of CMA in alkaline and acidic environments was investigated by introducing CMA to different concentrations of NaOH and HCl in 0.1(w/v)% Tween 80 PBS for 30 minutes (**Figure 5-1)**. In **Figure 5-1B**, the three HPLC peaks represent bisdemethoxycurcumin, demethoxycurcumin, and curcumin as elution time progresses respectively (5.45, 5.65, and 6 minutes). After 30 minutes of exposure to 0.003M NaOH, the diacrylate form of CMA (retention time peaks of 10.5, 10.8 and 11.1 minutes) decreased, while the monoacrylate form increased (7.95 and 8.35 minutes) with the emergence of curcumin peaks (**Figure 5-1C**). The decrease in diacrylate and increase in monoacrylate peaks indicated instability of the diacrylate form in alkaline conditions and a step-wise mechanism of hydrolysis that caused conversion back to curcumin. Exposure to 0.03M and 0.3M NaOH for 30 minutes resulted in complete hydrolysis of the multiacrylate compositions; however, the recovery of curcumin was low, at 12% and 8% (**Figure 5-1D and 5-1E**, respectively). In the presence of a strong base, curcumin itself could be degrading into other degradation products that may not be visible at 420 nm, such as feruloylmethane[150]. In **Figure 5-1E**, the curcumin peak decreased disproportionally to the curcumin standard, showing instability of curcumin in the presence of strong alkaline conditions; however, complete hydrolysis was observed.

CMA was then exposed to three different concentrations of HCl in 0.1% (w/v) Tween 80 PBS. HPLC data for this experiment are presented in **Figure 5-2**. After 30 minutes of exposure to 0.003M HCl, no hydrolysis occurred, and the recovery of curcumin was 0%. After 30 minutes in 0.03M HCl, a slight decrease in CMA was seen, but hydrolysis

to curcumin did not occur. Not until the material was exposed to 0.3M HCl for 30 minutes did the characteristic peaks of curcumin emerge in the sample. This only represented 2.5% of the theoretical amount of curcumin to be converted, and 50% of the initial CMA remained. Therefore, CMA appears to degrade in strong acidic environments before hydrolysis occurred.

The investigation of CMA conversion in strong acid and base conditions showed the alkaline sensitivity of the curcumin acrylate monomer that is incorporated in the PBAE polymer. The hydrolysis of the monomer is base-catalyzed, and so the reaction is less favored in acidic environments and the rate will slow drastically, which is consistent with the results for film degradation studies presented later in the chapter.

5.3.2 Degradation of 0 wt% curcumin conjugated PBAE Films

Curcumin free (0 wt% curcumin) films were synthesized, washed, and dried under vacuum at 50°C in preparation for degradation in three different citrate-phosphate buffered solutions of pH 3, 5, and 7, all with a constant strength of 0.5M (**Figure 5-3)**. All solutions were supplemented with 0.1% (w/v) Tween 80 to increase solubility of degradation products for all studies. The 0 wt% curcumin conjugated films in pH 7, I = 0.5M swelled to an equilibrium swelling ratio of 7.11 ± 1.1 over 3 hours (**Figure 5-3A**) until the film could not be handled. The hydrolysis of the hydrophilic network resulted in a degradation time of 3.5 hours (**Figure 5-3B**). The films were then investigated in pH 5, I = 0.5M and the swelling ratio of the film over time was found to be insignificant to the swelling ratio in pH 7; however, the maximum ratio was reached at 48 hours, 45 hours later than the neutral solution. The degradation time increased to 72 hours. Interestingly, the lowest pH solution of 3 at I = 0.5M had the slowest rate of swelling, and the longest degradation

period. The maximum swelling ratio was 7.08 ± 0.91, similar to the swelling ratios of pH 5, and pH 7; however, the duration of the degradation time extended up to 5 weeks. The rates of swelling and degradation were significantly different in all three solutions. Crosslinked PBAE result in base-catalyzed hydrolysis for degradation, where in acidic environments, the concentration of $[H^+]$ is greater, resulting in lower concentrations of $[OH^-]$ to play the role as a nucleophile. This effect decreases the rate of uptake in the polymer as well as the rate of hydrolysis, decelerating both responses within the network.

5.3.3 Degradation of 26 wt% curcumin conjugated PBAE Films

26 wt% curcumin conjugated films were degraded in three different environments: pH 3, 5, and 7, all with a constant ionic strength of 0.5M (**Figure 5-4**). As the acidity of the solution increased, the rate of degradation and polymer mass loss over time drastically decreased. The 26 wt% curcumin PBAE film in a neutral solution degraded within 8 hours, whereas the same film degraded in 24 hours in pH 5 and 240 hours in pH 3 (**Figure 5-4A**). The rate of hydrolysis decreased significantly with decrease in pH. Interestingly, the initial swelling ratio of the films in both pH 3 and 5 buffered solutions were greater over the first 2 hours (**Figure 5-4B**); however, a temporary plateau occurred over 2 days where 26 wt% film remained at 2.5 ± 0.067 until the initial hydrolysis of the film was initiated and the integrity was lost after 120 hours. The release of polymer degradation products that absorb at 420 nm, which include degradation products that absorb at curcumin's maximum wavelength, align with the total polymer content and ratio profiles in the three solutions. Release plateaued after 8 hours, 24 hours, and 144 hours for pH solutions at 7, 5, and 3, respectively (**Figure 5-4C**). Interestingly, in the low pH condition the total polymer content was not fully degraded until 168 hours, yet the absorbance of release products plateaued at

144 hours. This could be due to degradation of the curcumin release products in the acidic environment over time, or due to the higher incorporation of PEG(400)DA, which showed higher stability in pH of 3 and 5, and may be released after curcumin from the polymer. Therefore, the PBAE hydrolysis rate of the curcumin conjugated portion of the network could be faster than the portion of the network where the PEG(400)DA was incorporated.

5.3.4 Degradation of 32 wt% curcumin conjugated PBAE Films

32 wt% curcumin PBAE films were investigated in the same citrate-phosphate buffered solutions to investigate response to acidic environments (**Figure 5-5)**. In the pH 7 solution, the degradation time of the film was 12 hours. In lower pH conditions, the degradation time increased to 48 hours for pH 5 and 144 hours for pH 3 (**Figure 5-5A**). The shift in total mass remaining over time was significant as the pH changes from 7 to 3 where the degradation time of the network increased from 12 hours to 10 days. Similar to the 26 wt% curcumin films, the rate of swelling was enhanced for the first 6 hours at pH 5, seen in the inset of **Figure 5-5B**. The supernatant was analyzed over time to measure cumulative curcumin release products that absorb at 420 nm. The release profiles aligned with the swelling profiles and polymer mass content over time where the maximum release of curcumin products is 12 hours, 48 hours and 144 hours, respectively as the pH of the solution decreases (**Figure 5-5C**).

5.3.5 Comparative Effect of Curcumin Loading on pH Behavior and Release Time

When comparing the various polymer compositions, some interesting trends arose that are shown in **Table 5-2**. The degradation time increased as curcumin content increased for both pH 5 and 7. However, at the most acidic condition of pH 3, this trend inverts and the degradation time decreased with increasing curcumin loading. This may be due to the

degradation of curcumin in the polymer network in addition to the degradation of the ester bonds alone at very acidic conditions, causing faster degradation times when compared to the stable network in the 100 mol% PEG(400)DA films. This degradation of curcumin at acidic conditions was consistent with the initial pH-sensitivity studies of the monomer (**Figure 5-2**).

An interesting phenomenon observed with the crosslinked PBAE polymers is highlighted in the inset of **Figure 5-4B** and **Figure 5-5B**. Although the overall degradation time decreased in acidic conditions, the crosslinked polymers undergo an initial increased swelling at low pH. This increase in polymer swelling at low pH may be explained by charge-charge interactions. Hydrogel polymers that are pH-responsive exhibit greater swelling in environments that have a pH greater than their local pKa or lower than their local pKa depending on their ionic properties. These amphiphilic pH-responsive hydrogels can develop charges that contribute to repulsive forces responsible for swelling that are dependent on the pH of the solution [13]. The increased swelling of the hydrogel at low pH indicate that crosslinked curcumin-conjugated PBAE polymers may become charged at low pH. This creates repulsive forces that swell the polymer. After some time, the hydrolysis of the polymer backbone surpasses charge effects and the swelling at pH 7 will surpass that at pH 3. This explains why the polymer in a solution of pH 5 has a greater swelling ratio for only a short period. After this point, the rate of hydrolysis exceeds the rate of swelling between the two solutions.

To our knowledge, this is the first investigation showing a base-catalyzed, crosslinked PBAE polymer for drug release. Additionally, it has shown that the combination of a base-catalyzed monomer (CMA) with a hydrophilic monomer (PEGDA)

allows for the precise control of both pH responsive behavior and the release time of a drug payload. This method may be used in the future to fine tune the pH-sensitivity of crosslinked polymers by varying the composition of monomers with differing pH behaviors.

5.4 Conclusions

Three hydrolytically degradable crosslinked networks were investigated in three different citrate-phosphate buffered solutions to investigate degradation in the presence of acidic environments. Initially, the acrylate monomer, CMA, was investigated in strong acidic and basic conditions. This showed a favoring of base-catalyzed hydrolysis of the CMA monomer causing a conversion back to curcumin in alkaline conditions.

The CMA was crosslinked into PBAE networks using a TTD crosslinker with different ratios of PEG(400)DA. The three polymers were compared for their total polymer content, swelling ratio, and absorbance of release products, in three different pH conditions. The release profiles of curcumin were compared for 26 wt% curcumin and the 32 wt% curcumin films. Overall, the hydrogels containing only PEG(400)DA and TTD had rapid uptake of PBS and degraded quickly within 3.5 hours due to the hydrophilicity of the network. Looking at hydrophobicity of the network, the rate of degradation and hydrolysis was significantly slower in pH 7 due to the increase in curcumin content, where the maximum swelling ratio of these networks decrease as well. Overall, the degradation rates decreased drastically in pH 3 and 5 environments for all three polymer systems, especially with no incorporation of CMA.

Future studies with these pH-tunable polymers will incorporate environmental changes over time within each system to look at the stability and change of hydrolysis rates

by first placing the hydrogels in neutral environments and then changing the pH to acidic conditions. The opposite stimuli can be compared as well to observe pulsatile pH response and the inhibition of degradation within the polymer systems. This may hold potential for pH-responsive hydrogel systems that have an on/off switch for drug release in response to pH stimuli.

Table 5-1: Compositions of the curcumin-conjugated poly(beta-amino ester) films investigated.

CMA (mol%)	PEG(400)DA (mol%)	Curcumin (wt%)
0	100	0
50	50	26
60	40	32
all synthesized at a ratio of total acrylate to amine proton moles (RTAAP) of 1.0		

Table 5-2: Comparison of degradation times for each polymer composition in different pH solutions.

Degradation Time (hr)			
pH	Curcumin Loading (%)		
	0	26	32
3	840	240	144
5	48	24	48
7	3.5	8	12

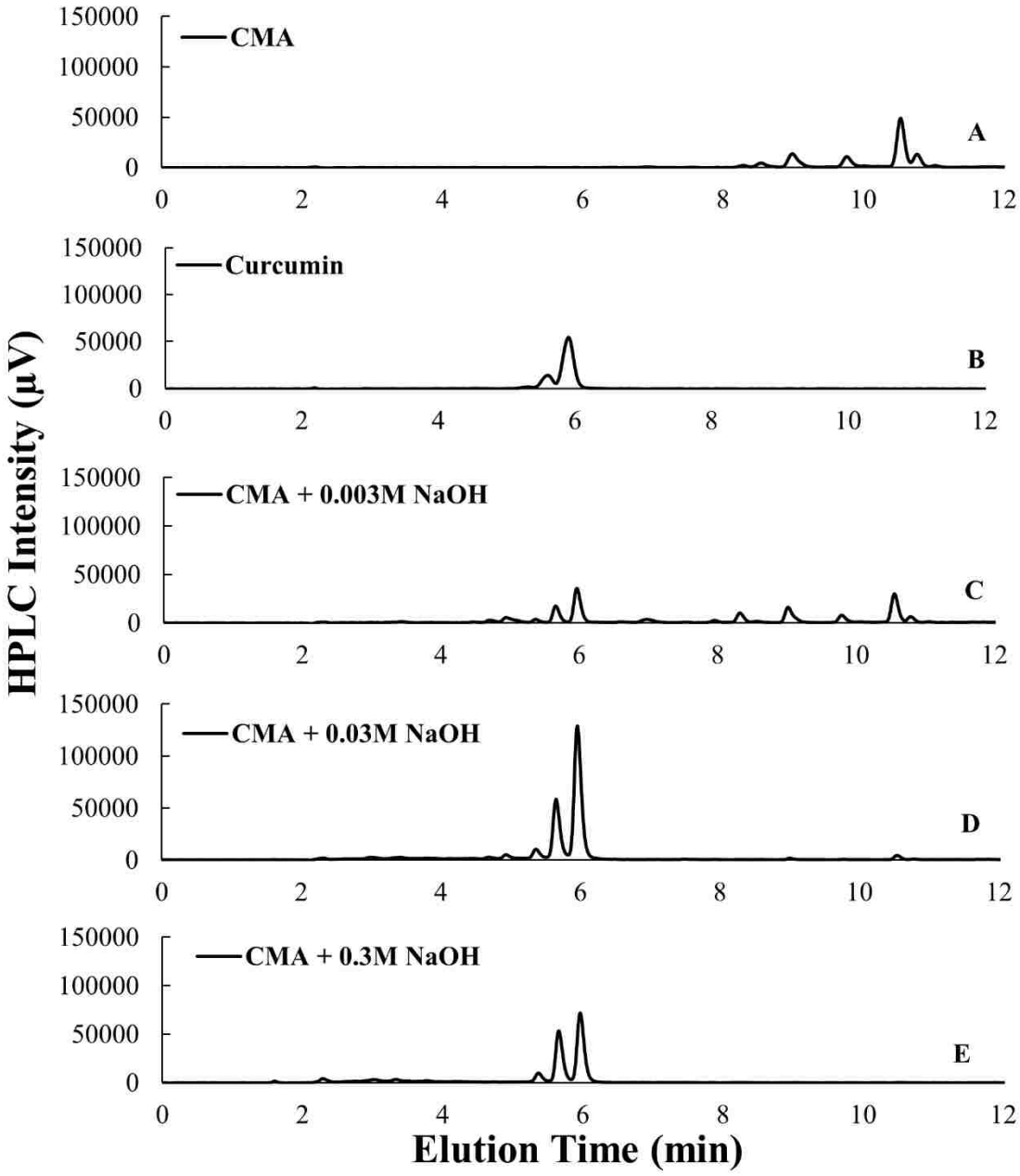

Figure 5-1: HPLC Chromatograms of CMA exposed to 0.003M, 0.03M, 0.3M NaOH for 30 minutes.

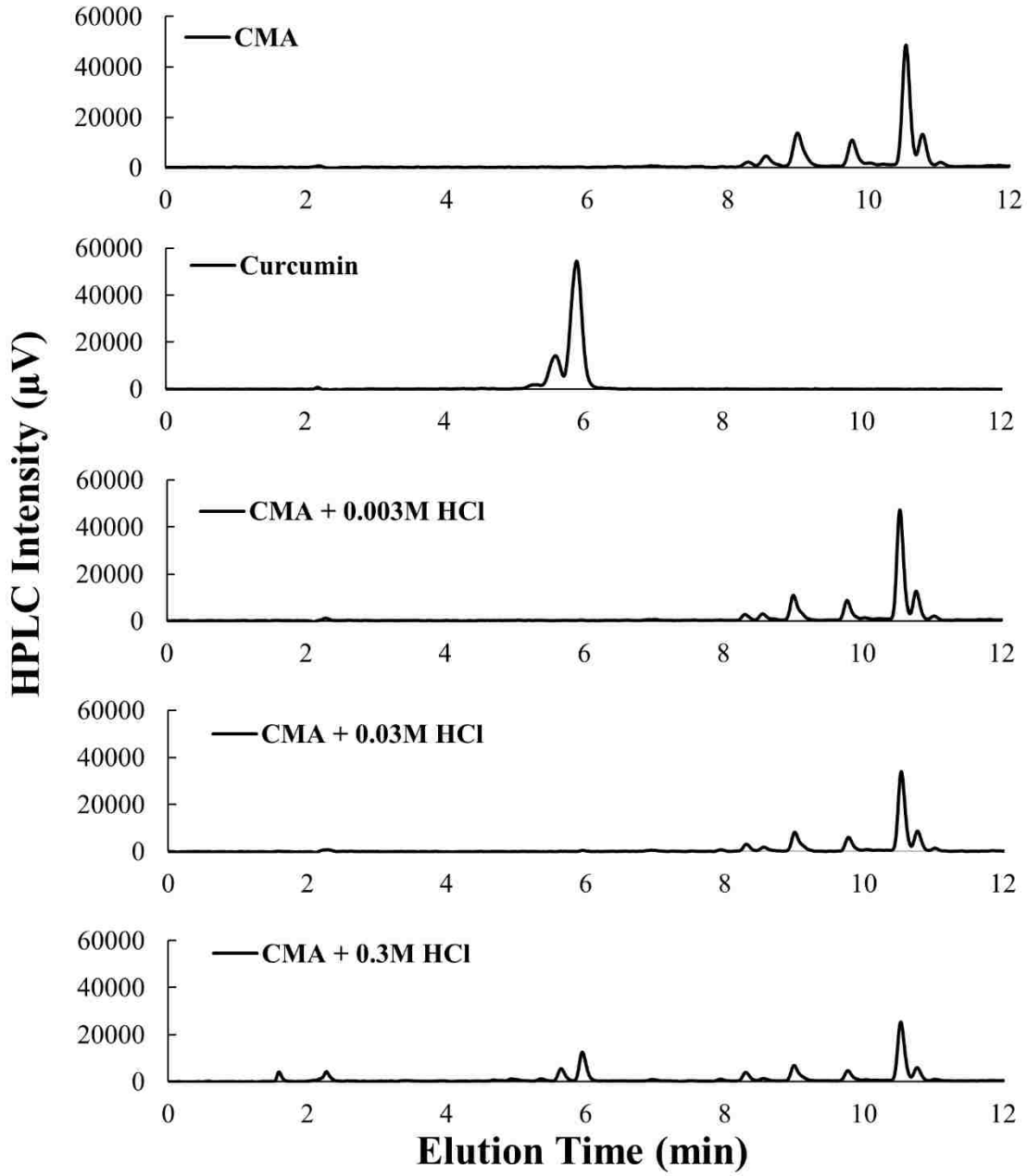

Figure 5-2: HPLC chromatograms of CMA exposed to 0.003M, 0.03M, 0.3M HCl for 30 minutes.

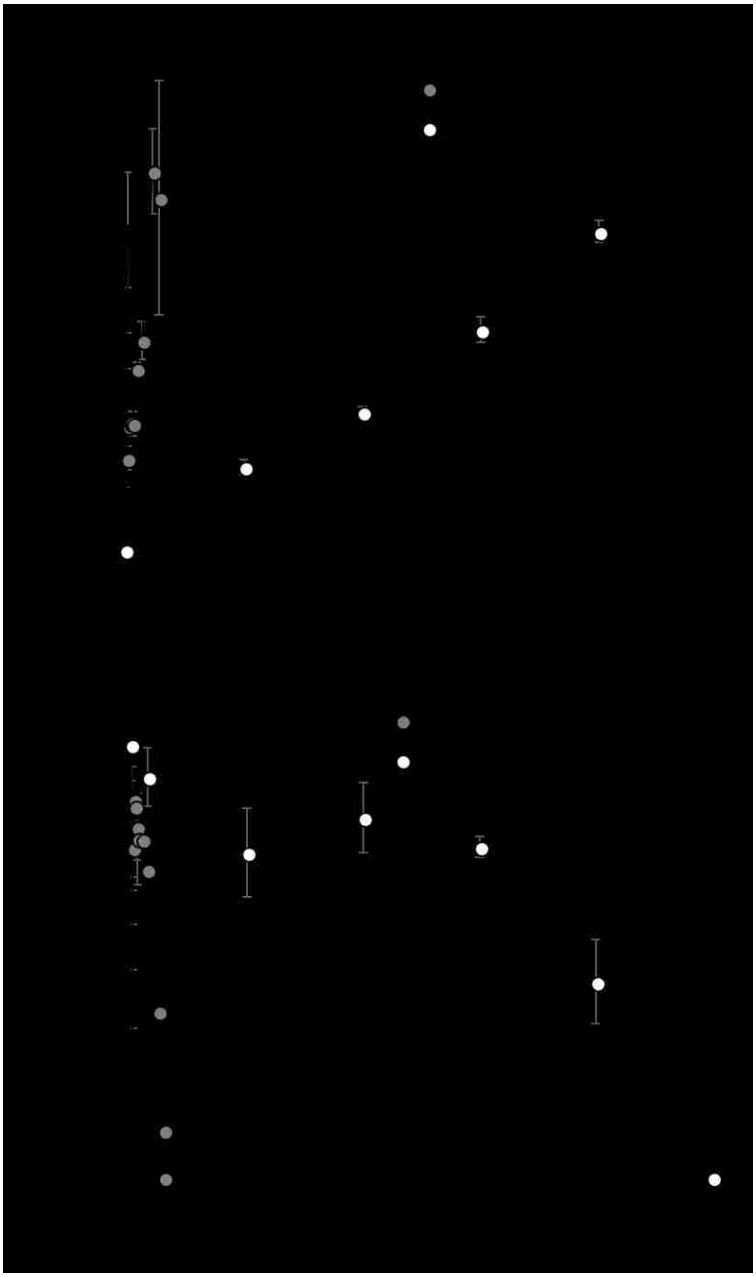

Figure 5-3: Swelling ratios (A), and mass remaining over time (B) of 0 wt% curcumin conjugated PBAE films. (n = 3, Mean ± SEM)

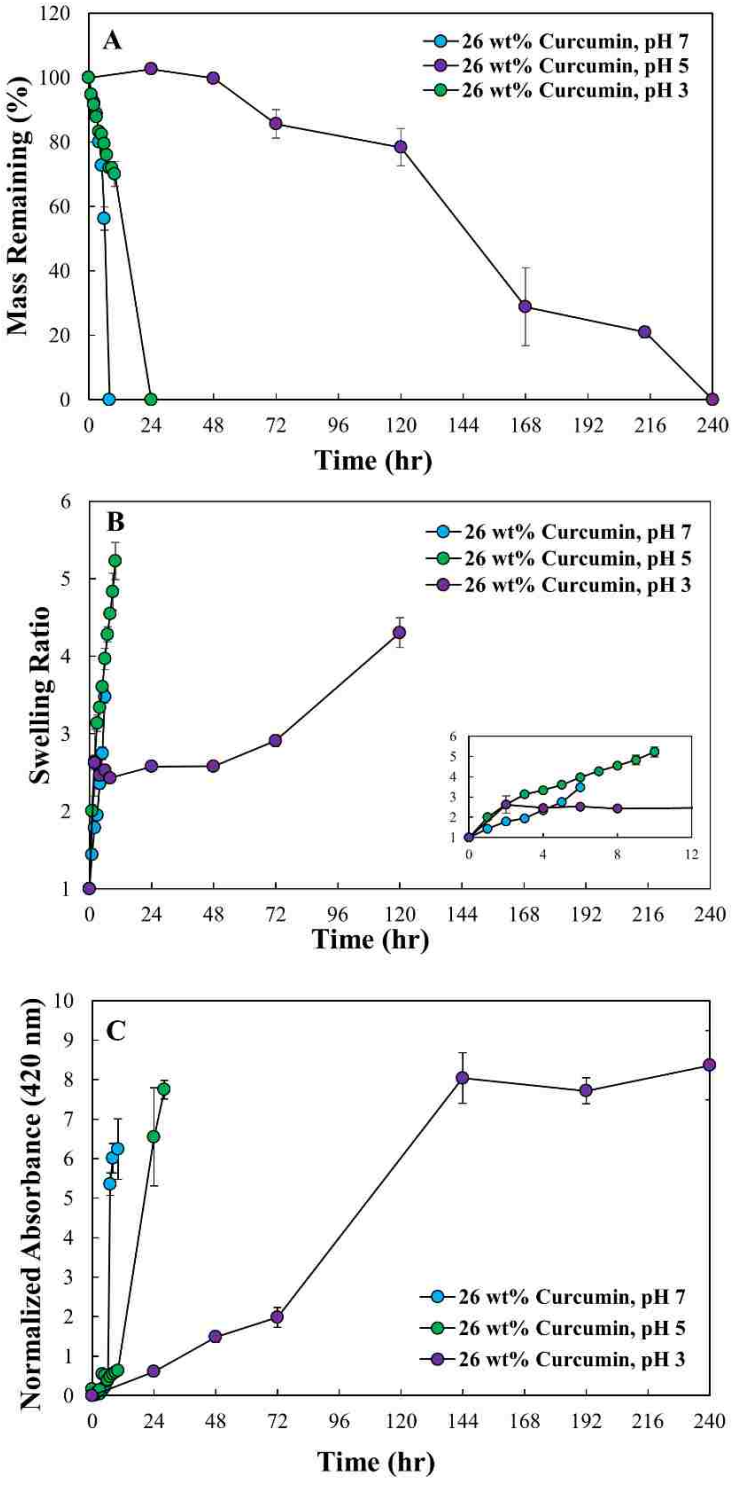

Figure 5-4: Mass remaining (A), swelling ratios (B), and cumulative release profiles (C) of 26 wt% curcumin conjugated PBAE films. (n = 3, Mean ± SEM)

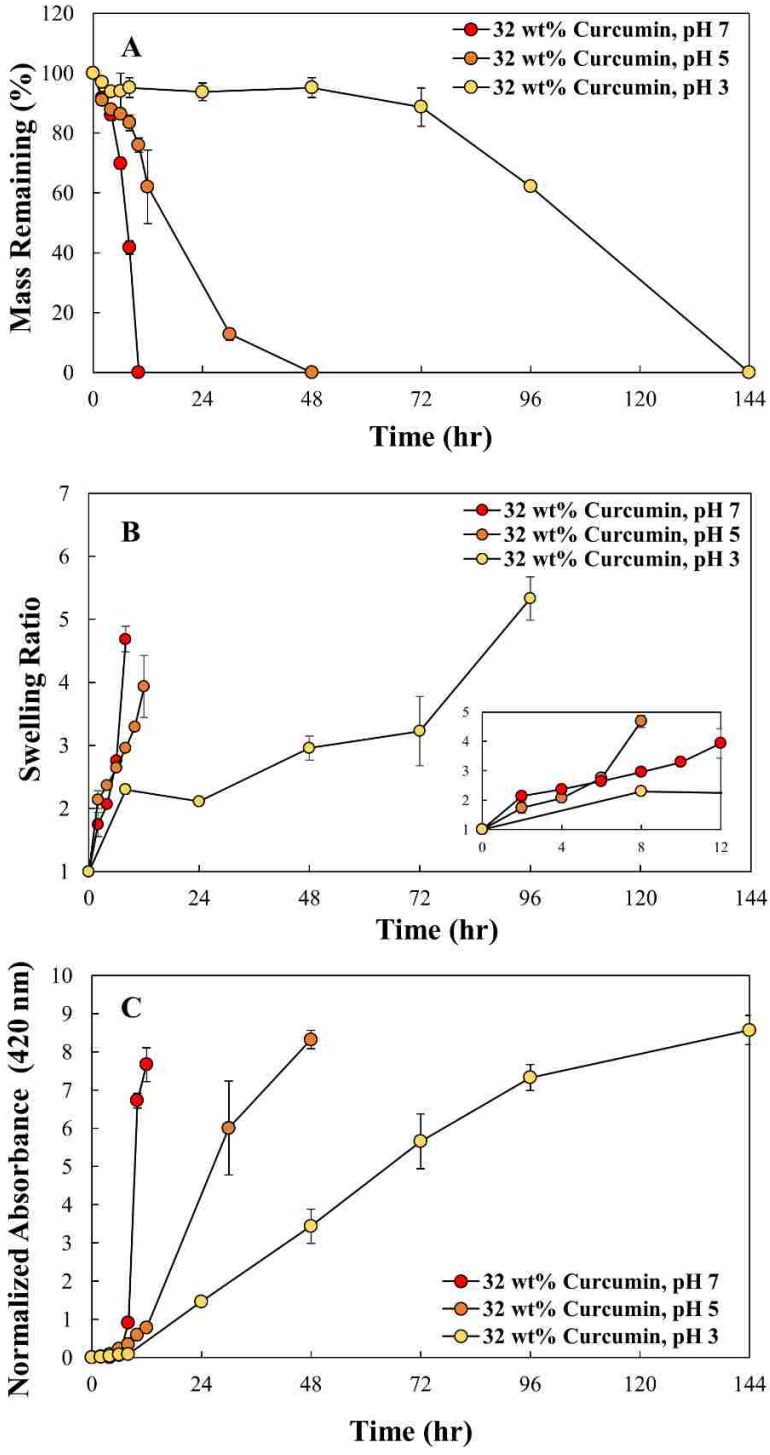

Figure 5-5: Mass Remaining (A), swelling ratio (B), and cumulative release profiles (C) of 32 wt% curcumin conjugated PBAE films. (n = 3, Mean ± SEM)

Chapter 6 Efficacy of Curcumin Conjugated Poly(beta-amino ester) Microparticles in the Treatment of Radiation-Induced Oral Mucositis in a Hamster Model

6.1 Introduction

Oral mucositis (OM) affects nearly 100% of head and neck cancer patients that undergo radiotherapy treatment. It is a debilitating side effect that damages healthy epithelial tissue in the oral cavity and results in severe ulcers. This is caused by oxidative stress (OS), where the antioxidant-free radical concentration in the cellular environment is imbalanced. While preferably the exposure only impacts the tumor site, the initial insult of high energy electrons can directly damage DNA in healthy proliferating epithelial cells and indirect radiation can create hydroxyl radical formation from the water content present in the cell. The initiation of free radical generation triggers secondary messengers that lead to the upregulation of pro-inflammatory cytokines and transcription factors that cause apoptosis and cell damage [19]. As the signaling cascades, the cytokines infiltrate through the submucosa and cause amplified injury within the oral cavity [151]. Parallel signaling pathways are initiated and lead to the destruction of the mucosal membrane and ulceration occurs. Due to the high epithelial proliferation rate, the mucosal can return to a healthy state, so long as the patient's health was not impaired initially or bacterial infection did not occur [152].

Treatments for OM include topical analgesics, antiseptics, and even turmeric oral rinses; however, patient compliance is low due to excessive rinse and application regimens for any considerable therapeutic effect. Without these treatments, oral mucositis often

becomes so severe that patients are susceptible to 2infection and will often halt treatment due to extreme pain and discomfort.

In this chapter, the efficacy of an 18 and 24 hour-controlled release antioxidant drug delivery system is investigated in a radiation-induced oral mucositis in a hamster model. Curcumin, a potent antioxidant extracted from turmeric with anti-inflammatory properties, is incorporated into the backbone of a hydrolytically degradable microparticle network that can release curcumin up to 24 hours. Its extended release over time eliminates excessive rinse patterns and combats excess free radical production to alleviate severity of injury in patients.

6.2 Materials and Methods

6.2.1 Materials

Curcumin was obtained from Chem-Impex, Inc. (Wood Dale, IL). Dichloromethane (DCM) and Acetonitrile (ACN) were purchased from Pharmco-Aaper (Brookfield, CT). Ketamine, Xylazine, and Buprenorphine were obtained through Henry Schein (Melville, NY). Enzyme-Linked Immunosorbent Assay Kits for TNF-α, 4-HNE, IL-10, Protein Carbonyl, and IL-6 were purchased through MyBioSource (San Diego, CA). BCA Protein Assay, Formalin, Ethanol, Hematoxylin, Eosin Y, Xylene, Lithium Carbonate, and Cytoseal were obtained through VWR (Radnor, PA), and 4,7,10-trioxa-1,13-tridecandediamine (TTD), Protein Cocktail Inhibitor, Tween 80, triethylamine, acryloyl chloride, isoflurane and PEGDA, MW = 575 were purchased through Sigma Aldrich (St. Louis, MO). Noveon® AA- Polycarbophil and Carbopol® 971P NF Polymer were acquired from Lubrizol (Cleveland, OH), and Eudragrit L100 was obtained from

Evonik Industries (Essen, Germany). No further purification was necessary for items obtained.

6.2.2 Synthesis of Curcumin Multiacrylate

Curcumin multiacrylate was synthesized with the same method as previously described in Chapters 3-5. Briefly, curcumin was reacted in the presence of triethylamine with acryloyl chloride at a molar ratio of curcumin:triethylamine:acryloyl chloride of 1:3:3 for 18 hours under a purged nitrogen environment and ice bath. After 18 hours, the TEA-HCl salt was filtered, and the THF was evaporated using a rotary evaporator. The product was reconstituted in anhydrous DCM and a 0.1M HCl and 0.1M K_2CO_3 liquid-liquid extract was completed to remove any excess TEA-HCl salt and acrylic acid. The organic solvent layer was collected and treated with magnesium sulfate to remove any residual water content. The DCM solution was then evaporated overnight on a rotary evaporator and the CMA product was collected and stored with a desiccant at -20°C.

6.2.3 Synthesis of Curcumin Conjugated Poly(beta-amino ester) Microparticles

Curcumin conjugated poly(beta-amino ester) films of 70 mol% CMA/30 mol% PEGDA, MW = 575 (C70) and 90 mol% CMA/10 mol% PEGDA, MW = 575 (PEGDA) (C90) were synthesized similar to Patil et al[116]. Briefly, curcumin multiacrylate and poly(ethylene glycol) diacrylate were reacted with 4,7,10-trioxa-1,13-tridecanediamine (TTD) to form a crosslinked ampiphilic network utilizing Michael Addition in anhydrous dichloromethane. The ratio of total acrylates to amine protons was set to a value of 1.0. 1.5 times the total monomer mass of aDCM was used for the reaction. CMA was solubilized in half of the desired aDCM. PEGDA and TTD were added to the remaining aDCM in separate tube for 5 minutes to allow for initial crosslinking. CMA was added directly to the

PEGDA/TTD mixture and the entire reaction solution was added to a casting ring and left for 1 hour at room temperature. After 1 hour, the film was placed in a drying oven at 50 °C for 24 hours. Synthesized films were washed at 40 mL per 1 gram of polymer in anhydrous acetonitrile 5x for 1 hour each to remove any unreacted monomers. Washed films were dried under vacuum at 50°C for 24 hours. Films were then cryomilled to obtain microparticles using a SPEX Sample Prep 6875D Freezer/Mill. Films were cut to fit within the stainless-steel milling tubes with 1 wt% magnesium stearate as a lubricant. The films were pre-cooled for 3 minutes, milled for 2 minutes at 15 cycles per second CPS (max), and then cooled for 2 minutes. This was repeated 5 times with a total milling time of 10 minutes. Microparticles were then dried overnight on a lyophilizer to remove any excess moisture and stored at -20°C with a dessicant until used.

6.2.4 Microparticle Characterization

Curcumin release and size analysis of C70 and C90 were measured. Degradation studies of C70 and C90 microparticles were completed at a theoretical final concentration in solution of 100 μg/mL curcumin in phosphate-buffered saline solution (pH 7.4) with 0.1% (w/w) SDS added to increase curcumin solubility. At desired time points, supernatant was collected, free from microparticles, and stored for analysis. Fresh buffer was replenished to the system to maintain constant volume throughout the degradation. A Cary 50 UV-Vis Microplate Reader spectroscopy instrument was used to observe total release time at curcumin's maximum wavelength at 420 nm. The final degradation time point for each system was also run through high performance liquid chromatography (HPLC, Water Phenomenex C18 column, 5 μm, 250 mm (length) x 4.6 mm (ID) on a Shimadzu Prominence LC-20 AB HPLC) coupled with a Waters Refractive Index Detector set to 420

nm to obtain quality of degradation products. Microparticle size distribution was obtained with a Size Analyzer (Shimadzu SALD-7101) utilizing ultraviolet laser diffraction to measure size distribution.

6.2.5 Mucoadhesive Solution Preparation

Mucoadhesive Solution was prepared based on Example 4 in the Mumper et al patent. 400 mL of DI water was added to a beaker and stirred with a coil impeller at 2000 rpm. 0.2% w/w Noveon was added slowly to DI water and left to stir for 30 minutes until Noveon was completely dispersed. 0.1% (w/w) Carbomer was then added and the mixing was increased to 1200 rpm for 30 minutes. Finally, the Eudragit was added to the solution and the mixing was increased to 2000 rpm for 30 minutes until completely dispersed. Sodium hydroxide was then used to partially neutralize the solution to pH 5.65 while constant mixing. The dispersion was stored in 50 mL tubes at room temperature.

6.2.6 Animals

Female and male golden Syrian hamster aged 4-6 weeks, with starting weight between 90-120 g were used (Envigo). Animals were individually housed in the Division of Laboratory Animal Resources and separated randomly in to treatment groups. Dietary restrictions included the ingestion of any fruit or vegetables with polyphenolic content, but were fed grain pellets and water ad libitum. All protocols were approved by the University of Kentucky Institutional Animal Care and Use Committee.

6.2.7 Radiation Dose

A pilot study was performed to select radiation dose that would onset the progression of oral mucositis between 8-12 days and peak at an OM score above 3 (rubric presented in **Table 6-1**). Hamsters were randomly divided in to two groups subject to an

acute dose of 40 and 60 Gy radiation. Hamsters were given standard rodent dosage of 100 mg/kg Ketamine + 10 mg/kg Xylazine intraperitoneally for anesthesia during radiation. Once anesthetized, the left cheek pouch of each hamster was extracted outside of the oral cavity and clamped using two acrylic pieces of material without hindering blood flow. A slab of solid water was placed on top of the acrylic piece to optimize delivery at the site of the pouch. Using a linear accelerator (LINAC), high-energy x-rays were delivered locally to the extracted pouch in the field, exposing the pouches at desired times for a total delivery 40 and 60 Gy. The acute dosage with desired results was then used for the acute dosage in the efficacy studies presented.

6.2.8 Treatment Groups and MP Dose

The treatment groups were randomly divided in to n = 5 females and n = 5 males groups to investigate the efficacy of C70 and C90 delivered topically to the hamster pouch using a syringe in the mucoadhesive solution. The microparticles investigated were observed at three polymer weight loadings in the mucoadhesive solution of 5%, 10%, and 20% (w/w) presented in **Table 6-2**. The desired amount of microparticles was measured and the mucoadhesive solution was added to the microparticles and mixed well right before dosing occurred to refrain from any premature degradation. Depending on the treatment group, 200 μL of DI water or microparticle suspension in mucoadhesive solution was syringed in to the hamster cheek pouch and the outside of the cheek was gently massaged to ensure full coverage. Dosing was performed every 24 hours for 28 days beginning 2 days prior to radiation exposure (**Figure 6-1**).

6.2.9 OM Rubric

The oral mucositis rubric used for assessment was based on a six point system developed by Sonis et al [153]. The hamsters were anesthetized with 2.5% isoflurane supplemented with oxygen by nose cone and cheek pouches were everted on Day 1-27 and scored. The cheek pouches were scored blindly by two individuals on a 0.25 point scale based on the following criteria in **Table 6-1**. Hamsters given a score of 3 were administered 0.1 mg/kg buprenorphine intraperitoneally (IP) once daily, and scores 4 and greater received 0.1 mg/kg buprenorphine IP twice daily, until OM lessened in severity.

6.2.10 Tissue Collection for H&E and OS Markers

After 28 days of treatment and observation, hamsters were sacrificed using isoflurane overdose and thoracic cavity destruction. The left and right cheek pouches were excised from each hamster, and each cheek pouch was cut into two. One sample was pinned and fixed in 10% formalin, and the other half was snap frozen in liquid nitrogen and stored at -80°C for tissue processing for ELISAs of various OS biomarkers.

Tissues that were fixed in 10% neutral buffered formalin overnight were then processed through paraffin, sectioned at 5 μm, and stained for hematoxylin and eosin (H&E). Slides were dipped in filtered hematoxylin for 2 minutes, rinsed in warm tap water, and blued using saturated lithium carbonate. Following dehydration, slides were dipped in Eosin Y and rinsed in alcohol. They were then cleared in xylene and coverslipped using Cytoseal. Slides were imaged on an Olympus BX41 microscope with a mounted Olympus DP71 camera.

The frozen pouches were weighed and a target tissue concentration of 200 mg/mL in 1x protease cocktail inhibitor was used extract protein content from the connective tissue

using a glass tissue homogenizer. Enzyme-linked immunosorbent assay kits for quantifying biomarkers related to oxidative stress were performed according to the Manufacturer's Protocol. These included TNF-α, 4-HNE, Protein Carbonyl, IL-10, and IL-6. A bicinchoninic acid assay (BCA) was performed to normalize biomarker levels between samples; each marker was reported in molar concentration per milligram protein. Statistical significance compared to the control analyzed by Dunnett's test.

6.3 Results and Discussion

6.3.1 Microparticle Characterization

C70 and C90 MP were milled and characterized by measuring the size distribution of the sample using laser diffraction. Degradation time of the particles was measured by using an ultra violet-visible (UV-vis) spectroscopy microplate reader to measure the cumulative absorbance at 420 nm over time of the 0.1% (w/w) SDS PBS (pH 7.4). The microparticles have comparable size distribution profiles as seen in **Figure 6-2A**. C70 MPs have a slight left shoulder, shifting the average particle size to 15.7 ± 0.27 μm compared to the C90 MP average size of 20.8 ± 0.37 μm; however, both systems have the same MP distribution between 0.5 and 100 μm.

Degradation of MPs was measured by collecting supernatant until microparticles were fully degraded and the absorbance plateaued. C70 MPs had 38 wt% of curcumin incorporated into the network and fully degraded over 15 hours, where C90 MP had 50 wt% curcumin and released over 24 hours (**Figure 6-2B)**. For example, if 1 mg of C70 and C90 microparticles were degraded, up to 0.38 mg of curcumin would be released from C70, whereas up to 0.5 mg of curcumin would be released from C90. C90 contained more

curcumin than C70, but the rate of release was slower due to the hydrophobicity of the network.

6.3.2 Radiation Dose Selection

A pilot study was executed to identify the exposure to use for the radiation-induced oral mucositis in a hamster model. Extracted and clamped left buccal tissue pouches were exposed to an acute dose of 40 Gy and 60 Gy radiation using a LINAC. Every day for 28 days, the hamsters were anesthetized and the pouches were extracted. Picture documentation was collected, and the pouch injury was blindly scored (**Figure 6-3**) using the rubric in **Table 6-1**. An example for each score can be observed in **Figure 6-4**. Delayed onset of injury was seen in both radiation groups where erythema was observed by day 10. Between day 10 and 18, redness and swelling increased and the sloughing of the mucosal lining began. For 40 Gy exposure, the injury never progressed further than slight sloughing of the pouch and resolved completely back to baseline after 22 days. For the 60 Gy exposure, the entire mucosal lining completely sloughed off from the buccal tissue and the formation of ulcers within the bed of the pouch developed in each hamster. The peak day of injury was Day 17, where the pouches were swollen and challenging to extract from the mouth with over 50% of the pouch ulcerated. The pouch quickly resolved due to the fast proliferation rate of epithelial cells, scoring 1 by Day 24.

6.3.3 Evaluation of Microparticle Efficacy

Hamsters were treated daily with a 200 μL dose of C70 or C90 MPs at three different weight loading of particle in mucoadhesive solution to determine efficacy of the MP rinse. Two doses were administered prior to radiation exposure and continued for 26 days following radiation exposure while the pouches were observed and scored daily. A

slight increase in erythema was seen in all groups for up to two days after radiation due to irritation of initial exposure and extraction. For the untreated groups, slight erythema onset by day 9 and mucosal sloughing was observed by day 15. The untreated groups peaked in injury by day 17 at a score of 3.63 ± 0.27 with the loss of elasticity and formation of ulcers that cover more than 50% of the cheek pouch. After a plateaued peak injury for two days, buccal tissue began to fully resolve with visible fibrosis by day 27. Based on the standard error of the mean (**Figure 6-5** and **Figure 6-6**), significant suppression of injury was seen by day 17 in C90 5 wt%, 10 wt%, and 20 wt% of microparticle dosages with a score of 2.5 ± 0.35, 2.2 ± 0.095, and 2.6 ± 0.25, respectively. The scoring for the 5% and 10% C90 dose initially scored lower than 20%, but by day 18 and 19, the injury was insignificant to the control group. The suppression of injury remains significant in 20 wt% C90 until Day 20. At the point of resolving, there appeared to be change in healing besides 20 wt% C90 on Day 22.

No significant change was seen in any of the microparticle dosages of the C70 polymer suspension over the 28 days of monitoring (**Figure 6-7** and **Figure 6-8**). Based on scoring, 5 and 20 wt% C70 appear to have an acceleration in healing; however, pouches treated with C70 MPs developed curcumin incorporated exophytic masses, usually found from chemical damage, that were unable to be scored as an ulcer, but delineated significantly from healthy buccal tissue. The important note is that all C90 treated pouches never received above a score of 3, which represents no observation of ulcers throughout the duration of the study.

6.3.4 OS Biomarkers

Biomarkers, such as protein carbonyl, 4-HNE, TNF-α, IL-10, and IL-6 have been found to be related to oxidative stress injury and the levels were evaluated in the tissue at day 28 [154, 155]. Protein carbonyl levels were measured in all samples to look for the presence of lipid peroxidation. All groups treated with curcumin incorporated microparticles had lower levels of protein carbonyl content (nmol/L/mg protein) than the treatment group, showing protection from lipid peroxidation within the buccal tissue collected (**Figure 6-9A)**. 4-HNE, a lipid alkenal byproduct of lipid peroxidation, was also another marker evaluated in all treatment groups[156]. Although normal levels of protein carbonyls were found in C70 20% (w/w) MP treatments, a significantly higher ($p<0.05$) level of 4-HNE (nmol/L/mg protein) was found compared to the controls (**Figure 6-9B**). This could be due to the abnormal exophytic mass that was seen in all groups treated with C70, with the highest weight loading having the highest degree of debris.

TNF-α and IL-10 levels in curcumin treated pouches remained insignificant to the levels found within the control groups (**Figure 6-9C** and **6-9D**). Since these samples were measured after the injury had been resolved, the pro-inflammatory cytokines and anti-inflammatory markers that aid in the signaling and amplification of injury or infiltration of cellular defenses may have also decreased in levels and returned to baseline. These levels would be beneficial to study throughout the experiment, specifically when peak injury is present in the model. IL-6 levels in all the curcumin microparticle treated tissue were on average lower than the control levels, with C90 20% (w/w) treatment group significantly lower level ($p<0.05$) (**Figure 6-9E**). This pro-inflammatory marker seen heightened in oral mucositis patients was suppressed in each curcumin treatment group [157].

6.3.5 H&E Analysis

Hematoxylin and eosin staining was used to differentiate between healthy and abnormal histology of tissue pouches exposed to radiation with or without microparticle treatment (**Figure 6-10**). In the baseline slide, healthy, intact epithelium was seen (black arrow) with normal nucleated muscle tissue, and connective tissue. In the irradiated sample, intact epithelial covered submucosa had present neutrophil and lymphocytic infiltration (densely populated area with nuclei) where the destruction of the epithelium occurred, and ulceration was seen (white arrow). Plump fibroblasts were also seen throughout the sample as commonly seen in patients that have been exposed to radiotherapy[158]. The formation of fibrous tissue was also seen (blue arrow). All untreated irradiated hamsters had prominent ulceration even at day 28 when sacrificed.

The C90 MP treatment group (**Figure 6-10** representative of 20% (w/v) C90) had prominent fibrous tissue, but observably lower than the untreated irradiated sample. The epithelium appeared healthy and intact. One sample in this microparticle treatment group had perivasculitis, inflammation that occurs around blood vessels (gray arrow). This could be due to extended direct contact with a foreign body, variable to the specific hamster, as it was only seen in one sample. This could be from the microparticle treatment, or extended contact of food on the inflamed tissue from stuffing of the pouch. All hamsters treated with C90 MPs had no ulceration. Hamsters treated with C70 MP had the formation of exophytic mass that consisted of denucleated necrotic tissue (red arrow). These masses were the most severe in the pouches treated with the highest weight loading of microparticle treatment.

Interestingly, the two MP systems investigated were made up of the same three starting materials at different molar ratios; however, one leads to curcumin exophytic masses, usually seen from tissue injury from chemical exposure. This suggested that the degradation products of the two systems are potentially different. To investigate the degradation products present, HPLC of the final degradation time point supernatant from the release profiles in **Figure 6-2B** was run for both systems (**Figure 6-11A**). Released products not only include curcumin (5.25-6.25 min), but also curcumin monoacrylate (7.75-8.5 min), and curcumin diacrylate (10.5-11 min) (**Figure 11B: I, II, III**). These were identified with standards and the work previously completed by Patil et al [118]. Although the release of acrylated curcumin is not ideal as suggested by literature on acrylate release and production toxicity [159], the products were released in the same proportions between the two systems. C90 MP would result in higher release of acrylate products, but was shown to have better efficacy than C70. The hydrolysis of the network also led to the release of the TTD-amino carboxylic acids (**Figure 11B: V**) and poly(ethylene glycol) (**Figure 11B: IV**). The TTD-amino carboxylic acid is not commercially available, but based on its structure, the acidic groups and short ether chain backbone could lead to toxicity. C70 would theoretically have a higher concentration of this degradation product, which could be noteworthy given the abnormal effect that resulted to the pouches treated with this material.

6.4 Conclusions

In this chapter, we found that a daily C90 MP treatment that delivered curcumin to the hamster cheek pouch over 24 hours provided protection against radiation-induced oral

mucositis, and was able to suppress protein carbonyl levels, and significantly suppress IL-6 levels found in the tissue lysate after 28 days of treatment.

Ultimately, we would hypothesize a network that would release only generally regarded as safe (GRAS) compounds would be the most beneficial for efficacy. However, to select crosslinkers such as ethylene diamine which would release an EDTA-like degradation product, we could eliminate potential toxic degradation products with the removal of PEGDA and TTD, but significantly increase the hydrophobicity of the network. The removal of PEGDA and TTD from our starting materials decreases the hydrophilicity of the network, which could change the release rate of curcumin. The promising results we obtained from these initial PBAE MP treatments provide successful insight into the development of these products for clinical applications.

Table 6-1: Oral mucositis grading rubric.

Score	Description
0	Pouch completely healthy. No erosion or vasodilation.
1	Erythema
2	Severe erythema, vasodilation and superficial erosion.
3	Formation of ulcer in one or more places, but not affecting more than 25% of the surface area of the pouch. Severe erythema and vasodilation.
4	Cumulative ulcer formation of about 50% of pouch surface area.
5	Complete ulceration of pouch mucosa. Unable to extract

Table 6-2: Treatment groups for the efficacy microparticle study.

Treatment	Number of Hamsters	Microparticle Dose/200 µL Mucoadhesive Solution
DI Water	5 male + 5 female	N/A
C70	5 male + 5 female	5% (w/w)
C70	5 male + 5 female	10% (w/w)
C70	5 male + 5 female	20% (w/w)
C90	5 male + 5 female	5% (w/w)
C90	5 male + 5 female	10% (w/w)
C90	5 male + 5 female	20% (w/w)

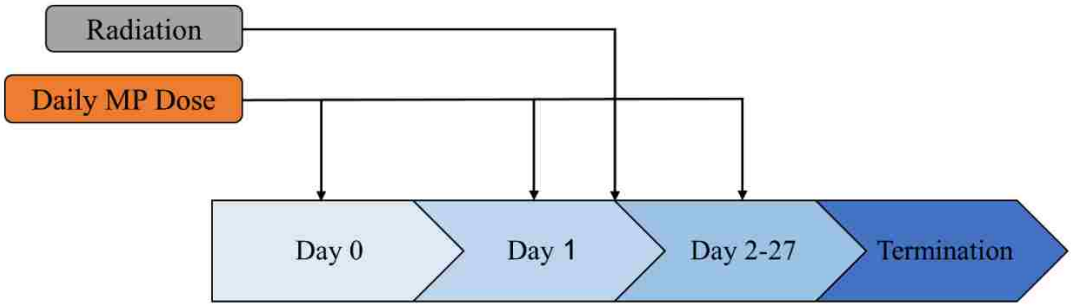

Figure 6-1: Treatment and radiation exposure set-up.

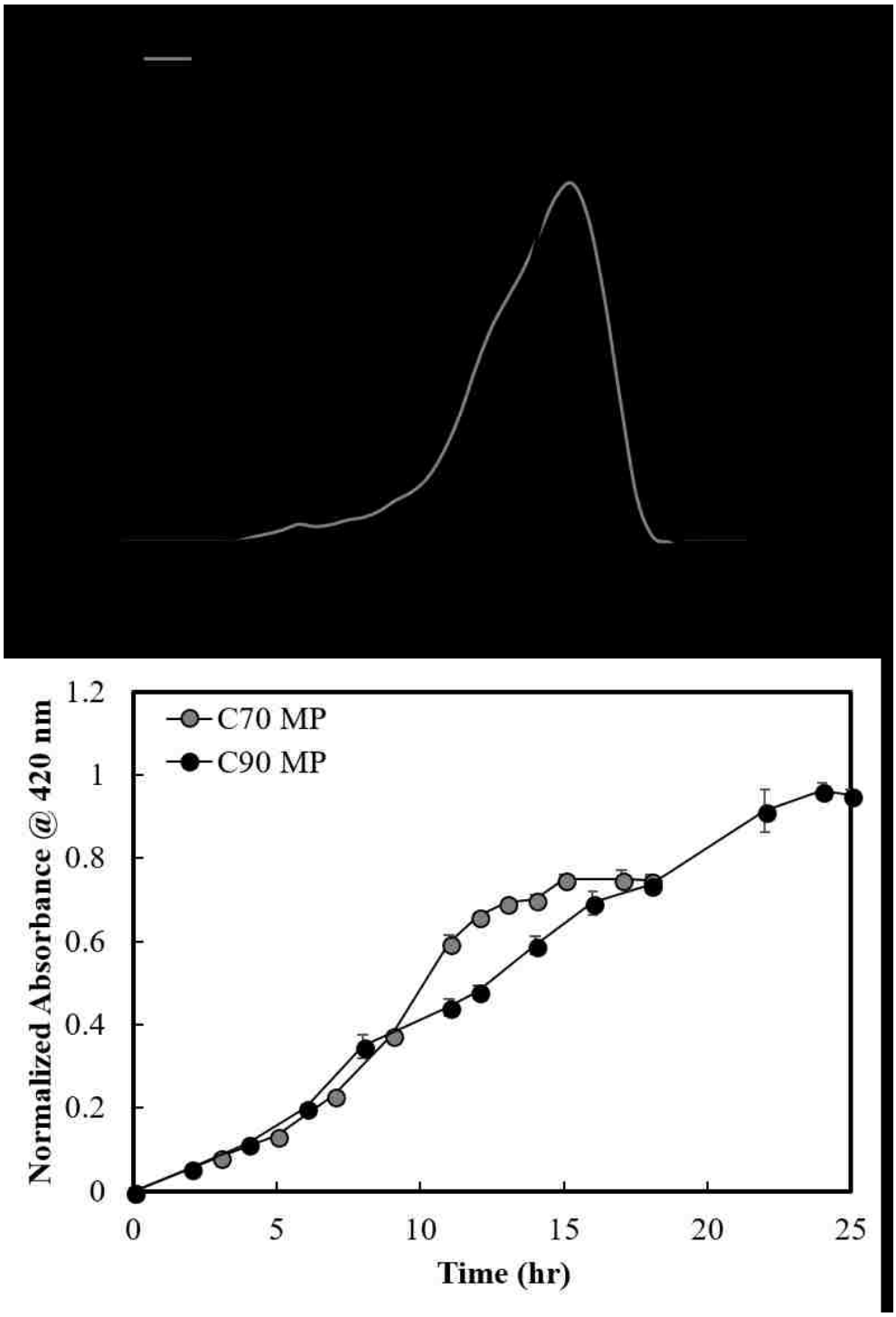

Figure 6-2: Microparticle size distribution (A) and release profile (B) of C70 (70 mol% CMA:30 mol% PEGDA, MW=575) and C90 (90 mol% CMA:10 mol% PEGDA, MW=575), both reacted with TTD at a ratio of total acrylate to amine proton of 1.0.

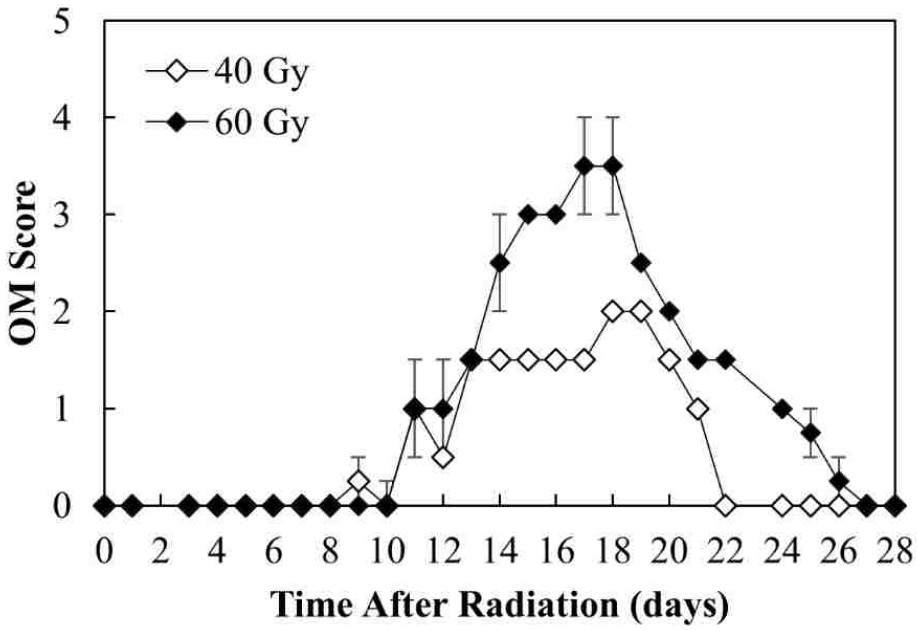

Figure 6-3: Comparison of the radiation induced oral mucositis from 40 and 60 Gy exposure.

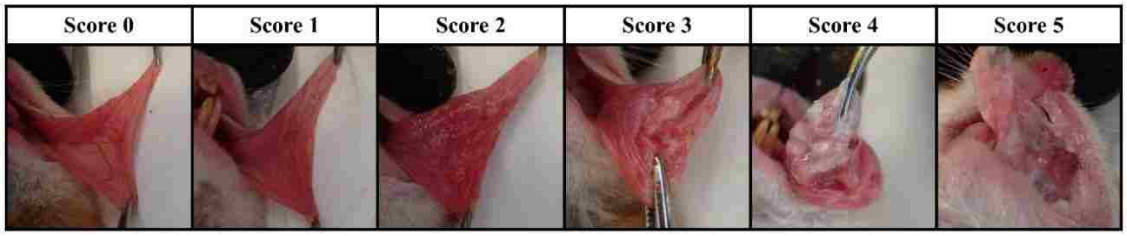

Figure 6-4: Examples of each score in the oral mucositis rubric.

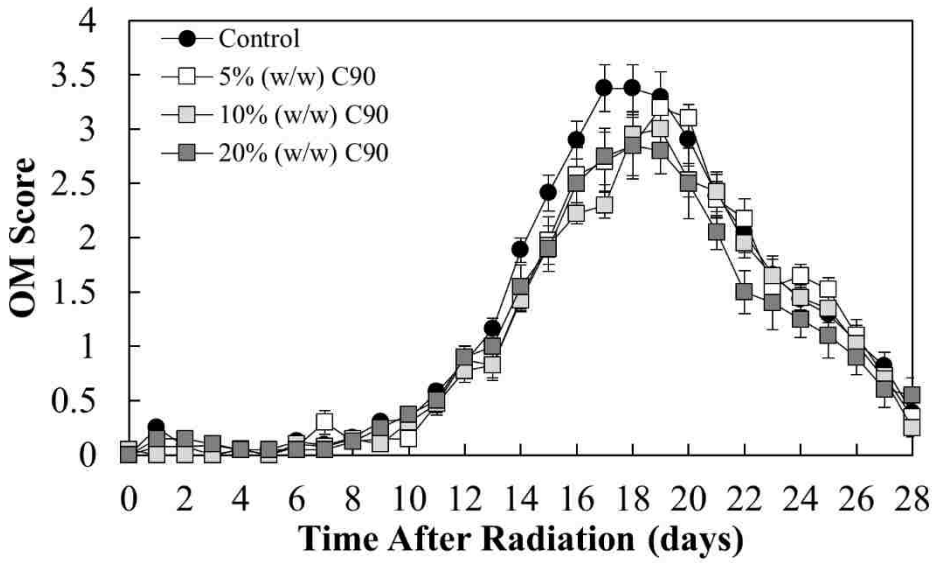

Figure 6-5: OM scoring assessment of C90 MP treatment after radiation exposure. Error bars represent standard error (Control: n = 22, Treatment groups: n = 10).

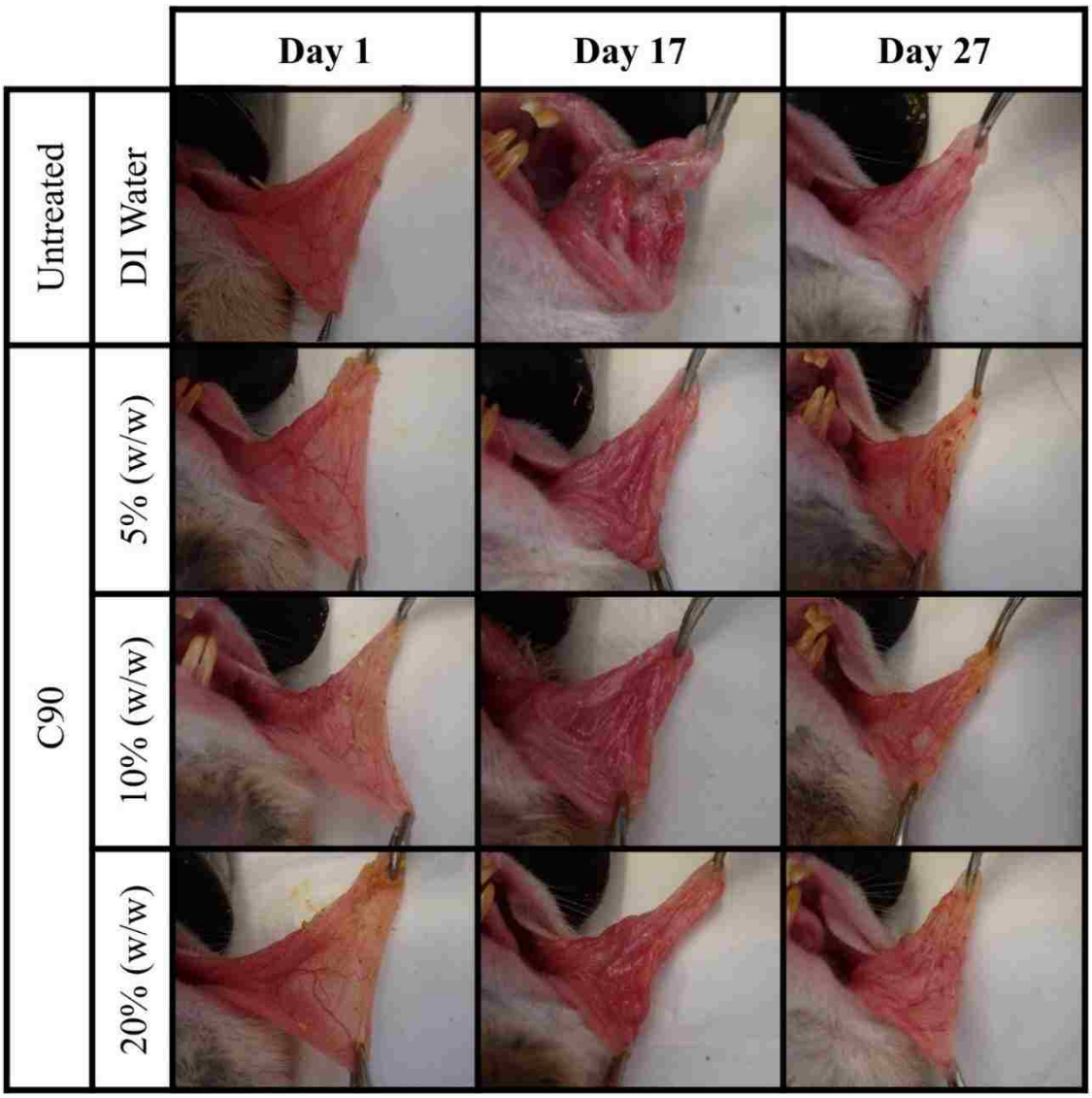

Figure 6-6: The progression of OM on untreated and C90 MP treated cheek pouches at three different MP weight loadings (5%, 10%, 20% (w/w)).

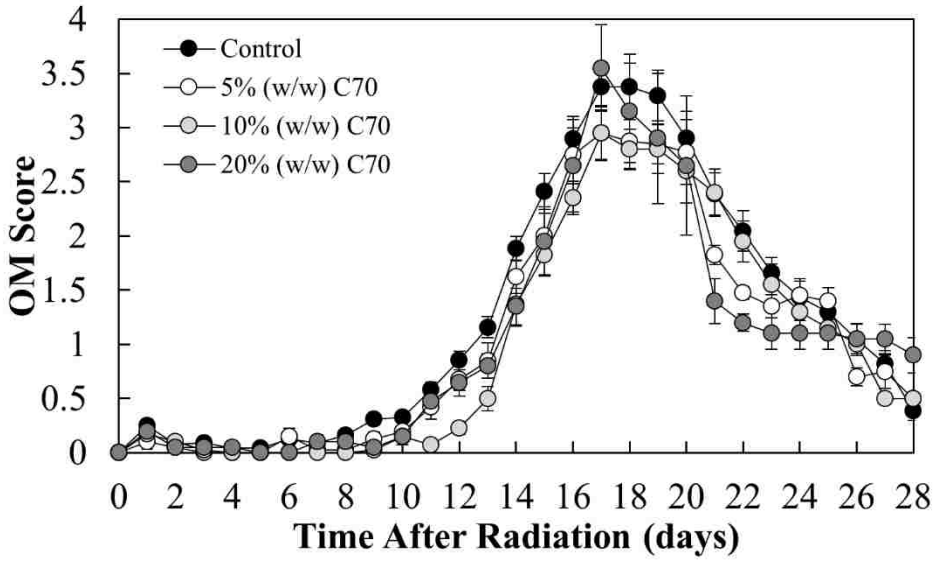

Figure 6-7: OM scoring assessment of C70 MP treatment after radiation exposure. Error bars represent standard error (Control groups: n = 22. Treatment groups: n = 10).

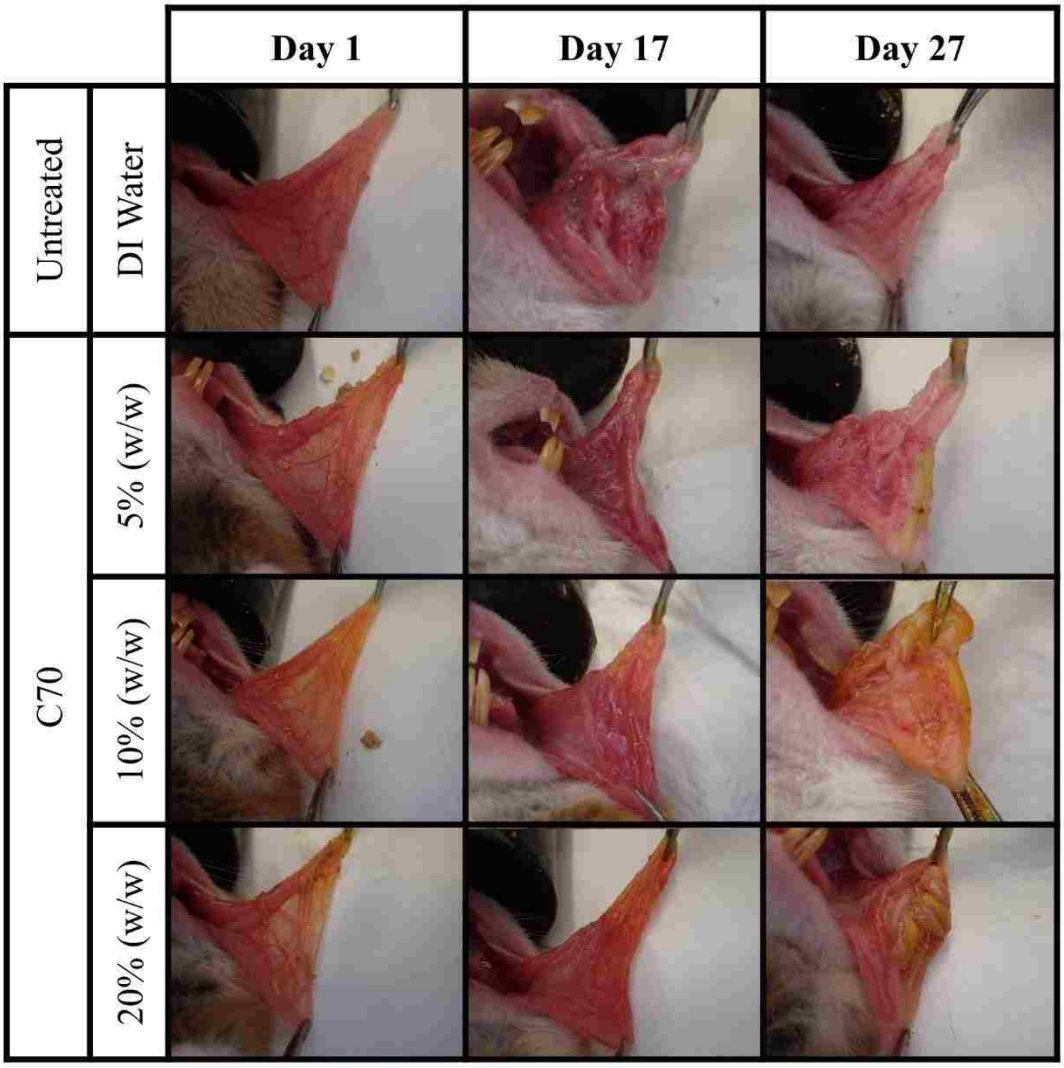

Figure 6-8: The progression of oral mucositis on untreated and C70 MP treated cheek pouches at three different weight loadings (5%, 10%, 20% (w/w)).

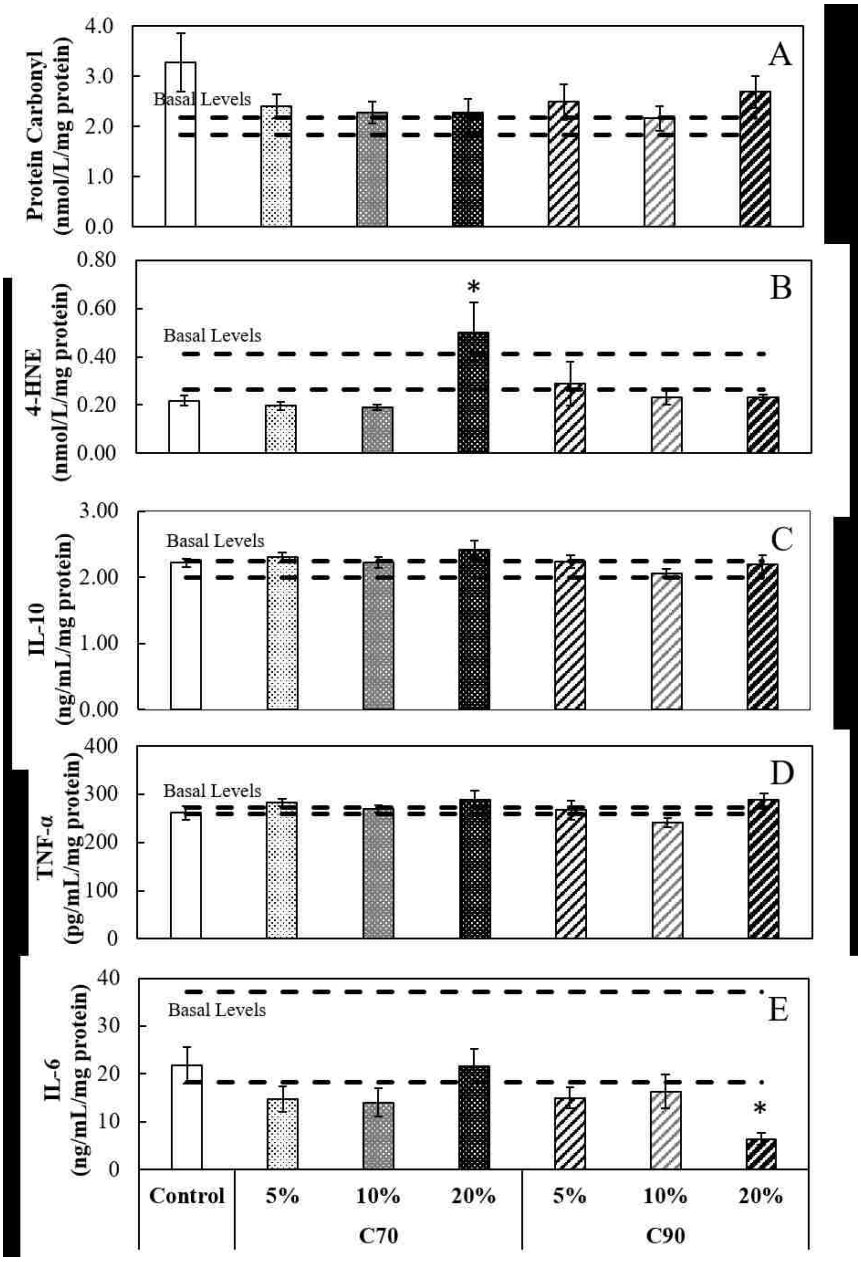

Figure 6-9: Protein carbonyl (nmol/L/mg protein) (A), 4-hydroxynonenal (nmol/L/mg protein) (B), interleukin-10 (IL-10) (nmol/L/mg protein) (C), tumor necrosis factor alpha (TNF-α) (nmol/L/mg protein) (D), and interleukin-6 (IL-6) (nmol/L/mg protein) (D) levels of control and treatment groups. Error bars represent standard error. * represent significance when compared to the control ($p<0.05$) using Dunnett's test. The dotted line represents the basal levels of each marker.

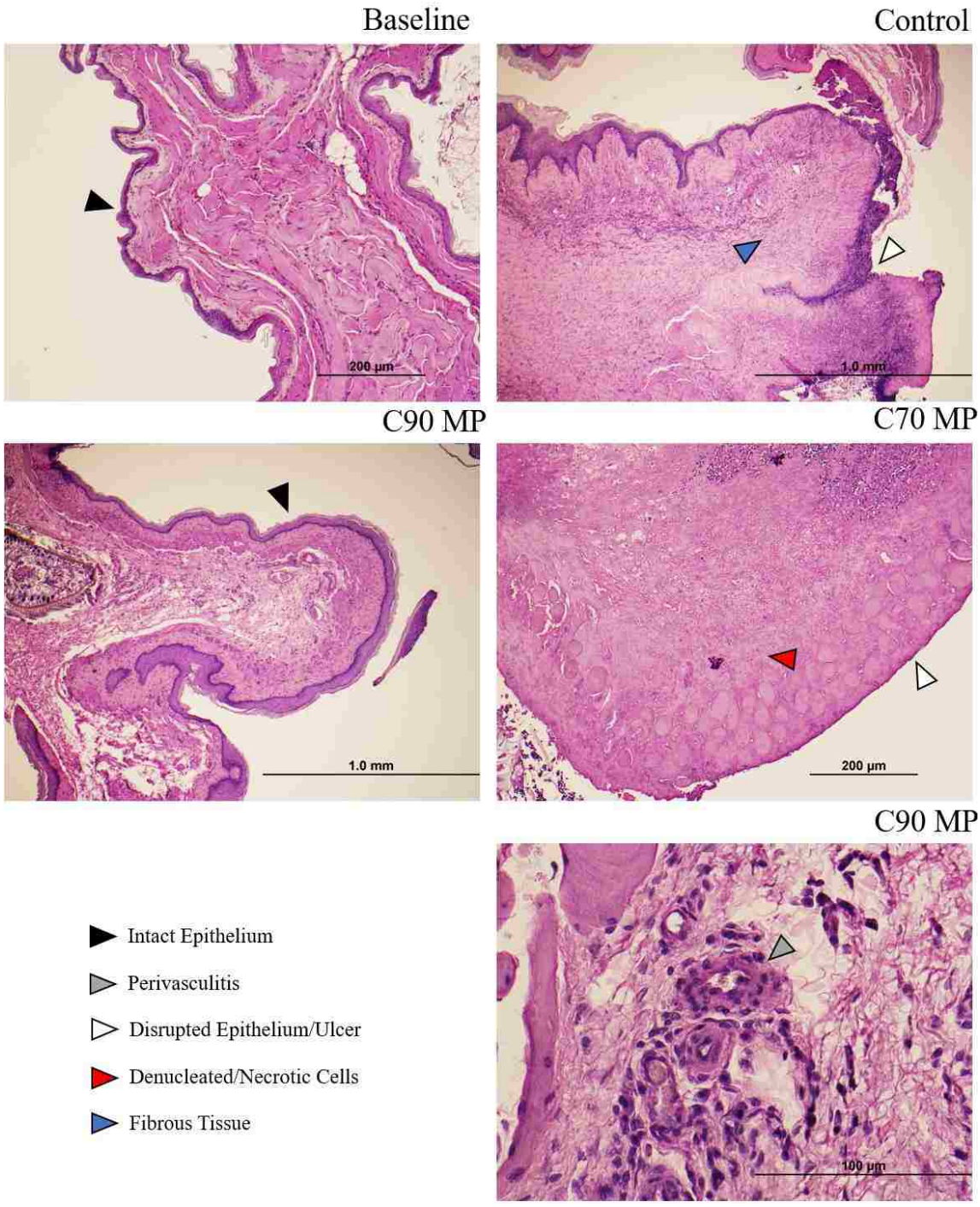

Figure 6-10: Hematoxylin and Eosin analysis of buccal tissue slides 28 days after exposure to radiation with either no microparticle treatment, C70, or C90 MP treatment.

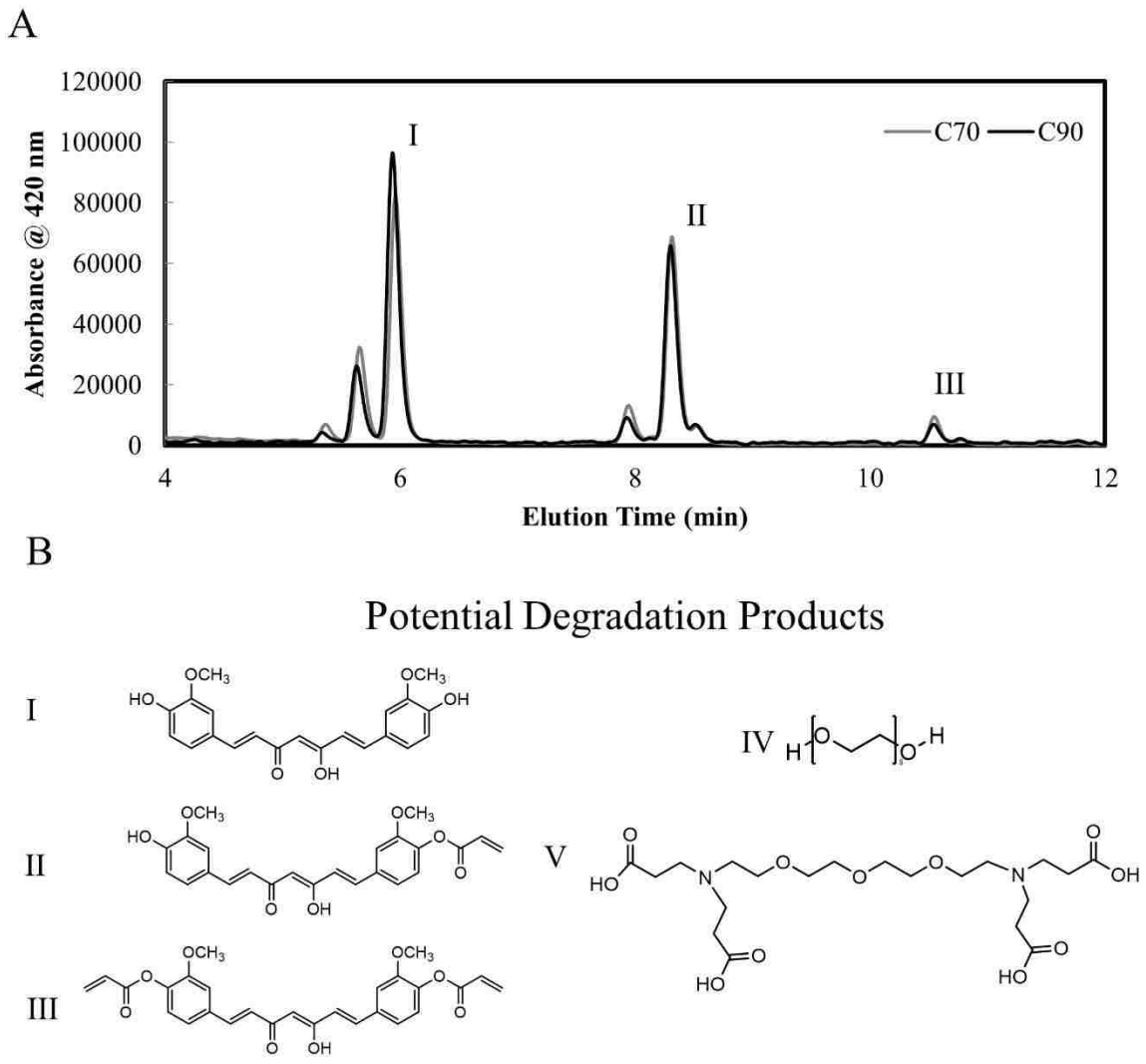

Figure 6-11: HPLC chromatograms at 420 nm of the final degradation products of C70 and C90 MPs (A) and all potential degradation products (B).

Chapter 7 The Reduction of Curcumin Monoacrylate in Curcumin Conjugated Poly(beta-amino ester) Films

7.1 Motivation

The release of safe and active degradation products from the curcumin-conjugated poly(beta-amino ester) films and microparticles is important to obtain the greatest therapeutic effect. To recapitulate the methodology of hydrolytically degradable antioxidant crosslinked networks, curcumin is modified at its active hydroxyl sites to form acrylated curcumin as a mixture of curcumin monoacrylate, diacrylate, and triacrylate. Michael Addition chemistry is utilized between acrylate and amines and a hydrolytically degradable crosslinked poly(beta-amino ester) network is formed. When hydrolyzed from the network, curcumin is released; however, acrylated curcumin products, which are less active curcumin products, are also found in the release products. This is due to hindered conversion of the acrylate-amine reaction, which results in only partial incorporation of triacrylate into the network. Therefore, free acrylate groups are still present in the network, and once hydrolyzed, the product of curcumin monoacrylate and diacrylate can be released. This is demonstrated in **Figure 3-4B** for 26 wt% curcumin-conjugated films in Chapter 3, and **Figure 6-9A**, in Chapter 6.

Not only does the scavenging capacity of curcumin decrease with the addition of acrylates, as seen in Chapter 3, but acrylated compounds have been found to be cytotoxic in cosmeceutical and pharmaceutical applications[160]. Acrylates are found in many nail products, such as acrylic nails, and nail enhancing polishes[161], as well as in adhesives in medical devices or to hold electrodes in place [162]. Although found in starting material and excipients, they are evident in development and reproductive toxicity, organ-system

toxicity, and neurological damage. Specifically, evidence shows that workers exposed to acrylates such as ethyl methacrylate and methyl methacrylate developed generalized and peripheral nerve damage[163]. Ideally, free curcumin and GRAS compounds would be the only degradation products released from the network.

Efficacy has been shown with polyphenol conjugated PBAE materials with curcumin acrylated release products present [33, 131]; however, attempts to reduce or remove the acrylate altogether would be beneficial. Efforts using several post-modification techniques, and changes in the reaction synthesis were completed. Significance between modified films and the control was defined as $p<0.05$ using a paired t-test.

7.2 Acrylate Capping using Isobutylamine (IBA) or Diethylamine (DEA)

Isobutylamine and diethylamine, purchased through Sigma Aldrich (St. Louis, MO) were selected as capping agents, utilizing the small secondary amines to diffuse through the network and react with any unreacted acrylates on the partially incorporated curcumin multiacrylate compound. The reacted site was hypothesized to undergo base-catalyzed hydrolysis just as the rest of the ester bonds present in the network, and only curcumin would be released. 38 wt% curcumin-conjugated PBAE films (C70) were synthesized as previously described in Chapter 6. Films were synthesized, washed in anhydrous acetonitrile, and dried for 24 hours in a vacuum oven at 50°C. Films were then introduced to either 5 mL of anhydrous dichloromethane, 0.5 mg/mL IBA, or 0.5 mg/mL DEA in a vented container and left at 50°C for 6 hours. Films were all washed once with anhydrous acetonitrile and then dried in a vacuum oven at 50°C for 24 hours. The films were degraded in 0.1% (w/v) Tween 80 phosphate buffered saline (PBS) solution (pH 7.4) in an agitating shaker bath at 37°C, and supernatant was collected over 18 hours. UV-Vis Spectroscopy

was used to quantify total recovery of the theoretical absorbance at 420 nm, and the final degradation product sample was run through HPLC to quantify the curcumin, curcumin monoacrylate, and curcumin diacrylate peaks (**Figure 7-1**). The film recovery based on total absorbance at 420 nm was unaffected by the post-modification step; however, the rate of release appears faster as all three groups that were treated, compared to the control film. Curcumin percent significantly increases to 71.8% in 0.5 mg/mL DEA ($p<0.05$) and 73.8% in 0.5 mg/mL IBA ($p<0.05$) compared to the control, resulting in a significant decrease in curcumin monoacrylate ($p<0.05$) and observable decrease in diacrylate. No change was seen in film incubated with DCM compared to the control film.

The same film compositions were incubated in the same three conditions; however, the incubation time was extended to 48 hours in a convection oven at 50°C for further reacting and drying time. After 48 hours, the films were washed once with anhydrous acetonitrile for 1 hour, and then dried in a vacuum oven at 50°C. Films were then degraded in 0.1% (w/v) Tween 80 PBS (pH 7.4) and time points were collected over 18 hours. No significant increase in curcumin was observed between the 6-hour incubation time and 48 hour incubation time, but a slight decrease in the curcumin diacrylate percentage in all three treatment groups was observed **(Figure 7-2**). Promising results were found with 0.5 mg/mL IBA, so IBA of three different concentrations were investigated to place IBA in excess of the free acrylates present.

The same film compositions were incubated in 0.5, 1.0, and 1.5 mg/mL IBA in 5 mL of DCM for 6 hours at 50°C. After 6 hours of reaction time, films were washed with anhydrous acetonitrile, and then dried at 50°C under vacuum. The percent contribution of the pure curcumin products significantly increased in 0.5 and 1.5 mg/mL IBA ($p<0.05$) and

the release profile was slightly accelerated where the recovery of the total absorbance at 420 nm was insignificantly affected (**Figure 7-3**). Capping the free acrylates in the network to a significant extent was successful within each release product; however, these statistically significant changes are unlikely to enhance the quality of the degradation products as out of the total degradation products, there still remain a significant amount of acrylate product. This could be due to the volatile nature of dichloromethane, where the secondary amines did not have enough time to impregnate the network and react before the DCM was fully evaporated in the oven.

7.3 Change in Ratio of Total Acrylate to Amine Protons

The ratio of total acrylate to amine protons (RTAAP) was investigated to increase the presence of free amines present in the network. The presence of excess amine was hypothesized to act as a nucleophile and increase base-catalyzed hydrolysis of the acrylates present. Films synthesized at 50 mol% CMA and 50 mol% PEG(400)DA were reacted with TTD at different RTAAPs of 0.9, 0.8, 0.7, 0.6. As the RTAAP decreases, the amount of amine present increases. The films were degraded in 0.1% (w/v) Tween 80 PBS (pH 7.4) and supernatant was collected over 8 hours. The final degradation time point was run on HPLC to determine percent release in the samples that contributed to curcumin, curcumin monoacrylate, and curcumin diacrylate.

The total percent recovery of the theoretical absorbance at 420 nm decreases as the RTAAP decreases. As more amine is present during the reaction, the kinetics between hydrolysis and ester formation are in competition and could result in premature hydrolysis of the acrylate groups on curcumin, resulting in lower incorporation of curcumin in to the network. The degradation time is also accelerated to 6 hours for RTAAP of 0.9, 0.8, and

0.7 and 5 hours for RTAAP of 0.6, due to the excess amines present within the network (**Figure 7-4**).

The recovery of curcumin in the final supernatant increases significantly at an RTAAP of 0.6, with 91% of the contribution of curcumin release products being curcumin, 8.7% curcumin monoacrylate, and 0% curcumin diacrylate. As the RTAAP increases, curcumin monoacrylate and curcumin diacrylate percent release increases.

7.4 Starting Material (CMA 1:3 vs CMA 1:2)

Curcumin multiacrylate was synthesized by reacting curcumin, triethylamine, and acryloyl chloride at a 1:3:3 molar ratio to undergo acid-chloride alcohol zication to produce a curcumin multiacrylate product to use as a starting material for curcumin-conjugated PBAE films[118]. A 1:3:3 stoichiometric ratio was used to synthesize the CMA starting material for all of the films throughout this dissertation (CMA 1:3). This results in 55% curcumin triacrylate, 45% curcumin diacrylate, and 0.9% curcumin monoacrylate based on LC-MS and HPLC-PDA [118]. The acrylated release products stem from the inability to fully react all acrylates in to the crosslinked network. This could be due to steric hindrance to react with all three acrylate groups on the curcumin triacrylate component. To investigate better conversion in to the network, CMA was synthesized at a 1:2:2 molar ratio to produce a higher percentage of curcumin diacrylate. This resulted in 12.4% curcumin triacrylate, 62% curcumin diacrylate, 23.3% curcumin monoacrylate, and 2.3% curcumin averaging 2 acrylate groups per CMA molecule vs 2.5 acrylate groups.

50 mol% CMA(1:2) and 50 mol% PEG(400)DA with TTD at an RTAAP of 1.0 were synthesized, washed, and dried. Films were degraded in 0.1% (w/w) Tween 80 PBS (pH 7.4) at 37°C in an agitating shaker bath, and the percent of curcumin and curcumin

monoacrylate were compared to the 50 mol% CMA(1:3)-50 mol% PEG(400)DA degradation products. Recovery of the total absorbance of release products at 420 nm was similar in both systems; however curcumin's percentage in the supernatant increased to 90% compared to 42%. The change in percentage of starting material components is noteworthy. The rate of reaction could decrease with the decrease in acrylates present, which allows for better conversion in to the network.

7.5 Conclusions

Post modification and synthesis modification on curcumin conjugated PBAE films with PEG(400)DA and TTD were investigated. Post modification has led to a slight decrease in monoacrylate, which resulted in slight increase of curcumin release; however, the change was unimpressive as it accelerated hydrolysis due to incubation times with amines.

The modification of the synthesis was promising. The increase in free amines present in the network aided in base-catalyzed hydrolysis of the acrylates present and a significant decrease in the curcumin monoacrylate present. The change in multiacrylate composition of the starting material also had promising effects, showing a decrease in curcumin monoacrylate present in the release products when a higher percentage of curcumin diacrylate was used in the reaction.

Future investigation continues with the purification of the curcumin's starting materials, made up of curcumin, curcumin demethoxycurcumin, and bisdemethoxycurcumin. This mixture of curcuminoids could be purified to curcumin, and the acid-chloride esterification reaction could be completed with one compound. This

could result in a multiacrylate mixture of only three compounds, rather than nine. The three compounds can be further purified to curcumin diacrylate. This not only leads to pure starting materials to provide better incorporation of curcumin in to the network, it also creates an avenue for linear PBAE synthesis, which opens many other methods of therapeutics while utilizing the novel chemistry in delivery methods such as aerosols, or nanoparticles.

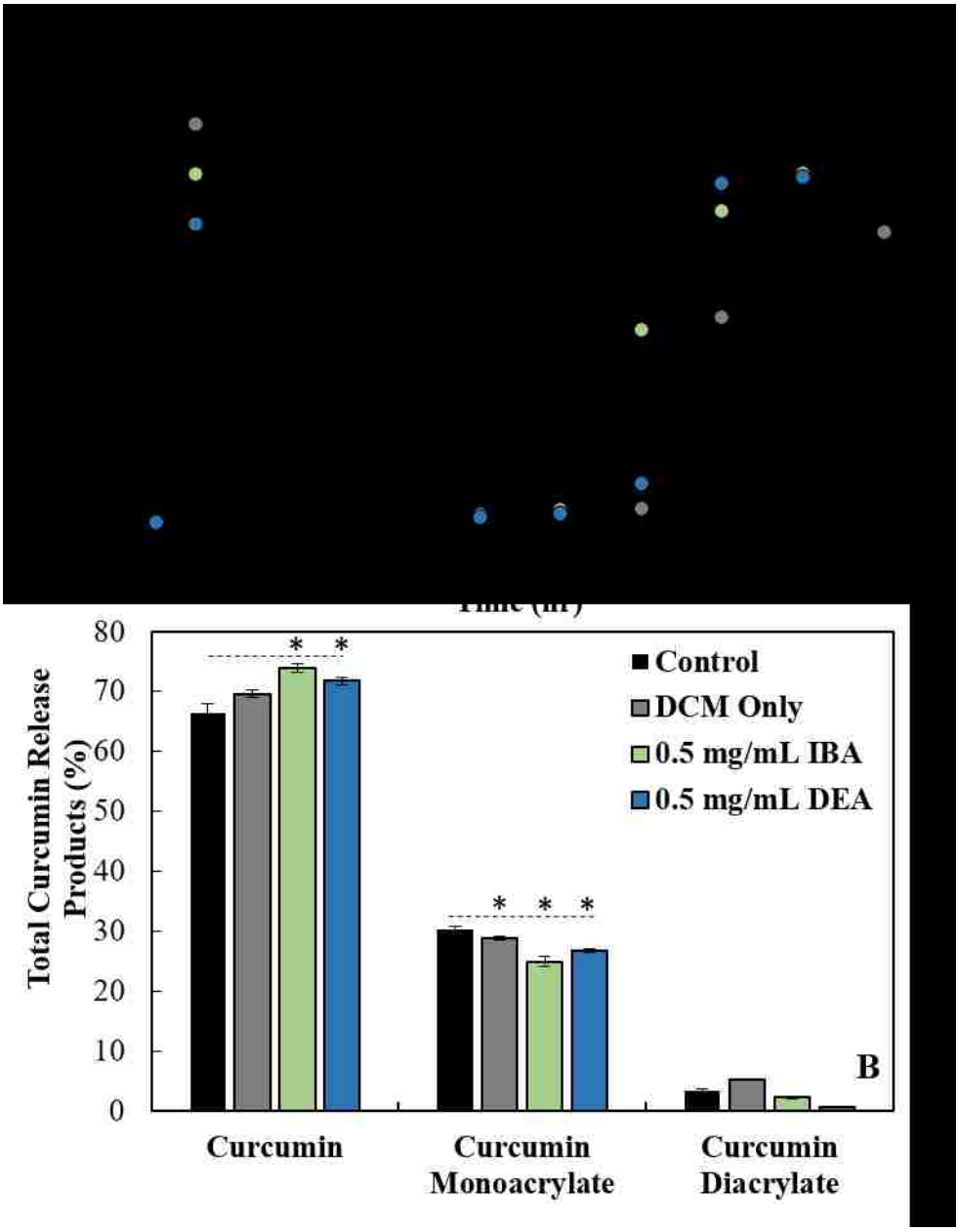

Figure 7-1: 38 wt% curcumin conjugated films incubated in DCM, 0.5 mg/mL IBA, and 0.5 mg/mL DEA for 6 hours at 50°C. The percent recovery based on the total theoretical absorbance released at 420 nm (A), and the percent contribution of curcumin release products at the final degradation time point (B). Error bars represent standard error of the mean, and * represent significant differences ($p<0.05$) compared to the control release products using a paired t-test.

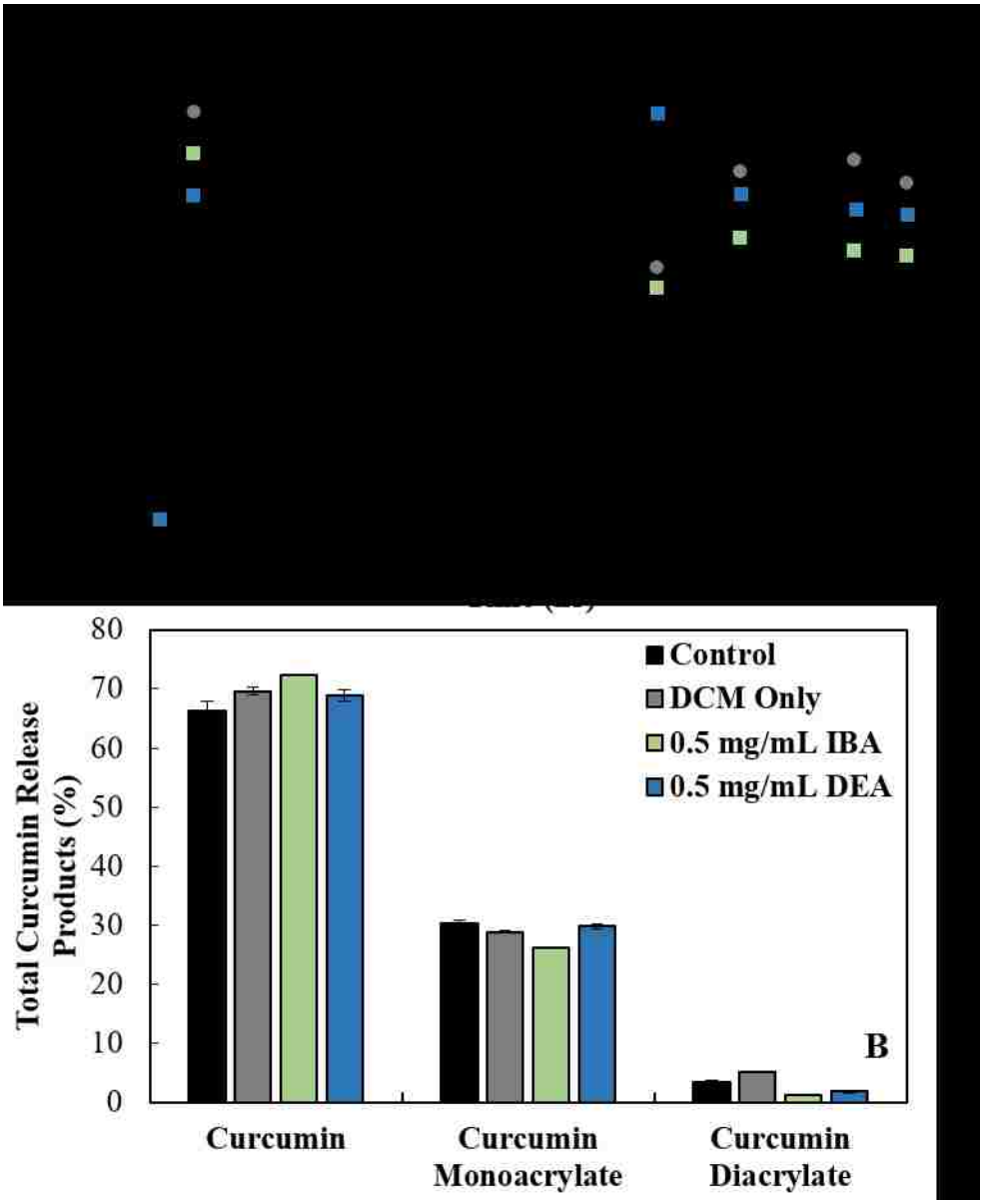

Figure 7-2: 38 wt% curcumin conjugated PBAE films incubated with DCM, 0.5 mg/mL IBA, and 0.5 mg/mL DEA for 48 hours at 50°C. The percent recovery based on the total theoretical absorbance released at 420 nm (A), and the percent contribution of curcumin release products at the final degradation time point (B). Error bars represent standard error of the mean. No significant changes in modified films compared to the control ($p>0.05$) using a paired t-test.

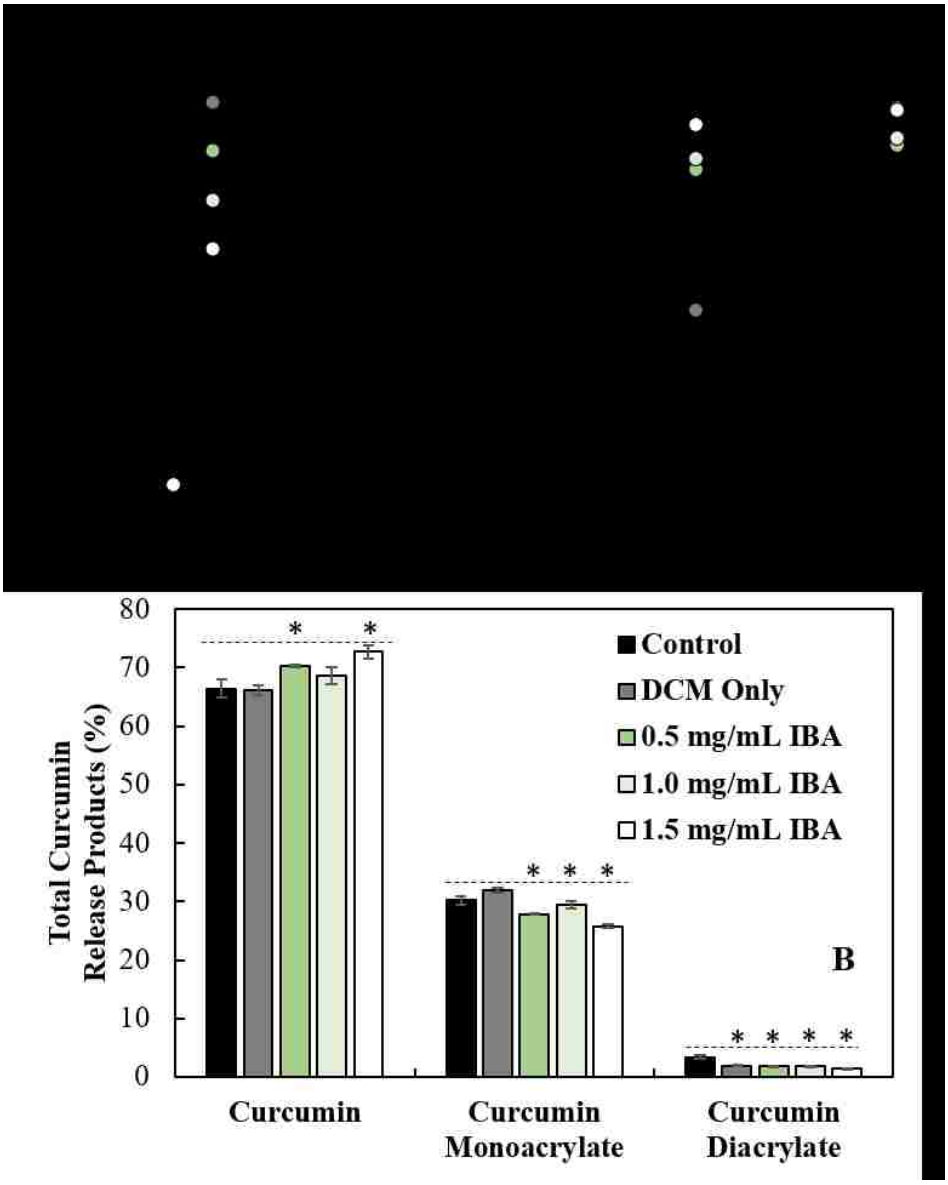

Figure 7-3: 38 wt% curcumin conjugated PBAE films were incubated with DCM, 0.5, 1, and 1.5 mg/mL IBA in DCM for 6 hours at 50°C. The percent recovery based on the total theoretical absorbance released at 420 nm (A), and the percent contribution of curcumin release products at the final degradation time point (B). Error bars represent standard error of the mean, and * represent significant differences ($p<0.05$) compared to the control release products using a paired t-test.

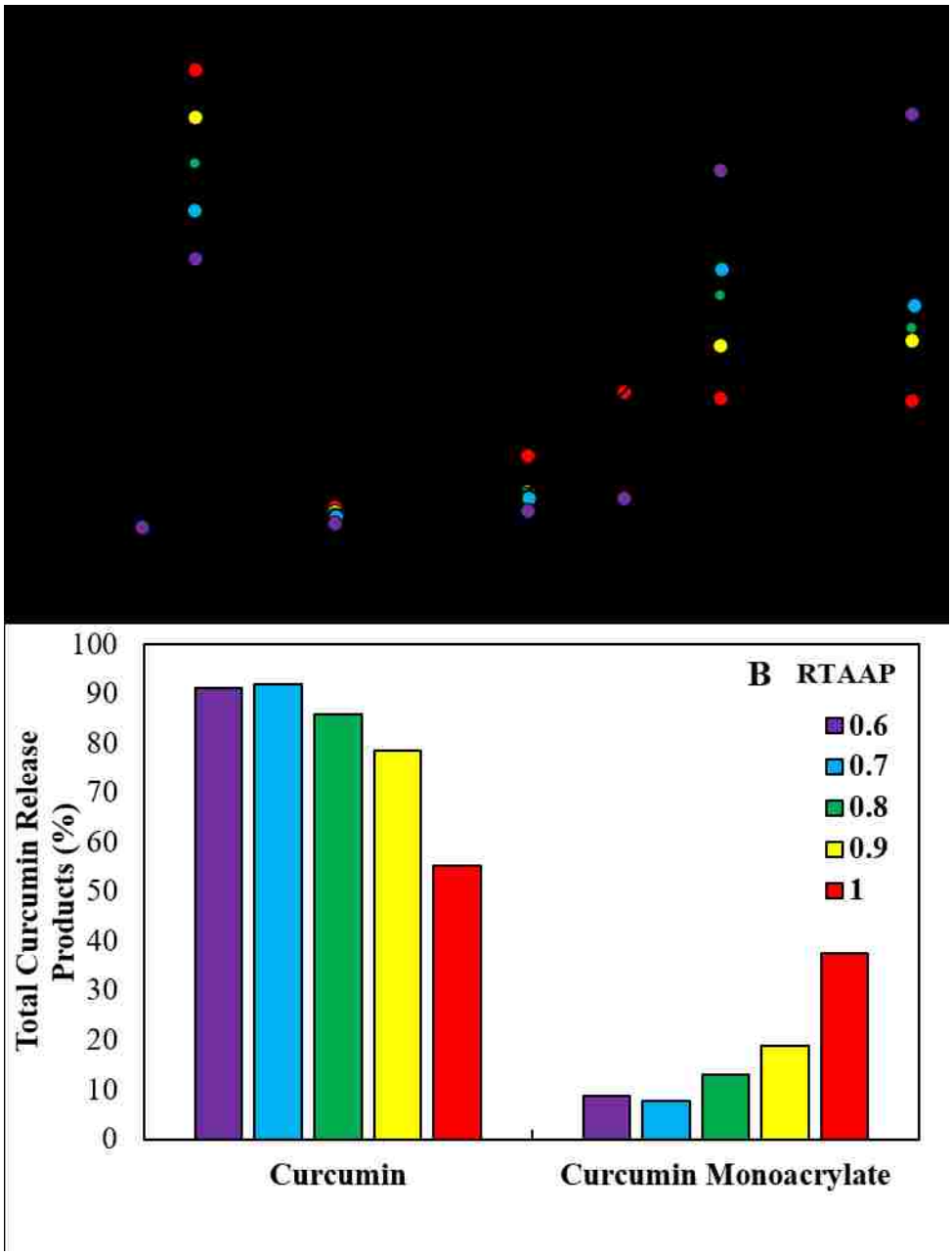

Figure 7-4: 26 wt% curcumin conjugated PBAE films were synthesized at different ratio of total acrylate to amine protons (RTAAP = 0.6, 0.7, 0.8, 0.9, 1.0). The percent recovery based on the total theoretical absorbance released at 420 nm (A), and the percent contribution of curcumin release products at the final degradation time point (B).

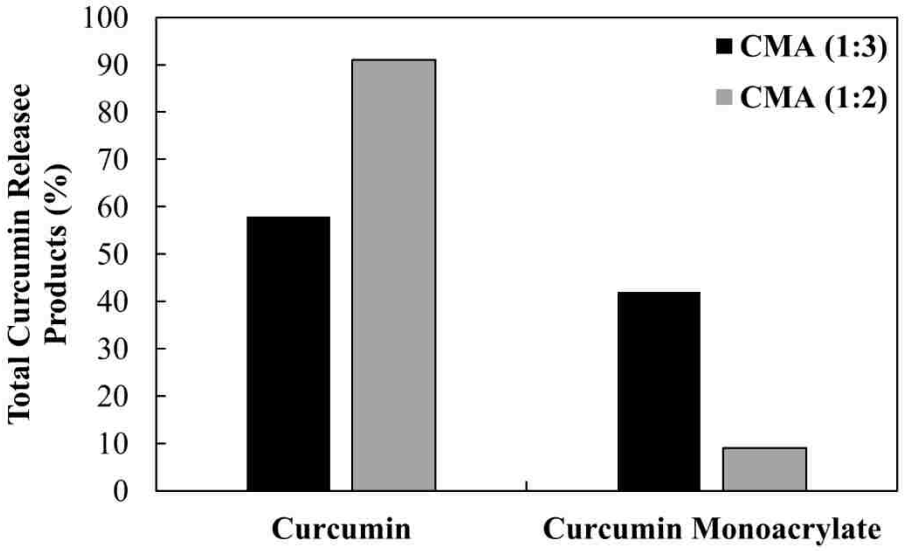

Figure 7-5: Comparison of CMA (1:3) and CMA (1:2) starting material in 26 wt% curcumin conjugated PBAE film release products.

Chapter 8 Conclusions

In this work, curcumin, a potent antioxidant with anti-inflammatory properties, was modified into a multiacrylate starting material, and incorporated into the backbone of a hydrolytically degradable network. The stability of the curcumin and the response of the polymer was explored by varying the curcumin content of the network in the presence of AAPH, H_2O_2, and acidic environments.

In **Chapter 3**, the oxidative consumption rates of curcumin were explored. Curcumin was highly unstable in the presence of a free radical generating environment, AAPH. A kinetic rate model was developed to find the oxidative consumption of curcumin as a free molecule. Efforts were made to develop a model that represented the rate of release and rate of consumption from a microparticle network simultaneously; however, simple models were unable to capture the effects of AAPH. Curcumin degradation products were further analyzed to find a second curcumin acrylated release product present. The fully degraded networks were then studied in AAPH solutions, and the oxidative consumption rate of curcumin and curcumin monoacrylate were found. Curcumin monoacrylate was found to have a slower rate of consumption than curcumin, resulting in lower scavenging ability with the acrylate group present. The rate models were then used to predict consumption profiles in the presence of higher concentrations of AAPH and were used to demonstrate the importance of controlled release antioxidant systems compared to bolus doses in the presence of a free radical generating environment.

In **Chapter 4**, the response of curcumin and the polymer network were further investigated in the presence of AAPH and H_2O_2. The sensitivity of the hydrolysis was found to be dependent on the source of the oxidizing environment and loading of curcumin

within the network. AAPH showed little to no effect on the swelling and total polymer content, and slight suppression of the total curcumin and curcumin monoacrylate released over time. For hydrogen peroxide, a significant effect was found on the polymer network where accelerated swelling, degradation, and increase in curcumin release was seen. It also promoted base catalyzed hydrolysis of the monoacrylate present on the curcumin product and the recovery of curcumin and total antioxidant activity increased.

Chapter 5 focused on the responsiveness of the PBAE networks in the presence of the different pH environments. The polymers of three different curcumin loadings were found to have dependent degradation times based on the amount of curcumin. Films that were only made with PEG(400)DA and TTD had fast degradation times in neutral conditions, but as the pH decreased the degradation was extended to 5 weeks. With curcumin incorporated in the network, at pH 3 the degradation time and swelling profiles were still extended significantly. This could be due to the change in localized pKa within the network as it degrades, limiting the swelling of the films with higher curcumin content, or even the degradation of curcumin in such acidic environments that compromised the network and allowed for faster hydrolysis and release.

Chapter 6 translated the microparticle system into an oral rinse formulation to study the effect of 18 and 24 hour curcumin-conjugated films for the treatment and suppression of oral mucositis in a hamster model. The greatest effect was seen by treating the cheek pouch daily for 28 days with 20% (w/w) C90 microparticles after an acute dose of radiation. And lastly, **Chapter 7** discusses the efforts on optimizing the polymer network to reduce the amount of curcumin monoacrylate released to achieve higher, more active, pure drug release over time.

These studies have demonstrated the response curcumin-conjugated poly(beta-amino ester) polymers have in the presence of oxidizing environments and the positive effect a particular formulation of the microparticle system can have oxidative stress induced diseases, such as oral mucositis. Using the knowledge of the polymer sensitivity in the presence of hydrogen peroxide concentrated environments, new applications using these networks could be investigated to treat other diseases that mimic burst release radical generation.

The understanding of the polymer's responsiveness to oxidative stress environments strengthens the platform being built for antioxidant poly(beta-amino ester) material design, and the possibilities remain endless for the application and impact these systems will make in the pharmaceutical industry.

REFERENCES

1. Kirkham, P.A. and P.J. Barnes, *Oxidative Stress in COPD.* CHEST. **144**(1): p. 266-273.

2. Waris, G. and H. Ahsan, *Reactive oxygen species: role in the development of cancer and various chronic conditions.* Journal of Carcinogenesis, 2006. **5**: p. 14-14.

3. Maria, O.M., N. Eliopoulos, and T. Muanza, *Radiation-Induced Oral Mucositis.* Frontiers in Oncology, 2017. **7**: p. 89.

4. Pham-Huy, L.A., H. He, and C. Pham-Huy, *Free Radicals, Antioxidants in Disease and Health.* International Journal of Biomedical Science : IJBS, 2008. **4**(2): p. 89-96.

5. Huang, M., et al., *Encapsulation of flavonoids in liposomal delivery systems: the case of quercetin, kaempferol and luteolin.* Food & Function, 2017. **8**(9): p. 3198-3208.

6. Watkins, R., et al., *Natural product-based nanomedicine: recent advances and issues.* International Journal of Nanomedicine, 2015. **10**: p. 6055-6074.

7. Pisoschi, A.M. and A. Pop, *The role of antioxidants in the chemistry of oxidative stress: A review.* European Journal of Medicinal Chemistry, 2015. **97**: p. 55-74.

8. Jordan, C., et al., *The Role of Carrier Geometry in Overcoming Biological Barriers to Drug Delivery.* Current pharmaceutical design, 2015.

9. Liechty, W.B., et al., *Polymers for Drug Delivery Systems.* Annual review of chemical and biomolecular engineering, 2010. **1**: p. 149-173.

10. Gemma, V., T.-P. Judit, and A. Fernando, *Polymers and Drug Delivery Systems.* Current Drug Delivery, 2012. **9**(4): p. 367-394.

11. Wattamwar, P.P., et al., *Synthesis and characterization of poly (antioxidant β-amino esters) for controlled release of polyphenolic antioxidants.* Acta biomaterialia, 2012. **8**(7): p. 2529-2537.

12. Giacco, F. and M. Brownlee, *Oxidative stress and diabetic complications.* Circulation research, 2010. **107**(9): p. 1058-1070.

13. Waisundara, V.Y. and L.Y. Hoon, *Free radical scavenging ability of Aspalathus linearis in two in vitro models of diabetes and cancer.* Journal of Traditional and Complementary Medicine, 2015. **5**(3): p. 174-178.

14. Wright, E., J.L. Scism-Bacon, and L.C. Glass, *Oxidative stress in type 2 diabetes: the role of fasting and postprandial glycaemia.* International Journal of Clinical Practice, 2006. **60**(3): p. 308-314.

15. Redding, S.W., *Cancer therapy-related oral mucositis.* Journal of dental education, 2005. **69**(8): p. 919-929.

16. Naidu, M.U.R., et al., *Chemotherapy-Induced and/or Radiation Therapy-Induced Oral Mucositis—Complicating the Treatment of Cancer.* Neoplasia (New York, N.Y.), 2004. **6**(5): p. 423-431.

17. Foundation, T.O.C. *Mucositis*. Information - Support - Advocacy - Research.. and Hope 2018 [cited 2018 March 2].

18. Sonis, S., *Oral mucositis.* Anti-cancer drugs, 2011. **22**(7): p. 607-612.
19. Krishnatry, R., et al., *Oral Radiation Mucositis: A Short Review*. Vol. 2. 2011. 37-43.

20. Houle, F. and J. Huot, *Dysregulation of the Endothelial Cellular Response to Oxidative Stress in Cancer.* InterScience, 2006.

21. Reuter, S., et al., *Oxidative stress, inflammation, and cancer: How are they linked?* Free radical biology & medicine, 2010. **49**(11): p. 1603-1616.

22. Houle, F. and J. Huot, *Dysregulation of the endothelial cellular response to oxidative stress in cancer.* Molecular carcinogenesis, 2006. **45**(6): p. 362-367.

23. Mircescu, G., *Oxidative Stress and Kidney Disease.* Acta Endocrinologica (1841-0987), 2008. **4**(4).

24. Putri, A.Y. and M. Thaha, *Role of oxidative stress on chronic kidney disease progression.* Acta Medica Indonesiana, 2016. **46**(3).

25. Fabbri, L.M., et al., *The Multiple Components of COPD*, in *COPD: A Guide to Diagnosis and Clinical Management*, N.A. Hanania and A. Sharafkhaneh, Editors. 2011, Humana Press: Totowa, NJ. p. 1-20.

26. Uttara, B., et al., *Oxidative Stress and Neurodegenerative Diseases: A Review of Upstream and Downstream Antioxidant Therapeutic Options.* Current Neuropharmacology, 2009. **7**(1): p. 65-74.

27. Jarrett, S.G. and M.E. Boulton, *Consequences of oxidative stress in age-related macular degeneration.* Molecular Aspects of Medicine, 2012. **33**(4): p. 399-417.
28. Society, A.C. *Global Cancer: Facts and Figures*. 2015; 3rd.

29. Ott, M., et al., *Mitochondria, oxidative stress and cell death.* Apoptosis, 2007. **12**(5): p. 913-922.

30. McArdle, F., et al., *Effects of oral vitamin E and β-carotene supplementation on ultraviolet radiation–induced oxidative stress in human skin.* The American Journal of Clinical Nutrition, 2004. **80**(5): p. 1270-1275.

31. Valavanidis, A., T. Vlachogianni, and K. Fiotakis, *Tobacco Smoke: Involvement of Reactive Oxygen Species and Stable Free Radicals in Mechanisms of Oxidative Damage, Carcinogenesis and Synergistic Effects with Other Respirable Particles.* International Journal of Environmental Research and Public Health, 2009. **6**(2): p. 445-462.

32. Gupta, P., et al., *The environmental pollutant, polychlorinated biphenyls, and cardiovascular disease: a potential target for antioxidant nanotherapeutics*. 2017. 1-20.

33. Gupta, P., et al., *Controlled Curcumin Release via Conjugation into PBAE Nanogels Enhances Mitochondrial Protection against Oxidative Stress.* International Journal of Pharmaceutics.

34. Abe, J. and B.C. Berk, *Reactive oxygen species as mediators of signal transduction in cardiovascular disease.* Trends in Cardiovascular Medicine, 1998. **8**(2): p. 59-64.

35. Panieri, E. and M.M. Santoro, *ROS homeostasis and metabolism: a dangerous liason in cancer cells.* Cell Death &Amp; Disease, 2016. **7**: p. e2253.

36. Lehnert, S., *Biomolecular action of ionizing radiation*. 2007: CRC Press.

37. Chen, J., S.C. Rogers, and M. Kavdia, *Analysis of Kinetics of Dihydroethidium Fluorescence with Superoxide Using Xanthine Oxidase and Hypoxanthine Assay.* Annals of Biomedical Engineering, 2013. **41**(2): p. 327-337.

38. Gupta, P., A. Lakes, and T. Dziubla, *Chapter One - A Free Radical Primer*, in *Oxidative Stress and Biomaterials*. 2016, Academic Press. p. 1-33.

39. Bienert, G.P., J.K. Schjoerring, and T.P. Jahn, *Membrane transport of hydrogen peroxide.* Biochimica et Biophysica Acta (BBA)-Biomembranes, 2006. **1758**(8): p. 994-1003.

40. Kaur, R., et al., *Oxidative stress—implications, source and its prevention.* Environmental Science and Pollution Research, 2014. **21**(3): p. 1599-1613.

41. Nimse, S.B. and D. Pal, *Free radicals, natural antioxidants, and their reaction mechanisms.* RSC Advances, 2015. **5**(35): p. 27986-28006.

42. Aguilar, T.A.F., B.C.H. Navarro, and J.A.M. Pérez, *Endogenous Antioxidants: A Review of their Role in Oxidative Stress*, in *A Master Regulator of Oxidative Stress - The Transcription Factor Nrf2*, J.A. Morales-Gonzalez, A. Morales-Gonzalez, and E.O. Madrigal-Santillan, Editors. 2016, InTech: Rijeka. p. Ch. 01.

43. Cochran, D. and T.D. Dziubla, *Antioxidant Polymers for Tuning Biomaterial Biocompatibility: From Drug Delivery to Tissue Engineering.* Antioxidant Polymers: Synthesis, Properties, and Applications, 2012: p. 459-484.

44. Lin, Y.-H., et al., *Approach To Deliver Two Antioxidant Enzymes with Mesoporous Silica Nanoparticles into Cells.* ACS Applied Materials & Interfaces, 2016. **8**(28): p. 17944-17954.

45. Kusumawati, I. and G. Indrayanto, *Chapter 15 - Natural Antioxidants in Cosmetics*, in *Studies in Natural Products Chemistry*, R. Atta ur, Editor. 2013, Elsevier. p. 485-505.

46. Celestino, M.T., et al., *Rational use of antioxidants in solid oral pharmaceutical preparations.* Brazilian Journal of Pharmaceutical Sciences, 2012. **48**: p. 405-415.

47. Velioglu, Y.S., et al., *Antioxidant Activity and Total Phenolics in Selected Fruits, Vegetables, and Grain Products.* Journal of Agricultural and Food Chemistry, 1998. **46**(10): p. 4113-4117.

48. Jayaprakasha, G.K., L. Jaganmohan Rao, and K.K. Sakariah, *Antioxidant activities of curcumin, demethoxycurcumin and bisdemethoxycurcumin.* Food Chemistry, 2006. **98**(4): p. 720-724.

49. Gambini, J., et al., *Properties of Resveratrol: In Vitro and In Vivo Studies about Metabolism, Bioavailability, and Biological Effects in Animal Models and Humans.* Oxidative Medicine and Cellular Longevity, 2015. **2015**: p. 13.

50. Lommen, A., et al., *Application of Directly Coupled HPLC−NMR−MS to the Identification and Confirmation of Quercetin Glycosides and Phloretin Glycosides in Apple Peel.* Analytical Chemistry, 2000. **72**(8): p. 1793-1797.

51. Paritosh P. Wattamwar, T.D.D., *Chapter 12: Modulation of the wound healing response through oxidation active materials*. University of Kentucky

52. Ahsan, H., et al., *Pro-oxidant, anti-oxidant and cleavage activities on DNA of curcumin and its derivatives demethoxycurcumin and bisdemethoxycurcumin.* Chemico-biological interactions, 1999. **121**(2): p. 161-175.

53. Aggeli, I.-K., et al., *Curcumin Acts as a Pro-Oxidant Inducing Apoptosis Via JNKs in the Isolated Perfused Rana ridibunda Heart.* Journal of Experimental Zoology Part A: Ecological Genetics and Physiology, 2013. **319**(6): p. 328-339.

54. Rahal, A., et al., *Oxidative Stress, Prooxidants, and Antioxidants: The Interplay.* BioMed Research International, 2014. **2014**: p. 19.

55. Sandur, S.K., et al., *Role of Prooxidants and Antioxidants in the Anti-Inflammatory and Apoptotic Effects of Curcumin (Diferuloylmethane).* Free radical biology & medicine, 2007. **43**(4): p. 568-580.

56. Wattamwar, P.P., et al., *Tuning of the pro-oxidant and antioxidant activity of trolox through the controlled release from biodegradable poly (trolox ester) polymers.* Journal of Biomedical Materials Research Part A, 2011. **99**(2): p. 184-191.

57. Jiao, Y., et al., *Iron chelation in the biological activity of curcumin.* Free Radical Biology and Medicine, 2006. **40**(7): p. 1152-1160.

58. Wilken, R., et al., *Curcumin: A review of anti-cancer properties and therapeutic activity in head and neck squamous cell carcinoma.* Molecular Cancer, 2011. **10**: p. 12-12.

59. Shakibaei, M., et al., *Suppression of NF-κB activation by curcumin leads to inhibition of expression of cyclo-oxygenase-2 and matrix metalloproteinase-9 in human articular chondrocytes: Implications for the treatment of osteoarthritis.* Biochemical Pharmacology, 2007. **73**(9): p. 1434-1445.

60. Agrawal, M., et al., *Ischemic insult induced apoptotic changes in PC12 cells: Protection by trans resveratrol.* European Journal of Pharmacology, 2011. **666**(1): p. 5-11.

61. Karthaus, M., et al., *Effect of topical oral G-CSF on oral mucositis: a randomised placebo-controlled trial.* Bone marrow transplantation, 1998. **22**(8): p. 781-785.

62. Watanabe, S., et al., *Assessment of the hamster cheek pouch as a model for radiation-induced oral mucositis, and evaluation of the protective effects of keratinocyte growth factor using this model.* International journal of radiation biology, 2014. **90**(10): p. 884-891.

63. Veeck, E.B., V.M. Trucci, and A.R.C. Morosolli, *Current strategies for the management of oral mucositis induced by radiotherapy or chemotherapy.* 2009.

64. Volpato, L.E.R., et al., *Radiation therapy and chemotherapy-induced oral mucositis.* Revista Brasileira de Otorrinolaringologia, 2007. **73**(4): p. 562-568.

65. Biswal, B.M., *Current Trends in the Management of Oral Mucositis Related to Cancer Treatment.* The Malaysian Journal of Medical Sciences : MJMS, 2008. **15**(3): p. 4-13.

66. Petkau, A., W. Chelack, and S. Pleskach, *Protection of post-irradiated mice by superoxide dismutase.* International Journal of Radiation Biology and Related Studies in Physics, Chemistry and Medicine, 1976. **29**(3): p. 297-299.

67. Miyamoto, H., et al., *The relationship between the severity of radiation-induced oral mucositis and the myeloperoxidase levels in rats.* Oral Surgery, Oral Medicine, Oral Pathology and Oral Radiology, 2015. **120**(3): p. 329-336.

68. Napoli, C., et al., *Effects of Nitric Oxide on Cell Proliferation: Novel Insights.* Journal of the American College of Cardiology, 2013. **62**(2): p. 89-95.

69. Olivera, A., et al., *Inhibition of the NF-κB signaling pathway by the curcumin analog, 3,5-Bis(2-pyridinylmethylidene)-4-piperidone (EF31): anti-inflammatory and anti-cancer properties.* International Immunopharmacology, 2012. **12**(2): p. 368-377.

70. Lalla, R.V., S.T. Sonis, and D.E. Peterson, *Management of oral mucositis in patients who have cancer*. Dental Clinics of North America, 2008. **52**(1): p. 61-77.

71. Spielberger , R., et al., *Palifermin for Oral Mucositis after Intensive Therapy for Hematologic Cancers.* New England Journal of Medicine, 2004. **351**(25): p. 2590-2598.

72. David Evans, B.H., Inge Kowanko *Prevention and Treatment of Oral Mucositis In Cancer Patients*. Best Practice, 2016. **2**, 1-6.

73. Allison, R.R., et al., *Multi-institutional, randomized, double-blind, placebo-controlled trial to assess the efficacy of a mucoadhesive hydrogel (MuGard) in mitigating oral mucositis symptoms in patients being treated with chemoradiation therapy for cancers of the head and neck.* Cancer, 2014. **120**(9): p. 1433-1440.

74. Rao, S., et al., *The Indian Spice Turmeric Delays and Mitigates Radiation-Induced Oral Mucositis in Patients Undergoing Treatment for Head and Neck Cancer An Investigational Study.* Integrative cancer therapies, 2014. **13**(3): p. 201-210.

75. Esatbeyoglu, T., et al., *Curcumin—from molecule to biological function.* Angewandte Chemie International Edition, 2012. **51**(22): p. 5308-5332.

76. Sonis, S.T., *Mucositis as a biological process: a new hypothesis for the development of chemotherapy-induced stomatotoxicity.* Oral Oncology. **34**(1): p. 39-43.

77. Koren, E. and V.P. Torchilin, *Drug carriers for vascular drug delivery.* IUBMB Life, 2011. **63**(8): p. 586-595.

78. Lai, S.K., Y.-Y. Wang, and J. Hanes, *Mucus-penetrating nanoparticles for drug and gene delivery to mucosal tissues.* Advanced drug delivery reviews, 2009. **61**(2): p. 158-171.

79. Patel, A., et al., *Ocular drug delivery systems: An overview.* World journal of pharmacology, 2013. **2**(2): p. 47-64.

80. Barua, S. and S. Mitragotri, *Challenges associated with Penetration of Nanoparticles across Cell and Tissue Barriers: A Review of Current Status and Future Prospects.* Nano today, 2014. **9**(2): p. 223-243.

81. Govender, T., et al., *Implantable and transdermal polymeric drug delivery technologies for the treatment of central nervous system disorders.* Pharmaceutical development and technology, 2017. **22**(4): p. 476-486.

82. Best, J.P., Y. Yan, and F. Caruso, *The Role of Particle Geometry and Mechanics in the Biological Domain.* Advanced Healthcare Materials, 2012. **1**(1): p. 35-47.

83. Ting, J.M., et al., *Advances in Polymer Design for Enhancing Oral Drug Solubility and Delivery.* Bioconjugate chemistry, 2018.

84. Unagolla, J.M. and A.C. Jayasuriya, *Drug transport mechanisms and in vitro release kinetics of vancomycin encapsulated chitosan-alginate polyelectrolyte microparticles as a controlled drug delivery system.* European Journal of Pharmaceutical Sciences, 2018. **114**: p. 199-209.

85. Xiao, Y., et al., *Mechanical Testing of Hydrogels in Cartilage Tissue Engineering: Beyond the Compressive Modulus.* Tissue Engineering. Part B, Reviews, 2013. **19**(5): p. 403-412.

86. Akhtar, M.F., M. Hanif, and N.M. Ranjha, *Methods of synthesis of hydrogels … A review.* Saudi Pharmaceutical Journal, 2016. **24**(5): p. 554-559.

87. Maitra, J. and V.K. Shukla, *Cross-linking in hydrogels-a review.* American Journal of Polymer Science, 2014. **4**(2): p. 25-31.

88. West, J.L. and J.A. Hubbell, *Comparison of covalently and physically cross-linked polyethylene glycol-based hydrogels for the prevention of postoperative adhesions in a rat model.* Biomaterials, 1995. **16**(15): p. 1153-1156.

89. Hennink, W.E. and C.F. van Nostrum, *Novel crosslinking methods to design hydrogels.* Advanced Drug Delivery Reviews, 2012. **64**: p. 223-236.

90. Rizwan, M., et al., *pH sensitive hydrogels in drug delivery: Brief history, properties, swelling, and release mechanism, material selection and applications*. Vol. 9. 2017.

91. Paul, D.F., et al., *Multifunctional poly(β -amino ester) hydrogel microparticles in periodontal in situ forming drug delivery systems.* Biomedical Materials, 2016. **11**(2): p. 025002.

92. L. Lakes, A., et al., *Reducible Disulfide Poly(beta-amino ester) Hydrogels for Antioxidant Delivery*. 2017.

93. Fernando, I.R., et al., *Esterase- and pH-responsive poly([small beta]-amino ester)-capped mesoporous silica nanoparticles for drug delivery.* Nanoscale, 2015. **7**(16): p. 7178-7183.

94. Wattamwar, P.P., et al., *Antioxidant activity of degradable polymer poly (trolox ester) to suppress oxidative stress injury in the cells.* Advanced Functional Materials, 2010. **20**(1): p. 147-154.

95. Priya James, H., et al., *Smart polymers for the controlled delivery of drugs – a concise overview.* Acta Pharmaceutica Sinica B, 2014. **4**(2): p. 120-127.

96. Ward, M.A. and T.K. Georgiou, *Thermoresponsive Polymers for Biomedical Applications.* Polymers, 2011. **3**(3): p. 1215.

97. Lue, S.J., C.-H. Chen, and C.-M. Shih, *Tuning of Lower Critical Solution Temperature (LCST) of Poly(N-Isopropylacrylamide-co-Acrylic acid) Hydrogels.* Journal of Macromolecular Science, Part B, 2011. **50**(3): p. 563-579.

98. Tang, S., et al., *Synthesis and characterization of thermally responsive N-isopropylacrylamide hydrogels copolymerized with novel hydrophobic polyphenolic crosslinkers.* Materials Today Communications, 2017. **10**: p. 46-53.

99. Hatefi, A. and B. Amsden, *Biodegradable injectable in situ forming drug delivery systems.* Journal of Controlled Release, 2002. **80**(1): p. 9-28.

100. Liu, L., et al., *In situ forming hydrogels based on chitosan for drug delivery and tissue regeneration.* Asian Journal of Pharmaceutical Sciences, 2016. **11**(6): p. 673-683.

101. Bertrand, N., et al., *Cancer nanotechnology: The impact of passive and active targeting in the era of modern cancer biology.* Advanced Drug Delivery Reviews, 2014. **66**: p. 2-25.

102. Upreti, M., A. Jyoti, and P. Sethi, *Tumor microenvironment and nanotherapeutics.* Translational cancer research, 2013. **2**(4): p. 309-319.

103. Kozielski, K.L., S.Y. Tzeng, and J.J. Green, *Bioengineered Nanoparticles for siRNA delivery.* Wiley interdisciplinary reviews. Nanomedicine and nanobiotechnology, 2013. **5**(5): p. 449-468.

104. Lee, S.H., et al., *Current Progress in Reactive Oxygen Species (ROS)-Responsive Materials for Biomedical Applications.* Advanced healthcare materials, 2013. **2**(6): p. 908-915.

105. Day, B.J., *Antioxidant therapeutics: Pandora's box.* Free Radical Biology and Medicine, 2014. **66**: p. 58-64.

106. Agrawal, M., *Natural polyphenols based new therapeutic avenues for advanced biomedical applications.* Drug Metabolism Reviews, 2015. **47**(4): p. 420-430.

107. Bisson, J., et al., *Can Invalid Bioactives Undermine Natural Product-Based Drug Discovery?* Journal of Medicinal Chemistry, 2016. **59**(5): p. 1671-1690.

108. Felice, F., et al., *Delivery of natural polyphenols by polymeric nanoparticles improves the resistance of endothelial progenitor cells to oxidative stress.* European Journal of Pharmaceutical Sciences, 2013. **50**(3): p. 393-399.

109. Yan, H., et al., *Functional Mesoporous Silica Nanoparticles for Photothermal-Controlled Drug Delivery In Vivo.* Angewandte Chemie International Edition, 2012. **51**(33): p. 8373-8377.

110. Gupta, P., et al., *Controlled curcumin release via conjugation into PBAE nanogels enhances mitochondrial protection against oxidative stress.* International Journal of Pharmaceutics, 2016. **511**(2): p. 1012-1021.

111. Conner, E.M. and M.B. Grisham, *Inflammation, free radicals, and antioxidants.* Nutrition. **12**(4): p. 274-277.

112. He, G., et al., *Oxygen free radical involvement in acute lung injury induced by H5N1 virus in mice.* Influenza and Other Respiratory Viruses, 2013. **7**(6): p. 945-953.

113. Zweier, J.L. and M.H. Talukder, *The role of oxidants and free radicals in reperfusion injury.* Cardiovascular research, 2006. **70**(2): p. 181-190.

114. Ortiz, F., et al., *Melatonin blunts the mitochondrial/NLRP3 connection and protects against radiation-induced oral mucositis.* Journal of Pineal Research, 2015. **58**(1): p. 34-49.

115. Z.M. Malik Al-Rubaei, T.U.M., Layla Karim Ali, *Effects of Local Curcumin on Oxidative Stress adn Total Antioxidant Capacity in vivo Study.* Pakistan journal of pharmaceutical sciences, 2014. **17**(12): p. 1237-1241.

116. Patil, V.S., T.D. Dziubla, and D.S. Kalika, *Static and dynamic properties of biodegradable poly(antioxidant β-amino ester) networks based on incorporation of curcumin multiacrylate.* Polymer, 2015. **75**: p. 88-96.

117. Dash, S., et al., *Kinetic modeling on drug release from controlled drug delivery systems.* Acta Pol Pharm, 2010. **67**(3): p. 217-23.

118. Patil, V.S., et al., *Curcumin Acrylation for Biological and Environmental Applications.* Journal of Natural Products, 2017. **80**(7): p. 1964-1971.

119. Werber, J., et al., *Analysis of 2,2’-Azobis (2-Amidinopropane) Dihydrochloride Degradation and Hydrolysis in Aqueous Solutions.* Journal of Pharmaceutical Sciences. **100**(8): p. 3307-3315.

120. Steenken, S. and P. Neta, *Oxidation of substituted alkyl radicals by hexachloroiridate(2-), hexacyanoferrate(3-), and permanganate ions in aqueous solution. Electron transfer versus chlorine transfer from hexachloroiridate(2-) ion.* Journal of the American Chemical Society, 1982. **104**(5): p. 1244-1248.

121. Gruber, S. and W. Dörr, *Tissue reactions to ionizing radiation—Oral mucosa.* Mutation Research/Reviews in Mutation Research, 2016. **770**: p. 292-298.

122. McBath, R.A. and D.A. Shipp, *Swelling and degradation of hydrogels synthesized with degradable poly (β-amino ester) crosslinkers.* Polymer Chemistry, 2010. **1**(6): p. 860-865.

123. Ak, T. and İ. Gülçin, *Antioxidant and radical scavenging properties of curcumin.* Chemico-biological interactions, 2008. **174**(1): p. 27-37.

124. FERREIRA, I.M., et al., *Exhaled Nitric Oxide and Hydrogen Peroxide in Patients with Chronic Obstructive Pulmonary Disease.* American Journal of Respiratory and Critical Care Medicine, 2001. **164**(6): p. 1012-1015.

125. Halliwell, B., M.V. Clement, and L.H. Long, *Hydrogen peroxide in the human body.* FEBS Letters, 2000. **486**(1): p. 10-13.

126. Van Eeden, S.F. and D.D. Sin, *Oxidative stress in chronic obstructive pulmonary disease: A lung and systemic process.* Canadian Respiratory Journal : Journal of the Canadian Thoracic Society, 2013. **20**(1): p. 27-29.

127. Moghaddam, S.J., et al., *Curcumin inhibits COPD-like airway inflammation and lung cancer progression in mice.* Carcinogenesis, 2009. **30**(11): p. 1949-1956.

128. Lee, D., et al., *Hydrogen peroxide-responsive copolyoxalate nanoparticles for detection and therapy of ischemia–reperfusion injury.* Journal of controlled release : official journal of the Controlled Release Society, 2013. **172**(3): p. 1102-1110.

129. Cui, Y., et al., *Facile Synthesis of H2O2-Cleavable Poly(ester-amide)s by Passerini Multicomponent Polymerization.* ACS Macro Letters, 2017. **6**(1): p. 11-15.

130. Biswal, D., et al., *A single-step polymerization method for poly(β-amino ester) biodegradable hydrogels.* Polymer, 2011. **52**(26): p. 5985-5992.

131. Gupta, P., et al., *Quercetin conjugated poly(β-amino esters) nanogels for the treatment of cellular oxidative stress.* Acta Biomaterialia, 2015. **27**: p. 194-204.

132. Lynn, D.M. and R. Langer, *Degradable Poly(β-amino esters): Synthesis, Characterization, and Self-Assembly with Plasmid DNA.* Journal of the American Chemical Society, 2000. **122**(44): p. 10761-10768.

133. Zhang, Y., et al., *Trigger-Responsive Poly(β-amino ester) Hydrogels.* ACS Macro Letters, 2014. **3**(7): p. 693-697.

134. Kozielski, K.L. and J.J. Green, *Bioreducible poly(beta-amino ester)s for intracellular delivery of siRNA.* Methods in molecular biology (Clifton, N.J.), 2016. **1364**: p. 79-87.

135. Kim, T.-i. and S.W. Kim, *Bioreducible polymers for gene delivery.* Reactive and Functional Polymers, 2011. **71**(3): p. 344-349.

136. Sai Krishna Borra, P.G., Jaideep Mahendra, Jayamathi, K.M., Cherian, C. N. and Ram Chand, *Antioxidant and free radical scavenging activity of curcumin determined by using different in viro and ex vivo models.* Journal of Medicinal Plants Research, 2013. **7**(36): p. 10.

137. Prasad, S., A.K. Tyagi, and B.B. Aggarwal, *Recent Developments in Delivery, Bioavailability, Absorption and Metabolism of Curcumin: the Golden Pigment from Golden Spice.* Cancer Research and Treatment : Official Journal of Korean Cancer Association, 2014. **46**(1): p. 2-18.

138. Faraji, A.H. and P. Wipf, *Nanoparticles in cellular drug delivery.* Bioorganic & Medicinal Chemistry, 2009. **17**(8): p. 2950-2962.

139. Peppas, N.A., et al., *Hydrogels in pharmaceutical formulations.* European Journal of Pharmaceutics and Biopharmaceutics, 2000. **50**(1): p. 27-46.

140. Hu, Y.-B., et al., *The endosomal-lysosomal system: from acidification and cargo sorting to neurodegeneration.* Translational Neurodegeneration, 2015. **4**: p. 18.

141. Boskey, E.R., et al., *Origins of vaginal acidity: high d/l lactate ratio is consistent with bacteria being the primary source.* Human Reproduction, 2001. **16**(9): p. 1809-1813.

142. Dressman, J.B., et al., *Upper Gastrointestinal (GI) pH in Young, Healthy Men and Women.* Pharmaceutical Research, 1990. **7**(7): p. 756-761.

143. Little, S.R., et al., *Poly-β amino ester-containing microparticles enhance the activity of nonviral genetic vaccines.* Proceedings of the National Academy of Sciences of the United States of America, 2004. **101**(26): p. 9534-9539.

144. Shenoy, D., et al., *Poly(Ethylene Oxide)-Modified Poly(β-Amino Ester) Nanoparticles as a pH-Sensitive System for Tumor-Targeted Delivery of Hydrophobic Drugs: Part I. In Vitro Evaluations.* Molecular pharmaceutics, 2005. **2**(5): p. 357-366.

145. Gao, W., J.M. Chan, and O.C. Farokhzad, *pH-Responsive Nanoparticles for Drug Delivery.* Molecular Pharmaceutics, 2010. **7**(6): p. 1913-1920.

146. Little, S.R. and D.S. Kohane, *Polymers for intracellular delivery of nucleic acids.* Journal of Materials Chemistry, 2008. **18**(8): p. 832-841.

147. Sankaranarayanan, J., et al., *Multiresponse Strategies To Modulate Burst Degradation and Release from Nanoparticles.* ACS Nano, 2010. **4**(10): p. 5930-5936.

148. Kalra, J., et al., *Effect of oxygen free radicals, hypoxia and pH on the release of liver lysosomal enzymes.* Molecular and Cellular Biochemistry, 1990. **94**(1): p. 1-8.

149. Elving, P.J., J.M. Markowitz, and I. Rosenthal, *Preparation of Buffer Systems of Constant Ionic Strength.* Analytical Chemistry, 1956. **28**(7): p. 1179-1180.

150. Lee, W.-H., et al., *Curcumin and its Derivatives: Their Application in Neuropharmacology and Neuroscience in the 21st Century.* Current Neuropharmacology, 2013. **11**(4): p. 338-378.

151. Kwon, Y., *Mechanism-based management for mucositis: option for treating side effects without compromising the efficacy of cancer therapy.* OncoTargets and therapy, 2016. **9**: p. 2007-2016.

152. Al-Ansari, S., et al., *Oral Mucositis Induced By Anticancer Therapies.* Current Oral Health Reports, 2015. **2**(4): p. 202-211.

153. Sonis, S., et al., *Defining mechanisms of action of interleukin-11 on the progression of radiation-induced oral mucositis in hamsters.* Oral Oncology, 2000. **36**(4): p. 373-381.

154. M Logan, R., et al., *Serum levels of NF-κB and pro-inflammatory cytokines following administration of mucotoxic drugs.* Cancer biology & therapy, 2008. **7**(7): p. 1139-1145.

155. Raber-Durlacher, J.E., et al., *Systematic review of cytokines and growth factors for the management of oral mucositis in cancer patients.* Supportive Care in Cancer, 2013. **21**(1): p. 343-355.

156. Zhong, H. and H. Yin, *Role of lipid peroxidation derived 4-hydroxynonenal (4-HNE) in cancer: Focusing on mitochondria.* Redox Biology, 2015. **4**: p. 193-199.

157. Colley, H.E., et al., *Tissue-engineered oral mucosa to study radiotherapy-induced oral mucositis.* International Journal of Radiation Biology, 2013. **89**(11): p. 907-914.

158. Gehrke, T., et al., *Long-term changes in the properties of skin-derived fibroblasts following irradiation of the head and neck.* Oncology letters, 2017. **14**(3): p. 3780-3786.

159. Bettencourt, A.F., et al., *Biodegradation of acrylic based resins: A review.* dental materials, 2010. **26**(5): p. e171-e180.

160. Pemberton, M.A. and B.S. Lohmann, *Risk Assessment of residual monomer migrating from acrylic polymers and causing Allergic Contact Dermatitis during normal handling and use.* Regulatory Toxicology and Pharmacology, 2014. **69**(3): p. 467-475.

161. Tsigonia, A., et al., *Indoor Air in Beauty Salons and Occupational Health Exposure of Cosmetologists to Chemical Substances.* International Journal of Environmental Research and Public Health, 2010. **7**(1): p. 314.

162. Borelli, S. and F.O. Nestlé, *Sensitization and Development of Allergic Contact Dermatitis Caused by a Single Contact with an Electrosurgical Grounding Plate Containing Acrylates.* Dermatology, 1998. **197**(4): p. 381-382.

163. Vázquez-Osorio, I., et al., *Allergic contact dermatitis due to acrylates in acrylic gel nails: A report of 3 cases*. Vol. 105. 2013.

VITA

Carolyn Therese Jordan was born in St. Louis, MO and received her B.S. in Chemical Engineering in May 2013 at Illinois Institute of Technology in Chicago, Illinois. She joined the Department of Chemical and Materials Engineering at University of Kentucky in August 2013 to pursue a Doctor of Philosophy in Chemical Engineering under the advisory of Dr. Thomas Dziubla and co-advisory of Dr. J. Zachary Hilt.

HONORS AND AWARDS

- Chicago Undergraduate Research Symposium Poster Finalist, 2012
- Burt L. Sim's College of Engineering Fellow, FY 2015-2016
- 2nd Place Poster Session Award, Materials and Chemical Engineering Graduate Student Symposium, 2017
- Top 15 National Finalist, GORE Fellowship, 2017
- CME/MSE Outstanding Graduate Student Award, 2018
- College of Engineering Outstanding Doctoral Student Award Nominee, 2018
- 2nd Place Poster Session Award, Markey Cancer Research Day, 2018

PATENT APPLICATIONS

Dziubla, T.D., Hilt, J.Z., Jordan, C.T. "Oxidation Triggered Polymer Degradation." Approval to initiate patent application process by Intellectual Property Committee, March 28, 2018.

PUBLICATIONS

Jordan, C.T., Shuvaeuv, V.V., Bailey, M., Muzykantov, V.R., Dziubla, T.D., "The Role of Carrier Geometry in Overcoming Biological Barriers to Drug Delivery." *Current Pharmaceutical Design.* 2015, 22 (9). 1259-1273.

Gupta, P., Jordan, C.T., Mitov, M., Butterfield, D.A., Hilt, J.Z., Dziubla T. "Controlled curcumin release via conjugation into PBAE nanogels enhance mitochondrial protection against oxidative stress." *International Journal of Pharmaceutics.* 2016, 511. 1012-1021.

Gupta, P., Thompson, B., Wahlang, B., Jordan, C.T., Hilt, J.Z., Hennig, B., Dziubla, T. "The environmental pollutant, polychlorinated biphenyls, and cardiovascular disease: a potential target for antioxidant nanotherapeutics." *Drug Delivery and Translational Research.* 2017. 1-20.

Lakes, A., Jordan, C.T., Gupta, P., Puleo, D., Hilt, J.Z., Dziubla, T. "Reducible Disulfide Poly(beta-amino ester) Hydrogels for Antioxidant Delivery." *Acta Biomaterialia*. 2017. In Press.

Jordan, C.T., Hilt, J.Z., Dziubla, T. "Modeling the Oxidative Consumption of Curcumin from Controlled Released Poly(beta-amino ester) Microparticles in the Presence of a Free Radical Generating System." *Journal of Controlled Release.* 2018. To be submitted.

Jordan, C.T., Hilt, J.Z., Dziubla, T. "Triggered Response Poly(beta-amino ester) Thin Films in Oxidizing Environments." 2018. To be submitted.

Jordan, C.T., Wiegman, K., Vargason, A.M., Hilt, J.Z., Dziubla, T. "pH Responsive Poly(beta-amino ester) Crosslinked Hydrogels." 2018. To be submitted.

Jordan, C.T., Bhandari, R., Bradford, E., Vargason, A., Darby, D., Cheek, D., Wiegman, K., Savage, D., Howerton, B., Hilt, J.Z., Dziubla, T. "Poly(curcumin) Microparticle Efficacy for the Treatment of Radiation Induced Oral Mucositis in a Hamster Model." 2018. To be submitted.

PRESENTATIONS (oral/poster)

Sofia Hekmatfar, Carolyn T. Schumer, NW Karuri. *Development of an instructional module for fitting kinetic models to enzymatic degradation of proteins.* American Society of Engineering Education, 2012, poster

Carolyn T. Schumer, Paige L. Clark, Ava M. Vargason, J. Zach Hilt, Thomas D. Dziubla, Kimberly W. Anderson, *The Efficacy of Poly(trolox ester) Antioxidant Therapy and the Prevention of Metastatic Cancer Cell Adhesion,* Biomedical Research Day, University of Kentucky, March 2015, poster

Carolyn T. Jordan, Ava M. Vargason, J. Zach Hilt, Thomas D. Dziubla, Kimberly W. Anderson, *The Relationship Between Oxidative Stress and Breast Cancer Cell Adhesion Using an Ischemia/Reperfusion Injury Model,* AICHE Annual Meeting, November 2015, poster

Carolyn T. Jordan, J. Zach Hilt, Thomas D. Dziubla, *Evaluation of Microparticle Degradation and Activity in the Presence of Free Radical Generating Systems*, University of Kentucky CCTS Spring Conference, April 2016, poster

Carolyn T. Jordan, J. Zach Hilt, Thomas D. Dziubla, Evaluation of Microparticle Degradation and Activity in the Presence of Free Radical Generating Systems. American Institute of Chemical Engineers Annual Meeting 2016, San Francisco, CA, November 2016, oral

Carolyn T. Jordan, J. Zach Hilt, Thomas D. Dziubla, Modeling the Oxidative Consumption of Curcumin from Controlled Release Poly(beta-amino ester) Microparticles in the Presence of a Free Radical Generating System, UK College of Engineering Biomedical Research Day, Lexington, KY, March 2017 (oral)

Carolyn T. Jordan, J. Zach Hilt, Thomas D. Dziubla, Modeling the Oxidative Consumption of Curcumin from Controlled Release Poly(beta-amino ester) Microparticles in the Presence of a Free Radical Generating System, Society for Biomaterials 2017, Minneapolis, MN, April 2017 (poster)

Carolyn T. Jordan, J. Zach Hilt, Thomas D. Dziubla, Modeling the Oxidative Consumption of Curcumin from Controlled Release Poly(beta-amino ester) Microparticles in the Presence of a Free Radical Generating System, American Institute of Chemical Engineers Annual Meeting 2017, Minneapolis, MN, October 2017 (oral)